THE UNIVERSITY OF CALGARY


An Analysis of Airborne Gravity by Strapdown INS/DGPS


by


Craig L. Glennie


A DISSERTATION

SUBMITTED TO THE FACULTY OF GRADUATE STUDIES

IN PARTIAL FULFILLMENT OF THE REQUIREMENTS FOR THE

DEGREE OF DOCTOR OF PHILOSOPHY


DEPARTMENT OF GEOMATICS ENGINEERING

CALGARY, ALBERTA

MARCH, 1999

Canada

# ABSTRACT

Airborne gravity is a method of determining gravity disturbances from measurements taken on an aircraft. The method investigated is the use of a strapdown INS and differential GPS. The INS measures specific force (reaction force due to gravity plus aircraft acceleration) while DGPS measures aircraft acceleration only. Therefore, by differencing the two data streams an estimate of the gravity field, contaminated by measurement noise, is obtained. The question that arises is how accurately, and with what resolution, can the INS/DGPS system determine the disturbances.

This dissertation provides a detailed analysis of strapdown INS/DGPS for the determination of gravity disturbances from an airplane using both rotation invariant scalar gravimetry (RISG) and strapdown inertial scalar gravimetry (SISG). The analysis encompasses theoretical aspects and a detailed numerical study using real data from two flight tests in September 1996 and June 1998.

Results from the September 1996 test showed a best agreement of the system estimate with an upward continued reference of 2.8 mGal and 1.1 mGal at flight heights of 4350 and 7300 metres, respectively. An analysis of crossover point differences for the lower flight showed a repeatability of 1.6 mGal. The SISG method performed consistently better than RISG. These results are near the expected resolution of the current prototype system. However, the long-term non-linear drift of the system disturbance estimates was found to be a problem. This problem could be remedied by using accelerometers with better bias stability, or by combining the airborne disturbance estimates with other sources of gravity information in the flight area. The possibility of combining multiple observations of the specific force and GPS acceleration was also investigated for the September 1996 test, however, combining multiple estimates showed little improvement over estimates with a single INS/DGPS system.

The June 1998 test compared strapdown INS/DGPS airborne gravity to the more established airborne gravity using a LaCoste and Romberg gravimeter. The two systems agreed at the 2-3 mGal level, which is near the combined expected noise levels for the two systems. The excellent agreement shows that the use of a strapdown INS/DGPS system is a promising approach to airborne gravity.

# ACKNOWLEDGEMENTS

# TABLE OF CONTENTS

# LIST OF TABLES

# LIST OF FIGURES

# NOTATION

## 1. CONVENTIONS

1.1 Vectors are bold and lowercase

1.2 Matrices are bold and uppercase

1.3 A dot above a matrix or vector denotes time differentiation

1.4 "Vector" refers to components of a vector. Vector superscripts refer to the coordinate frame the vector is represented in, e.g.

$$\mathbf{r^b} = \begin{bmatrix} r_x^b & r_y^b & r_z^b \end{bmatrix}^T$$

1.5 Rotation matrices are specified by indices such that the transformation from the b-frame to the l-frame is given by

$$\mathbf{r^l} = \mathbf{R_b^l r^b}$$

1.6 Angular velocity of, for example, the b-frame with respect to the i-frame (subscripts) coordinated in the b-frame (superscript) is given by

$$\omega_{ib}^b = \begin{bmatrix} \omega_x & \omega_y & \omega_z \end{bmatrix}^T$$

or by the corresponding skew-symmetric matrix

$$\Omega_{ib}^b = \begin{bmatrix} 0 & -\omega_z & \omega_y \\ \omega_z & 0 & -\omega_x \\ -\omega_y & \omega_x & 0 \end{bmatrix}$$

## 2. COORDINATE FRAMES

2.1 Local Astronomic Frame (a-frame)
- origin: at observation point
- x-axis: tangent to astronomic meridian pointing north
- y-axis: completes a left-handed system
- z-axis: orthogonal to level surface at observation point

2.2 Operational Inertial Frame (i-frame)
- origin: at center of mass of the Earth.

- x-axis: pointing towards mean vernal equinox.
- y-axis: completes a right-handed system.
- z-axis: coincident with Earth mean spin axis.

## 2.3 Body Frame (b-frame)

- origin: centre of mass of accelerometer proof masses, assumed to coincide with centre of rotation of sensor unit.
- x-axis: pointing to the right when looking forward.
- y-axis: pointing forward longitudinally along body.
- z-axis: completes a right-handed system.

## 2.4 Earth-Fixed Frame (e-frame)

- origin: Earth's centre of mass.
- x-axis: orthogonal to z-axis in meridian plane of Greenwich.
- y-axis: completes a right-handed system.
- z-axis: parallel to Earth's mean spin axis.

The rotation of the e-frame with respect to the i-frame is given by

$$\omega_{ie}^{e} = \begin{bmatrix} 0 \\ 0 \\ \omega_{Earth} \end{bmatrix} = \begin{bmatrix} 0 \\ 0 \\ 7.2921158 * 10^{-5} (rad/s) \end{bmatrix}.$$

## 2.5 Local-Level Frame (l-frame)

- origin: at the origin of the sensor frame.
- x-axis: completes a right-handed system.
- y-axis: along the north direction of the ellipsoidal meridian.
- z-axis: orthogonal to reference ellipsoid, pointing outwards.

The rotation of the l-frame with respect to the e-frame is given by

$$\omega_{el}^{l} = \begin{bmatrix} -\dot{\varphi} & \dot{\lambda}\cos\varphi & \dot{\lambda}\sin\varphi \end{bmatrix}^{T}.$$

Where $\varphi$ and $\lambda$ are geodetic latitude and longitude, and the dot denotes time differentiation.

The rotation matrix between the l-frame and the e-frame is given by

$$
\mathbf{R}_l^e = \begin{bmatrix} -\sin\lambda & -\sin\varphi\cos\lambda & \cos\varphi\cos\lambda \\ \cos\lambda & -\sin\varphi\sin\lambda & \cos\varphi\sin\lambda \\ 0 & \cos\varphi & \sin\varphi \end{bmatrix}
$$

The rotation matrix between the l-frame and the b-frame is given by

$$
\mathbf{R}_b^l = \begin{bmatrix} \cos\psi\cos\phi - \sin\psi\sin\theta\sin\phi & -\sin\psi\cos\theta & \cos\psi\sin\phi - \sin\psi\sin\theta\cos\phi \\ \sin\psi\cos\phi + \cos\psi\sin\theta\sin\phi & \cos\psi\cos\theta & \sin\psi\sin\phi - \cos\psi\sin\theta\cos\phi \\ -\cos\theta\sin\phi & \sin\theta & \cos\theta\cos\phi \end{bmatrix}
$$

where $\phi, \theta, \psi$, are the roll, pitch and yaw of the body frame, defined as: roll about y-axis, pitch about x-axis, and yaw about z-axis. The rotations are all positive counter-clockwise when viewed from the positive end of the respective axis.

## 3.  ACRONYMS

- **AGMASCO**   airborne geoid mapping system for coastal oceanography
- **DEM**   digital elevation model
- **DGPS**   differential global positioning system
- **FIR**   finite impulse response
- **IMU**   inertial measurement unit
- **INS**   inertial navigation system
- **KMS**   Kort & Matrikelstyrelsen (Danish National Survey and Cadastre)
- **LCR**   LaCoste and Romberg
- **LRF III**   Honeywell Laseref III strapdown inertial system
- **LTN 101**   Litton 101 strapdown inertial system
- **PDOP**   position dilution of precision
- **PPS**   pulse-per-second
- **RISG**   rotation invariant scalar gravimetry
- **RMS**   root mean square
- **SISG**   strapdown inertial scalar gravimetry

## 4. SYMBOLS

| | |
|---|---|
| $\mathbf{A}$ | row matrix, last row of $\mathbf{R}_b^l$ matrix |
| $a_1, a_2 \cdots a_5$ | cross-coupling coefficients |
| $da_1, da_2 \cdots da_5$ | errors in the cross-coupling coefficients |
| $\mathbf{b}$ | vector of accelerometer biases |
| $b_i, b_j$ | flight lines i and j disturbance biases in crossover adjustment |
| $c_{cc}$ | cross-coupling correction |
| $c_{tilt}$ | platform tilt correction |
| $\mathbf{d}$ | vector of gyro drifts |
| $dT$ | time synchronization error |
| $\mathbf{F}$ | dynamics matrix |
| $\mathbf{F}^l$ | skew-symmetric matrix of specific force |
| $\mathbf{f}^b$ | vector of accelerometer specific force measurements |
| $\mathbf{df}^b$ | vector of accelerometer errors |
| $f_e, f_n, f_u$ | three components of specific force in the l-frame |
| $f_x, f_y, f_z$ | three components of the specific force in the b-frame |
| $df_x, df_y, df_z$ | accelerometer errors in the b-frame |
| $\mathbf{G}$ | shaping matrix |
| $g$ | magnitude of gravity |
| $\mathbf{g}^l$ | gravity vector in the l-frame |
| $\mathbf{g}^e$ | normal gravity in the e-frame |
| $h$ | geodetic height |
| $K$ | scale factor |
| $\mathbf{l}^b$ | position difference between the INS and GPS measurement origins in the INS b-frame |
| $\mathbf{N}^e$ | coefficient matrix relating normal gravity errors to position errors |
| $p_b$ | beam position |
| $dp_b$ | beam position error |

| | |
|---|---|
| $\mathbf{R}_b^e$ | transformation matrix from the b-frame to the e-frame |
| $\mathbf{R}_b^l$ | rotation matrix which transforms accelerometer measurements from the b-frame to the l-frame |
| $\mathbf{r}^e$ | position vector in the e-frame, |
| $\delta\mathbf{r}^e$ | errors in position (for Kalman filter) |
| $R_m$ | meridian radius of curvature |
| $R_n$ | prime vertical radius of curvature |
| $S$ | spring tension |
| $s_i, s_j,$ | slopes of flight lines i and j in crossover adjustment |
| $T_c$ | low-pass filtering cut-off period |
| $T_{ph}$ | period of the phugoid oscillation |
| $\mathbf{V}^l$ | skew-symmetric matrix of vehicle velocity |
| $v_b$ | beam velocity |
| $dv_b$ | beam velocity error |
| $\mathbf{v}^e$ | vehicle velocity vector |
| $\delta\mathbf{v}^e$ | errors in velocity (for Kalman filter) |
| $\mathbf{v}^l$ | vehicle velocity vector |
| $d\mathbf{v}^l$ | vehicle velocity error |
| $v_e, v_n, v_u$ | east, north and up components of the vehicle velocity |
| $\dot{\mathbf{v}}^l$ | vehicle acceleration |
| $d\dot{\mathbf{v}}^l$ | vehicle acceleration error |
| $d\dot{v}_e, d\dot{v}_n, d\dot{v}_u$ | vehicle acceleration errors in the l-frame |
| $\mathbf{x}$ | Kalman filter error states |
| $\mathbf{w}$ | random forcing functions |
| $\mathbf{w}_b$ | vector of accelerometer bias white noise |
| $\mathbf{w}_d$ | vector of gyro drift white noise |
| $\boldsymbol{\alpha}^l$ | kinematic acceleration vector |

| | |
|---|---|
| $\alpha_e$, $\alpha_n$, $\alpha_u$ | three components of the kinematic acceleration vector in the l-frame |
| $d\alpha_e$, $d\alpha_n$, $d\alpha_u$ | errors in kinematic acceleration vector in the l-frame |
| $\beta$ | diagonal matrix of inverse of correlation times for accelerometer bias processes |
| $\gamma^l$ | normal gravity vector |
| $d\gamma^l$ | errors in normal gravity vector |
| $\gamma$ | normal gravity |
| $\Delta\delta g$ | difference in disturbance estimates between flight lines at crossover points |
| $\Delta t_i$ | time differences between the start of the flight line and the time of the current crossover point. |
| $\delta g^l$ | gravity disturbance vector |
| $d\delta g^l$ | error in the gravity disturbance vector |
| $\varepsilon^l$ | attitude errors due to gyro measurement noise and initial misalignment |
| $\varepsilon_E$, $\varepsilon_N$, $\varepsilon_U$ | attitude errors in the l-frame |
| $\eta$ | deflection of the vertical in east-west direction |
| $\theta$ | pitch angle |
| $\kappa$ | diagonal matrix of inverse of correlation times for gyro drift processes |
| $\xi$ | deflection of the vertical in north-south direction |
| $\sigma$ | standard deviation |
| $\psi$ | yaw angle |
| $\Omega^l_{be}$ | skew-symmetric matrix of the angular velocity between the b-frame and the e-frame |
| $\Omega^l_{el}$ | skew-symmetric matrix of the angular velocity $\omega^l_{el}$ |
| $\Omega^b_{ib}$ | skew-symmetric matrix of the angular velocity, $\omega^b_{ib}$ |
| $\Omega^l_{ie}$, | skew-symmetric matrix of the angular velocity $\omega^l_{ie}$ |
| $\omega^l_{el}$ | angular vehicle rate over the ellipsoid |
| $d\omega^l_{el}$ | error in vehicle rate over the ellipsoid |

| | |
|---|---|
| $\omega_{ib}^{b}$ | angular velocity measured by INS gyroscopes |
| $\omega_{ie}^{l}$ | earth rotation vector |
| $d\omega_{ie}^{l}$ | error in earth rotation |
| $\omega_{e}$ | earth rotation rate |
| $\varphi_{xx}(\tau)$ | autocorrelation function |
| $\varphi$ | geodetic latitude |
| $\lambda$ | geodetic longitude |
| $\phi$ | roll angle |

# CHAPTER 1
## Introduction

In this dissertation, a detailed analysis of airborne gravity disturbance determination by strapdown INS/DGPS is presented.

## 1.1: Background and Objectives

Measuring gravity from an airborne platform has been a dream of geodesists and geophysicists for decades. Making accurate gravity measurements from an airplane is vastly superior to point-wise terrestrial measurements both in terms of economy and efficiency. It also offers the opportunity to survey remote areas that are not easily accessible. Proposals for such an airborne survey system go back 40 years, e.g. Thompson (1959). The first flight experiments were performed soon after, see Thompson and LaCoste (1960) and Nettleton et al. (1960). These first flight tests were disappointing as sufficiently accurate navigation data to determine aircraft position and velocity were not available.

Interest in airborne gravity waned for approximately the next twenty years, however, interest was rekindled in the mid-eighties which led to improvements in airborne gravity meter system design. The new designs employed damped stable platforms that were selected to optimize the results based on operational conditions; see for example LaCoste (1983). However, the navigational data used for vertical acceleration determination was still a cause for concern.

The second, and current, stage of airborne gravity system development began in the late 1980's with the use of the Global Positioning System (GPS) for kinematic applications. It was quickly realized that the emergence of GPS would allow the determination of the aircraft navigational parameters with sufficient accuracy to compensate gravimeter output for aircraft motion. In addition to making the stable platform systems developed in the early eighties into operational airborne gravity

systems, GPS also opened up the possibility of using other system concepts based on existing inertial sensors for gravity disturbance estimation.

In principle, there are two main problems when designing an airborne gravity system: the accurate maintenance of a direction in space, and separating the gravitational and non-gravitational accelerations that are sensed by instruments on an airborne platform. The inability to separate the gravitational and kinematic aircraft accelerations was the major downfall of the early airborne gravimetry tests. An accurate system for sensing kinematic vehicle acceleration was simply not available. However, the introduction of differential GPS (DGPS) positioning has for the most part solved the problem of determining aircraft acceleration. Accurate DGPS position and velocity information can be differentiated to determine aircraft acceleration. At the current time, DGPS is the method of aircraft acceleration determination used by all operational and prototype airborne gravity systems.

The maintenance of a direction in space is the area where there is some disparity in system designs. In principle there are four methods that can be used for attitude stabilization of a gravity meter, see Schwarz and Wei (1994). The four different methods are displayed in Figure 1.1. Three use inertial systems for attitude stabilization, while one uses a GPS multi-antenna system.
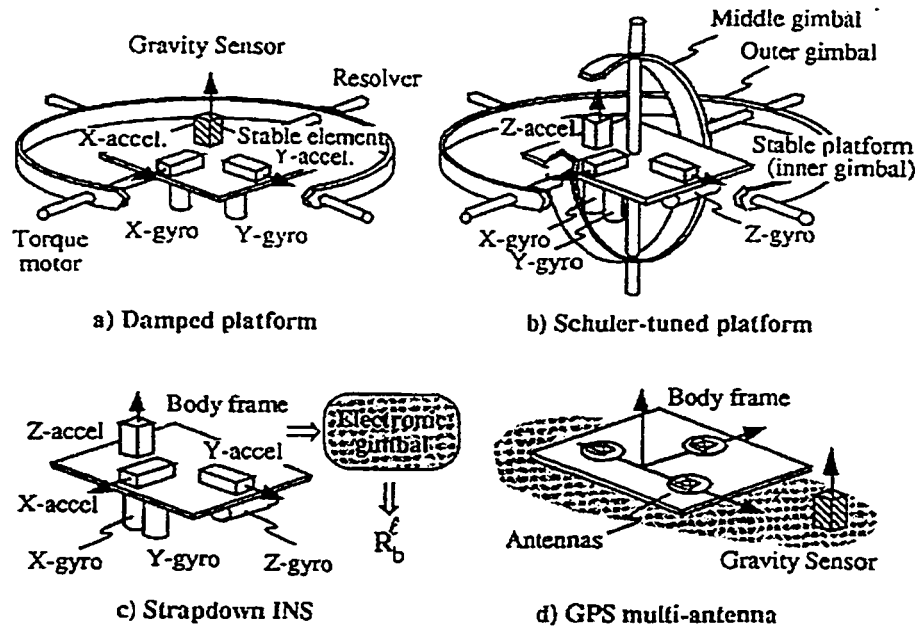


Figure 1.1: Attitude Stabilization for Airborne Gravity (after Schwarz and Wei, 1994)

The first two methods of attitude determination depicted employ a similar concept. A stable platform is used, and therefore orientation of the gravimeter sensor is replaced by stabilization. This has the obvious advantage that the gravity sensors are isolated from the aircraft rotations, and therefore, sensors with a much smaller dynamic range can be used. A smaller dynamic range in turn allows the sensor greater sensitivity. The first platform stabilization method ((a) in Figure 1.1) is a damped two-axes platform system. For this system the x and y axis gyros and accelerometers are used in a feedback loop to stabilize the platform. These sensors suffer from errors, and thus the feedback mechanism must be damped in order to optimize the gravity estimation for a certain time period. Typically damping periods of 4 to 18 minutes are used, Valliant (1992). To date, most operational airborne gravity results have been obtained with modified two-axes LaCoste and Romberg sea gravimeters; see for example Brozena (1992), Klingele et al. (1996) and Hehl et al. (1997).

Due to the design of the two-axes systems significant horizontal acceleration can degrade the accuracy of the results. Therefore, the second method of platform stabilization ((b) in Figure 1.1) can be applied. This is the so-called Schuler tuned three-axes stable platform system. The Schuler platform has a damping period of 84 minutes and therefore theoretically eliminates the errors due to horizontal accelerations. In practice these errors are not completely eliminated due to the inaccuracy of the platform sensors. The ITC-2 system developed at the Inertial Technology Scientific Center in Moscow is an example of a Schuler tuned three axis system; see for example Salychev (1995) and (1998) and Salychev and Schwarz (1995).

The final two methods of attitude stabilization presented in Figure 1.1 do not make an attempt to isolate the gravity sensors from the aircraft rotation. The aircraft dynamics are sensed by the gravity meter and then removed in post mission data processing. This has the conceptual drawback that the gravity sensors require a larger dynamic range. A larger dynamic range means decreased sensitivity. In theory, a GPS multi-antenna system could be used for attitude stabilization ((d) in Figure 1.1), and has been proposed in Boedecker and Neumayer (1995). The attitude of the aircraft is computed from the change in coordinate differences between a rigid antenna array

mounted on the aircraft. Currently, such systems are not of high enough accuracy to meet the stringent attitude requirements of airborne gravity. An additional drawback of such a system is that differential rotations between the attitude sensors and gravity sensor cannot be measured. This is due to the fact that the GPS antennas are mounted on the aircraft fuselage, and not on the gravity sensor itself.

The final method of attitude stabilization is the use of a strapdown inertial system ((c) in Figure 1.1). For a strapdown inertial system the platform stabilization is replaced by an electronic stabilization where the gyroscope angular velocities are integrated to compute a rotation matrix between the body frame and the local-level frame. Advantages to the use of a strapdown inertial system include size, cost, operational flexibility and a high data output rate for detailed post mission analysis. Airborne gravity by strapdown INS/DGPS has been mainly pursued by the University of Calgary; see Schwarz et al. (1991) and Wei and Schwarz (1994) for a theoretical analysis of strapdown INS potential for airborne gravity disturbance estimation.

There is in principle another method of scalar gravity disturbance determination that does not require a source of attitude stabilization. This approach is called Rotation Invariant Scalar Gravity (RISG); for details see Czompo (1994). In this approach an orthogonal accelerometer triad is used to determine the magnitude of the specific force vector. This magnitude can be related to the scalar gravity disturbance through the use of all three components of the aircraft kinematic acceleration. The obvious advantage of this approach is that gravity determination becomes independent of determining or maintaining a direction in space. In practice, this means that the system design becomes much simpler because no rotation sensors are needed. It also means that the RISG method can be implemented in any of the existing systems with an accelerometer triad by simply disregarding the rotation measurements.

In June 1995 the University of Calgary conducted a flight test of a strapdown INS/DGPS system for airborne gravity disturbance determination. It is believed that this was the first test of its kind. The test was carried out in the Rocky Mountains near Calgary, Canada. Three profiles were flown along approximately the same 250 km track. Dense ground gravity values in the area were used to determine an upward continued

reference for each flight line. Scalar gravity results were computed using both the strapdown INS attitude stabilization (called the SISG or strapdown inertial scalar gravimetry approach) and the RISG approach. The results of this test showed that the short-term accuracy and repeatability of such a system was at the level of 2 to 4 mGal. More information on the flight test can be found in Wei and Schwarz (1998).

The June 1995 flight test of the prototype strapdown INS/DGPS system had showed that there was great promise in this approach to gravity disturbance estimation. However, the test had only presented short-term accuracy and repeatability results for the system in a very limited study. There were still many questions to be answered, many possible improvements to explore, and a detailed analysis of the estimation procedure required. Some of the unsolved questions included:

- What was the expected noise level of the gravity estimates for the current prototype system?
- Was the accuracy of disturbance estimation dependent upon flight direction?
- What was the long-term behaviour of the gravity disturbance estimates, and could the long-term errors be accounted for?
- Could a procedure be implemented that allowed a better separation of the gravity disturbances and accelerometer biases?
- Were the errors in the SISG and RISG approaches different enough to allow the use of one approach as a check on the other, and could a combination of the two estimation techniques improve results?
- What was the cause of the remaining residuals in the solution? Were these residuals noise, or were they systematic in nature and caused, for instance, by some undetected processing error or an unaccounted dynamic effect?
- What type of accuracy improvements could be realized by multiple sensor configurations?
- Does strapdown INS/DGPS airborne gravity give the same accuracy and resolution for gravity field recovery as the more established airborne gravity using a LaCoste and Romberg air/sea gravimeter?

These questions set the stage for continuing research in strapdown airborne gravity. Data to answer these questions were obtained in two flight tests, performed in September 1996 and June 1998. The September 1996 flights were an extensive test performed over three days in an area with dense ground gravity coverage. This allowed for the calculation of an accurate upward continued reference for all of the flight lines. In addition, two strapdown inertial systems were flown side-by-side to provide independent system estimates for error checking and an investigation of multiple sensor configurations. The June 1998 test flew the strapdown INS/DGPS system side-by-side with a LCR gravimeter that allowed, for the first time, a direct comparison of these two approaches to airborne gravity. With the analysis of these data sets it is hoped that the contents of this dissertation will provide an answer, or at least an indication of the answer, for the above questions. In addition, the conclusions presented should help determine the future direction of research for the continuing improvement of strapdown airborne gravity.

## 1.2:Thesis Outline

The main objective of this dissertation is to give a detailed analysis of the use of strapdown inertial navigation systems and differential GPS for the determination of the vertical component of the gravity disturbance vector from an airplane. The analysis encompasses both theoretical aspects and a detailed numerical study using real data from two flight tests. The dissertation gives an in-depth analysis of the long-term accuracy and repeatability of the system as well as possible barriers for further system improvement; where system improvement is generally considered to be an increase in the accuracy and/or resolution of the system.

Chapter 2 of the dissertation introduces the principle of scalar gravity disturbance recovery by both the SISG (strapdown inertial scalar gravimetry) and RISG (rotation invariant scalar gravimetry) approaches. The error models for the two approaches are presented and briefly contrasted and compared in a theoretical manner. The SISG and RISG error models' response to actual aircraft dynamics is then given. The aircraft motion from two flight lines of the September 1996 test are used to analyze the

similarities and differences in the RISG and SISG error models under typical airborne gravity flight conditions. Finally, the chapter concludes with a discussion of the current data processing techniques to determine gravity disturbances at flight level from the raw strapdown INS and DGPS measurements.

The prototype strapdown INS/DGPS system developed at the University of Calgary along with the two flight tests analyzed in the dissertation are presented in Chapter 3. The estimated accuracy of the INS accelerometers and DGPS acceleration determination are presented to give an idea of the expected performance of the prototype system. A flight test of the prototype system in September 1996 is described. This test took place over three days in a 100 km by 100 km area of the Rocky Mountains. Two strapdown inertial systems were flown side-by-side in the September test. The second flight test, performed in June 1998 is also discussed. In this test the strapdown INS system was flown alongside a LaCoste and Romberg (LCR) modified air/sea gravimeter and an orthogonal triad of QA 3000 accelerometers. The chapter concludes with a brief discussion of the LCR gravimeter and its expected performance.

Airborne gravity by strapdown INS/DGPS provides relative gravity information. However, the relative gravity estimates are not self-consistent due to the long-term drift of the gravity disturbance estimates. This drift is mainly due to instability in the accelerometer biases of the strapdown inertial system. In Chapter 4 the problem of long-term accelerometer bias estimation and compensation is presented. Various attempts to model the long-term drift of the accelerometer biases are presented. These include the use of a first-order Gauss-Markov model, a combination polynomial fit and Gauss-Markov or random walk model, and an iterative technique to better separate accelerometer biases and gravity disturbances. Finally, a crossover adjustment is introduced as the first step in an alternative method of compensating for the accelerometer bias instability.

The results of the September 1996 and June 1998 flight tests are presented and discussed in Chapter 5. Both RISG and SISG results are given for the strapdown INS systems. For the September 1996 test the results are investigated in three ways: the two strapdown INS system estimates are inter-compared, the individual system estimates are

compared to an upward continued reference, and crossover point differences are analyzed. The June 1998 test data is examined in two ways: the strapdown INS system estimates are compared with the LCR disturbance estimates, and both the strapdown INS and LCR gravimeter estimates are compared to existing ship measurements of gravity below some of the flight lines.

Chapter 6 begins with an investigation of the improvement in disturbance estimation possible by combining the SISG and RISG estimates from one system. Results for an entire day of testing in September 1996 are presented. Some possible problems using solely the RISG approach for an airborne gravity survey system are also discussed. Finally, the chapter concludes with a discussion of gravity estimation improvement using multiple sensor configurations. The data collected during the September 1996 test is used to show the improvement obtained using multiple specific force measurements and multiple determinations of kinematic DGPS acceleration.

Finally, Chapter 7 gives a brief summary of the main results and also presents some conclusions and recommendations for future work.

# CHAPTER 2
## The Method of Scalar Airborne Gravity by Strapdown INS/DGPS

The description of two approaches to scalar airborne gravimetry by strapdown INS/DGPS will be given. The first, strapdown inertial scalar gravimetry (SISG), requires orientation information from the strapdown system. The second, rotation invariant scalar gravimetry (RISG) needs only the output of an orthogonal accelerometer triad. The error models for the two approaches will also be given and compared. Additionally, the behaviour of the SISG and RISG error models will be analyzed using actual aircraft dynamics. Finally, current data processing techniques for the strapdown INS/DGPS measurements will be briefly discussed.

## 2.1 The Measurement Models of Scalar Airborne Gravity

### 2.1.1 Strapdown Inertial Scalar Gravimetry (SISG)

In the local-level frame, the model of airborne gravimetry can be expressed by Newton's equation of motion in the gravitational field of the earth as:

$$\delta g^l = \dot{v}^l - R_b^l f^b + \left( 2\Omega_{ie}^l + \Omega_{el}^l \right) v^l - \gamma^l \tag{2.1}$$

where

$\delta g^l$ is the gravity disturbance vector,

$\dot{v}^l$ is vehicle acceleration (dot denotes time differentiation),

$R_b^l$ is a rotation matrix which transforms accelerometer measurements from b-frame to the l-frame,

$f^b$ is the vector of accelerometer specific force measurements,

$v^l$ is the vehicle velocity vector,

$\Omega^l_{ie}$, $\Omega^l_{el}$      are skew-symmetric matrices of the angular velocities $\omega^l_{ie}$ and $\omega^l_{el}$ due to earth rotation and vehicle rate over the ellipsoid, and

$\gamma^l$      is the normal gravity vector.

For a detailed derivation of this equation, the reader is referred to Schwarz and Wei (1997). When an integrated strapdown INS/DGPS system is used for airborne gravity, the specific force vector $f^b$ is measured by the three accelerometers of the inertial measuring units. The transformation matrix $R^l_b$ is obtained by integrating the angular velocities (after correction for earth rate and vehicle rate) sensed by the inertial systems gyroscopes. The kinematic quantities $\dot{v}^l$, $v^l$ are obtained from GPS Doppler and carrier phase measurements. Finally, the quantities $\omega^l_{el}$ and $\gamma^l$ are computed using GPS position and velocity results. Equation (2.1) can be used for both scalar and vector gravimetry. When considering scalar gravimetry, only the vertical component (the last of the three equations) is used:

$$\delta g = f_u - \dot{v}_u + \left( \frac{v_e}{R_n + h} + 2\omega_e \cos\varphi \right) v_e + \frac{v_n^2}{R_m + h} - \gamma \qquad (2.2)$$

where

$f_u$      is the upward component of specific force (from INS),

$v_e$, $v_n$, $v_u$      are the east, north and up components of the vehicle velocity (from GPS),

$R_m$, $R_n$      are the meridian and prime vertical radii of curvature,

$\varphi$, h      are geodetic latitude and height,

$\omega_e$      is the earth rotation rate, and

$\gamma$      is normal gravity.

The sum of the third and fourth terms in equation (2.2) is often called the Eötvös correction. This approach is often abbreviated as SISG (Strapdown Inertial Scalar Gravimetry).

## 2.1.2 Rotation Invariant Scalar Gravimetry (RISG)

An alternative approach to scalar gravimetry is called RISG (Rotation Invariant Scalar Gravimetry), see Czompo (1994). In this method all three specific force components of an orthogonal accelerometer triad are used to determine the changes in the magnitude of gravity. Precise orientation information for the accelerometer triad is not required, it is only needed approximately to account for the lever-arm correction due to the difference in origins of the INS and GPS measurement units.

Since the magnitude of the acceleration is not dependent upon orientation, the magnitude of gravity can be computed as:

$$g = \left| \mathbf{g}^l \right| = \left[ \left| \mathbf{f}^b \right|^2 - \left| \boldsymbol{\alpha}^l \right|^2 + 2\boldsymbol{\alpha}^a \mathbf{g}^a \right]^{1/2}, \tag{2.3}$$

where the superscripts a, l and b denote the local astronomic, local-level, and body frame respectively. The quantity $\boldsymbol{\alpha}^l$ is the kinematic acceleration vector which is defined as:

$$\boldsymbol{\alpha}^l = \dot{\mathbf{v}}^l + \left( 2\boldsymbol{\Omega}^l_{ie} + \boldsymbol{\Omega}^l_{el} \right)\mathbf{v}^l \tag{2.4}$$

and is the sum of vehicle and Coriolis accelerations. Solving the quadratic equation (2.3) for the magnitude of gravity, and assuming that the upward component of the acceleration in the local astronomic frame can be approximated by using the upward kinematic acceleration in the l-frame (i.e. neglecting the deflections of the vertical), the gravity disturbance $\delta g$ is given by

$$\delta g = \left[ \left| \mathbf{f}^b \right|^2 - \alpha_e^2 - \alpha_n^2 \right]^{1/2} - \alpha_u - \gamma, \tag{2.5}$$

where

$\alpha_e$, $\alpha_n$, $\alpha_u$    are the three components of the kinematic acceleration vector in the l-frame,

$\mathbf{f}^b$    is the specific force vector in the b-frame, and

$\gamma$    is normal gravity.

A more detailed derivation of the RISG equation can be found in Wei and Schwarz (1998).


## 2.2 Error Models for SISG and RISG Approaches to Airborne Gravity


### 2.2.1 Error Model of SISG

The error model of strapdown inertial vector gravimetry has been derived in, for example, Schwarz and Wei (1994) and Schwarz and Li (1996), and is obtained by linearizing equation (2.1) in the following way:

$$d\delta g^l = F^l \varepsilon^l - R_b^l df^b - d\dot{v}^l + \left(2\Omega_{ie}^l + \Omega_{el}^l\right)dv^l - V^l\left(2d\omega_{ie}^l + d\omega_{el}^l\right) - d\gamma^l \qquad (2.6)$$

where,

$d\delta g^l$    represents the error in the gravity disturbance vector,

$\varepsilon^l$    is attitude errors due to gyro measurement noise and initial misalignment,

$df^b$    is accelerometer errors,

$d\dot{v}^l$    is GPS vehicle acceleration error,

$dv^l$    is GPS vehicle velocity error,

$d\omega_{ie}^l$, $d\omega_{el}^l$    are angular velocity errors,

$d\gamma^l$    is errors in normal gravity computation, and

$F^l$, $V^l$    are skew-symmetric matrices of specific force and vehicle velocity respectively.

With current GPS technology it is possible to obtain post-mission position and velocity with standard deviations of approximately $\sigma_p = 20$ cm, and $\sigma_v = 5$ cm/s, respectively. Therefore, the errors generated by the fourth, fifth and sixth terms in equation (2.6) can be safely neglected since they will contribute less than 0.5 mGal error in determination of $\delta g$ given these position and velocity accuracies, Schwarz and Wei (1994). However, equation (2.6) assumes that the INS and GPS time series are perfectly synchronized, and this is impossible in practice. Therefore, an additional error term due to a time shift between the data series must be added. The error equation now takes the form

$$d\delta g^l = F^l \varepsilon^l - R_b^l df^b - d\dot{v}^l + \left(\dot{R}_b^l f^b + R_b^l \dot{f}^b\right) dT \,, \tag{2.7}$$

where dT is the time synchronization error. The first two error terms are due to the inertial system, the third due to GPS, and the fourth due to timing errors between the two systems. If we consider the scalar gravimetry (SISG) case, then equation (2.7) reduces to

$$d\delta g = f_e \varepsilon_N - f_n \varepsilon_E - A df^b - d\dot{v}_u + \left(\dot{A} f^b + A \dot{f}^b\right) dT \,, \tag{2.8}$$

where $A$ and $\dot{A}$ are row matrices of the form

$$A = \left[-\cos\theta\sin\phi \quad \sin\theta \quad \cos\theta\cos\phi\right] \tag{2.9a}$$

$$\dot{A} = \left[\dot{\phi}\sin\theta\sin\phi - \dot{\phi}\cos\theta\cos\phi \quad \dot{\theta}\cos\theta \quad -\dot{\theta}\sin\theta\cos\phi - \dot{\phi}\cos\theta\sin\phi\right] \tag{2.9b}$$

and $\phi, \theta$ are the roll and pitch angles of the transformation matrix from the b-frame to the l-frame, and the dot denotes time differentiation. Thus, the error in gravity disturbances for the scalar case is affected by errors in all three accelerometers ($df_x$, $df_y$, $df_z$). However, for a typical airborne gravity flight the roll and pitch angles will be quite small, and therefore, the vertical accelerometer error will dominate. Errors due to misalignment will only appear in the gravity disturbance estimation if specific forces in the horizontal

channels ($f_e$, $f_n$) are present. Therefore, operation at a constant velocity is desired to keep these errors minimal.

## 2.2.2 Error Model of RISG

An error model for the RISG approach can be obtained by linearizing equation (2.5) and adding a term (dT) which is due to imperfect time synchronization between the INS and GPS measurements (Wei and Schwarz, 1996). The resulting equation is of the form

$$d\delta g = \frac{f_x}{f_u}df_x + \frac{f_y}{f_u}df_y + \frac{f_z}{f_u}df_z - \frac{\alpha_e}{f_u}d\alpha_e - \frac{\alpha_n}{f_u}d\alpha_n - d\alpha_u + \left|\dot{f}^b\right|dT, \tag{2.10}$$

where

$f_u = \left[\left|f^b\right|^2 - \alpha_e^2 - \alpha_n^2\right]^{1/2}$ is the upward component of the specific force in the l frame,

$f_x$, $f_y$, $f_z$               are the three components of the specific force in the b-frame,

$df_x$, $df_y$, $df_z$         are the accelerometer errors, and

$d\alpha_e$, $d\alpha_n$, $d\alpha_u$       are the errors in kinematic acceleration.

Thus, as can be observed in equation (2.10), errors in the vertical channels affect the gravity disturbance determination almost directly while errors in the horizontal channels are attenuated. By examining the first three terms of equation (2.10) the optimal orientation for mounting a triad of orthogonal accelerometers for RISG gravity determination becomes apparent for a constant velocity flight. If three accelerometers, all with a standard deviation $\sigma$, are used in the RISG triad then the minimum error contribution in $d\delta g$ by the accelerometers will be of magnitude $\sigma$ if the b-frame is aligned with the l-frame. In this case the first and second terms will be approximately zero ($f_x/f_u$, $f_y/f_u \sim 0$) and $f_z/f_u \sim$ one. The error contributions for all other alignments will be greater than $\sigma$, up to a maximum of $1.7\sigma$ for a 45° umbrella-like configuration. This means that

the performance of the system could theoretically be improved by using a better z-accelerometer, or by using multiple z-accelerometers. If multiple z-accelerometers are used, and the accelerometer noise has white noise characteristics, then an improvement of $\sigma / \sqrt{n}$ could be expected, where n is the number of z-accelerometers.

## 2.3 Comparison of SISG and RISG Error Sources

### 2.3.1 Theoretical Comparison of SISG and RISG Error Sources

The SISG and RISG approaches to scalar airborne gravity determination are mathematically different. However, as will be shown below, despite the different formulations the error terms for the two methods can show quite similar behaviour. Comparisons of the error models for the two approaches can also be found in Wei and Schwarz (1996) and Schwarz and Glennie (1998). First, by assuming precise post-mission position and velocity from DGPS, the error in kinematic acceleration ($d\alpha_e$, $d\alpha_n$, $d\alpha_u$) in equation (2.10) can be replaced by $\left(d\dot{v}_e,\ d\dot{v}_n,\ d\dot{v}_u\right)$ since the errors in computing the Coriolis acceleration in equation (2.4) are negligible. Therefore, the error in GPS determined vertical acceleration has the same effect in both equation (2.8) and (2.10).

The effect of the accelerometer errors $\mathbf{df^b}$ and the synchronization error dT will only be the same in both equations if the flight is at constant height and constant velocity, and the b-frame is mounted in such a way that it corresponds to the l-frame. For the synchronization errors to be the same the following equation must hold:

$$\dot{\mathbf{A}}\mathbf{f^b} + \mathbf{A}\dot{\mathbf{f}}^b = \sqrt{\dot{f}_x^2 + \dot{f}_y^2 + \dot{f}_z^2}\ . \tag{2.11}$$

For the effect of the accelerometer errors $\mathbf{df^b}$ to be the same, the following three equations must be satisfied:

$$\frac{f_x}{f_u} = -\cos\theta\sin\phi \quad \frac{f_y}{f_u} = \sin\theta \quad \frac{f_z}{f_u} = \cos\theta\cos\phi .$$

(2.12)

If pitch, roll and their time derivatives are zero (i.e. b-frame corresponds to l-frame), then equations (2.11) and (2.12) reduce to the forms

$$\dot{f}_u = \sqrt{\dot{f}_e^2 + \dot{f}_n^2 + \dot{f}_u^2}$$

(2.13a)

$$\frac{f_e}{f_u} = 0 \quad \frac{f_n}{f_u} = 0 \quad \frac{f_u}{f_u} = 1 .$$

(2.13b)

If the deflections of the vertical are neglected, the only way in which these equations can be valid is if there are no horizontal accelerations present. As a result, for a constant velocity constant height flight the accelerometer errors and time synchronization errors will effect the SISG and RISG results in the same way if the b-frame corresponds to the l-frame. Airborne gravity flights are planned to be at constant velocity and height, and RISG accelerometer errors are minimized when the triad is aligned with the l-frame. Therefore, this situation is approximated in actual flights and, thus, actual results should have similar accelerometer and time synchronization error characteristics.

However, in actual flight conditions the horizontal accelerations cannot be kept to zero, and the b-frame and l-frame are never perfectly aligned. Experience has shown that the horizontal accelerations typically reach 0.5 m/s$^2$ during straight flights. Considering that g (and therefore $f_u$) is approximately 10 m/s$^2$, the effect of the horizontal accelerometer errors on gravity estimation in the RISG approach will be less than 5% of their total error. In the SISG approach, if we assume that pitch and roll are small enough to use a small angle approximation for $\theta$ and $\phi$ ( i.e. $\sin\alpha = \alpha$ and $\cos\alpha = 1$), then equation (2.12) shows that the rotation will have a small effect of approximately 1.7% of the horizontal accelerometer error for 1° of roll or pitch. Therefore, for actual flight conditions, the errors due to the horizontal accelerometers may be slightly different for

the two approaches. Obviously, the effect of the horizontal accelerometer errors becomes larger for a larger deviation of the b-frame from the l-frame.

Finally, we will consider the remaining terms in equations (2.8) and (2.10). If, for the terms in equation (2.8) we assume that the effects of the deflections of the vertical are negligible, the remaining errors are

$$f_e \varepsilon_N - f_n \varepsilon_E \approx \alpha_e \varepsilon_N - \alpha_n \varepsilon_E, \qquad (2.14a)$$

and the remaining errors in equation (2.10) are

$$-\alpha_e \frac{d\alpha_e}{f_u} - \alpha_n \frac{d\alpha_n}{f_u}. \qquad (2.14b)$$

These remaining errors do not match each other. The first is due to an orientation error, while the second is due to errors in DGPS horizontal accelerations. Dividing the horizontal accelerations by the upward specific force transforms them into an equivalent orientation error. However, considering the relative sizes of the $f_u$ and $d\alpha$ terms, the errors in equation (2.14b) should always be relatively small. The errors in equation (2.14a) on the other hand will only be small if the horizontal accelerations, not the acceleration errors, are small. This could cause a significant difference in the error spectrums of the RISG and SISG methods, especially if the misalignment is large. To investigate the error models further a detailed analysis of the modifying factors for the SISG and RISG approaches using aircraft dynamics from an actual airborne gravity flight will be presented in the next section.

## 2.3.2 Response of SISG and RISG Error Models to Aircraft Dynamics

In the previous section the error models for the SISG and RISG approaches to airborne gravity were presented. A theoretical comparison of the error models for the two

approaches was also given. The conclusion of this comparison was that accelerometer errors and time synchronization errors will affect both approaches in the same way if the b-frame corresponds to the l-frame, and if the aircraft is moving at constant velocity and constant height. Since such operational conditions can only be approximated an examination of the error models using actual aircraft dynamics will be presented here to provide a more realistic comparison. Two flight lines of the September 1996 test have been selected for this comparison.

The first-order error models of the SISG and RISG approach were previously presented; they are repeated here for convenience.

SISG
$$d\delta g = f_E \varepsilon_N - f_N \varepsilon_E - \mathbf{Adf}^b - d\dot{v}_u + \left(\dot{\mathbf{A}}\mathbf{f}^b + \mathbf{A}\dot{\mathbf{f}}^b\right)dT \qquad (2.8)$$

RISG
$$d\delta g = \frac{f_x}{f_u}df_x + \frac{f_y}{f_u}df_y + \frac{f_z}{f_u}df_z - \frac{\alpha_e}{f_u}d\dot{v}_e - \frac{\alpha_n}{f_u}d\dot{v}_n - d\dot{v}_u + \left|\dot{\mathbf{f}}\right|dT \qquad (2.10)$$

Errors in gravity determination are due to DGPS acceleration errors, INS specific force errors, INS misalignment errors, and time synchronization errors. These error terms, along with the factor that modifies them for both the SISG and RISG approach are summarized in Table 2.1. The final column in Table 2.1 (Figure) identifies the figure in which the specific error terms are graphically represented.

| Error Term | SISG Factor | RISG Factor | Figure |
|---|---|---|---|
| X-accelerometer ($df_x$) | $-\cos\theta\sin\phi$ | $f_x/f_u$ | Figure 2.1 |
| Y-accelerometer ($df_y$) | $\sin\theta$ | $f_y/f_u$ | Figure 2.2 |
| Z-accelerometer ($df_z$) | $\cos\theta\cos\phi$ | $f_z/f_u$ | Figure 2.3 |
| Synchronization (dT) | $\dot{\mathbf{A}}\mathbf{f}^b + \mathbf{A}\dot{\mathbf{f}}^b$ | $\left|\dot{\mathbf{f}}\right|$ | Figure 2.4 |
| East GPS Accel ($d\dot{v}_e$) | None | $\alpha_e/f_u$ | Figure 2.5 |
| North GPS Accel ($d\dot{v}_n$) | None | $\alpha_n/f_u$ | Figure 2.6 |
| Up GPS Accel ($d\dot{v}_u$) | -1.0 | -1.0 | None |
| East Misalignment ($\varepsilon_E$) | $-f_e$ | None | Figure 2.6 |
| North Misalignment ($\varepsilon_N$) | $f_n$ | None | Figure 2.5 |

**Table 2.1:** Error Terms for SISG and RISG approaches

The interaction of each error term with typical aircraft dynamics for two flight lines from the September 1996 flight test (see section 3.3) is presented. One flight line is in a north-south direction, and the other in an east-west direction. The north-south flight line is displayed in the top graphs, and the east-west line in the bottom graphs for Figures 2.1 to 2.6. All dynamic parameters (i.e. GPS acceleration, INS specific force and attitude) were low-pass filtered to 30 and 90 seconds $(T_c)$ for the generation of the figures. The 30 second graphs are the left two, and the 90 second graphs are on the right in Figures 2.1 to 2.6. It should be noted that the INS was mounted with its positive y-axis along the aircraft's flight direction toward the front of the aircraft, and the positive x-axis pointing towards the right of the plane (when facing the cockpit). The z-axis completes a right-handed system.

Figures 2.1, 2.2 and 2.3 display the modifying factors in columns 2 and 3 of Table 2.1 for the x accelerometer, y accelerometer, and z accelerometer, respectively.

$(T_c = 30 \text{ seconds})$     $(T_c = 90 \text{ seconds})$
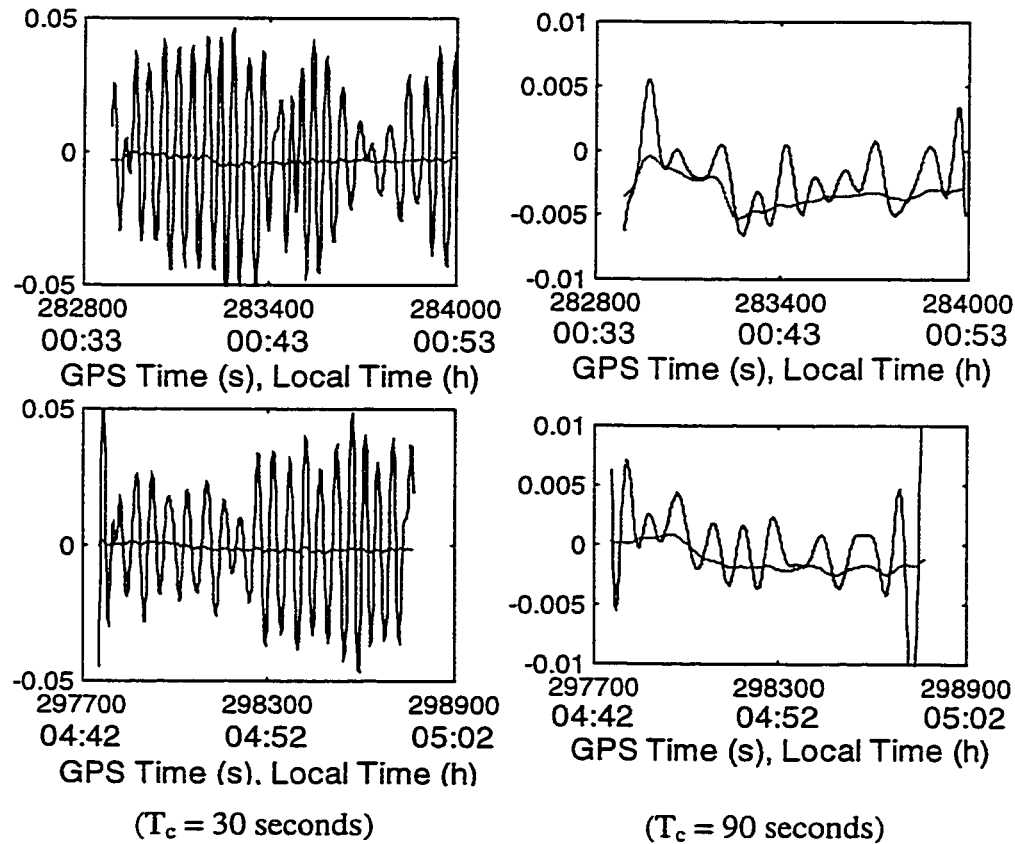
**Figure 2.1:** X-Accelerometer Factor, N-S and E-W Flight Lines, (RISG - dotted)

Figure 2.1 shows that the RISG and SISG modifying factors for the x-accelerometer error are quite different. The RISG factor is always fairly small, while the SISG factor varies between ±5% and ±1% for the 30 and 90 second filtering periods, respectively. The higher variation for the 30 second filtering period is due to an aircraft motion phenomenon known as phugoid motion. Phugoid motion is the natural oscillation of an aircraft at a certain frequency due to a symmetric disturbance, e.g. a sudden up-gust of wind, on the aircraft. The phugoid oscillation period for this flight test is at approximately 45 seconds (see section 5.1.1.1), and therefore this oscillation does not show up in the data filtered to 90 seconds. The RISG x-accelerometer factor is a quotient of translational parameters, while the SISG factor is due to rotational motion. Therefore, it appears that the phugoid oscillation has a larger rotational than translational effect about the axis perpendicular to the motion of the plane (i.e. the x-axis of the inertial system), and therefore the SISG factor is larger than the RISG factor.



($T_c$ = 30 seconds)          ($T_c$ = 90 seconds)
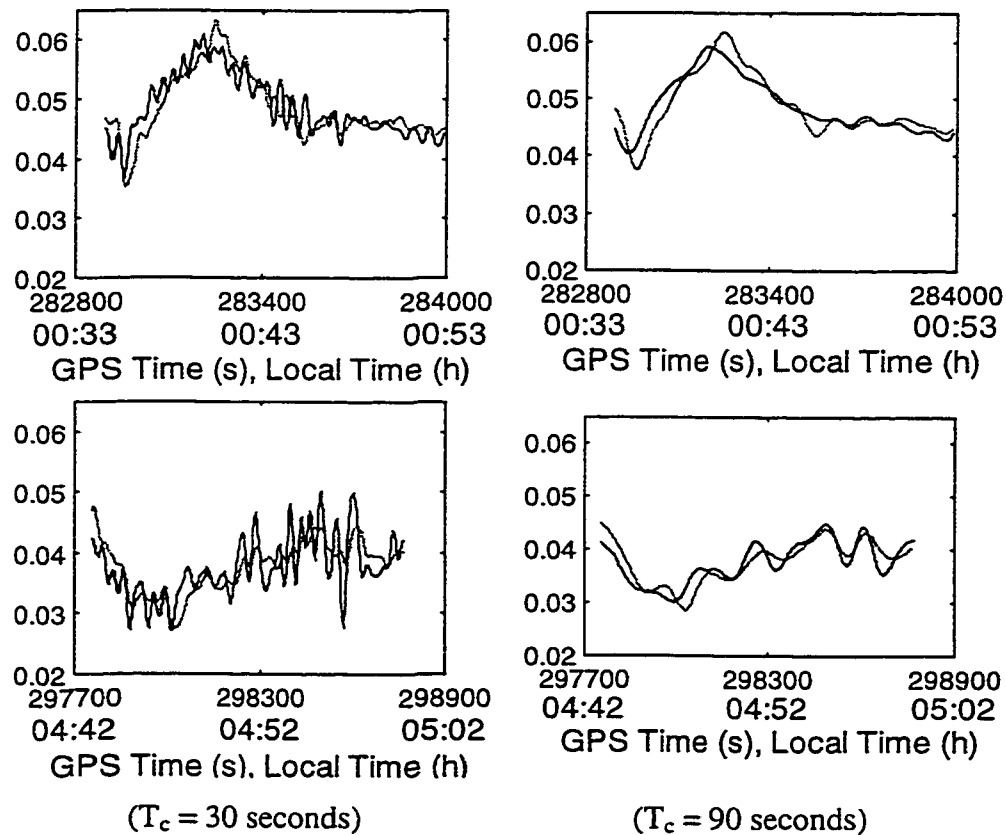
**Figure 2.2**: Y-Accelerometer Factor, N-S and E-W Flight Lines, (RISG - dotted)

The y-accelerometer error modifying factors in Figure 2.2 show a higher degree of correlation than those for the x-accelerometer. The correlation coefficient between the SISG and RISG y-accelerometer error modifying factors varies from 0.6 to 0.85. The maximum deviation between the y factors in Figure 2.2 never exceeds 1%. The effect of the phugoid oscillation is clearly evident in the 30 second modifying factors. Again, the RISG factor is due to translational motion while the SISG factor is due to rotational motion. However, in Figure 2.2 the RISG and SISG factors show similar behaviour. This suggests that the phugoid oscillation has a similar effect on translation and rotation about the axis along the airplane direction of travel (i.e. the y-axis of the inertial system). At a 90 second filtering period the RISG and SISG modifying factors for the y-accelerometer are nearly identical.



(T_c = 30 seconds)      (T_c = 90 seconds)
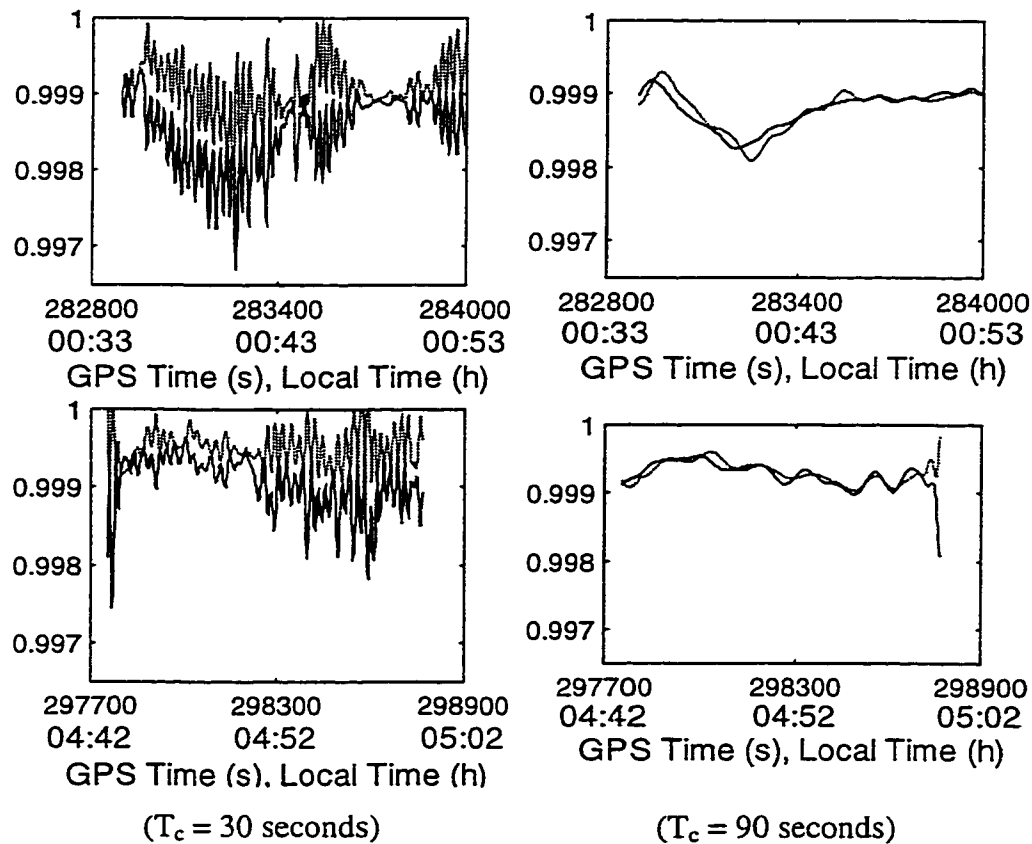
**Figure 2.3:** Z-Accelerometer Factor, N-S and E-W Flight Lines, (RISG - dotted)

An examination of Figure 2.3 reveals an interesting correlation between the RISG and SISG z-accelerometer error modifying factors. At 90 seconds the two factors are nearly identical. However, at 30 seconds the SISG and RISG factors appear to be mirror images of each other. This behaviour can be explained by examining the relationship between the two modifying factors. The RISG z-accelerometer factor is given by $f_z/f_u$, but $f_u$ can also be written as

$$f_u = \mathbf{A}\mathbf{f}^b = -\cos\theta\sin\phi \cdot f_x + \sin\theta \cdot f_y + \cos\theta\cos\phi \cdot f_z . \qquad (2.15a)$$

Rearranging this equation gives

$$\frac{f_z}{f_u} = \frac{1 + \cos\theta\sin\phi \cdot \dfrac{f_x}{f_u} - \sin\theta \cdot \dfrac{f_y}{f_u}}{\cos\theta\cos\phi} . \qquad (2.15b)$$

The denominator on the right hand side of equation (2.15b) is the SISG z-accelerometer error modifying factor. Therefore, it is clear that for the z-accelerometer error the RISG modifying factor is related to the inverse of the SISG factor, which explains the mirror image pattern found on the left-hand side of Figure 2.3. Again, the effect of the phugoid oscillation is clearly evident in the 30 second modifying factors. It should also be noted that the deviation between the SISG and RISG z-accelerometer error factors was never larger than 0.4%. Therefore, the differences displayed in Figure 2.3 cannot be considered significant.

It should be mentioned that the RISG and SISG modifying factors for the three accelerometer errors in Figures 2.1 to 2.3 do not show any significant dependence upon flight line direction. This is due to the fact that the inertial system is a strapdown system, and thus, the measurement axes are fixed to the airplane. Therefore, the y-axis was always aligned with the flight direction of the airplane.

Figure 2.4 displays the time synchronization error modifying factors for the RISG and the SISG approaches. The units of the modifying factors in Figure 2.4 are mGal/s.

By examining Figure 2.4 it is apparent that the two time synchronization error modifying factors are very different. In fact the correlation between them is less than 0.05. The reason for this becomes evident by examining the synchronization error factors for the RISG and SISG approach given in Table 2.1. The RISG factor is a magnitude, and therefore only has positive values; however, the SISG factor is not restricted to positive values. If the absolute value of the SISG factor is compared with the RISG factor then the two show almost perfect correlation; a correlation coefficient over 0.95 for all flight lines. Again, the effect of the phugoid oscillation is clearly evident in the 30 second modifying factors.

(T_c = 30 seconds)                    (T_c = 90 seconds)
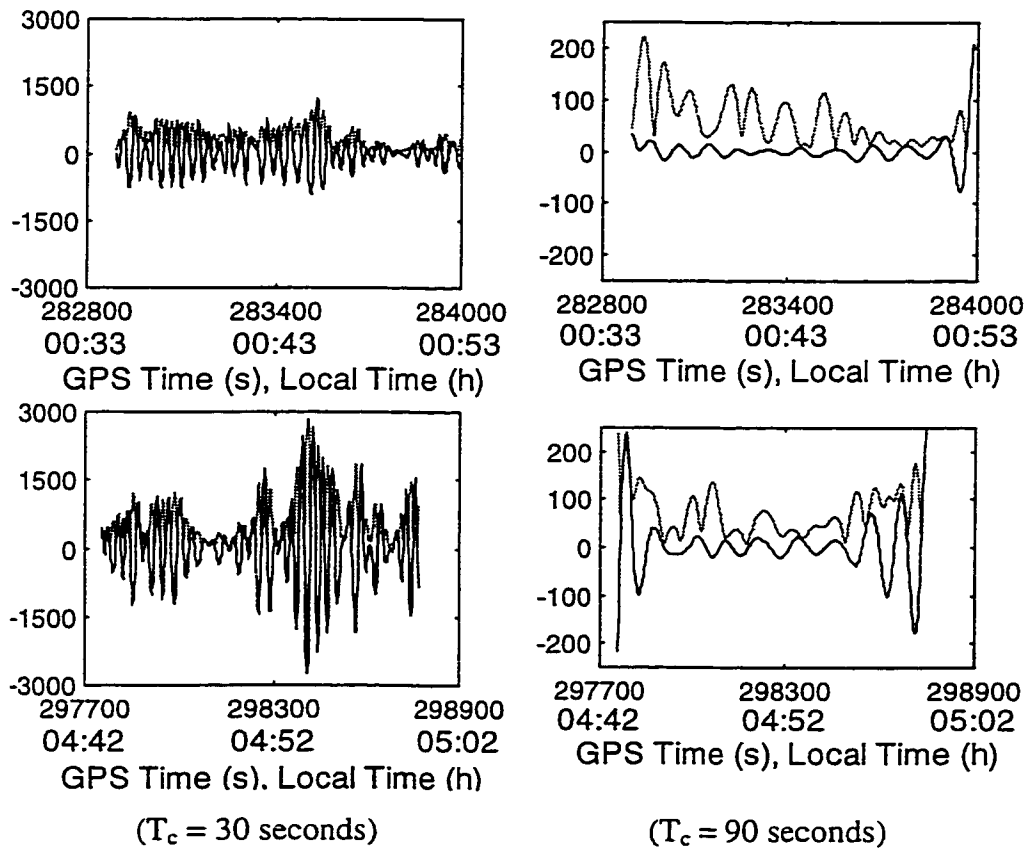
**Figure 2.4:** Time Synchronization Factor (mGal/s), N-S and E-W Flight Lines, (RISG - dotted)

Time synchronization is a very critical source of error for strapdown airborne gravimetry. By examining Figure 2.4 it is observed that even a one millisecond

synchronization error could cause up to a 3 mGal error at a 30 second filtering period. It should be noted that the bottom flight line in Figure 2.4 represents a fairly extreme case for the synchronization error modifying factor. Generally, the synchronization error factors vary between ±1000 mGal/s at 30 seconds. Obviously, for filtering periods above the phugoid motion period the time synchronization is not as critical. This can be verified by examining the 90 second modifying factors on the right hand side of Figure 2.4.

The remaining error model terms are due to INS misalignment and DGPS horizontal acceleration errors. The first is specific to the SISG approach, the second to the RISG approach. In Figure 2.5 the north misalignment error and east DGPS acceleration error modifying factors are presented, while Figure 2.6 displays the east misalignment error and the north DGPS acceleration error modifying factors. The misalignment error factors have been divided by 206265 to display them as scaling a misalignment in arcseconds instead of in radians.



(T_c = 30 seconds)                    (T_c = 90 seconds)
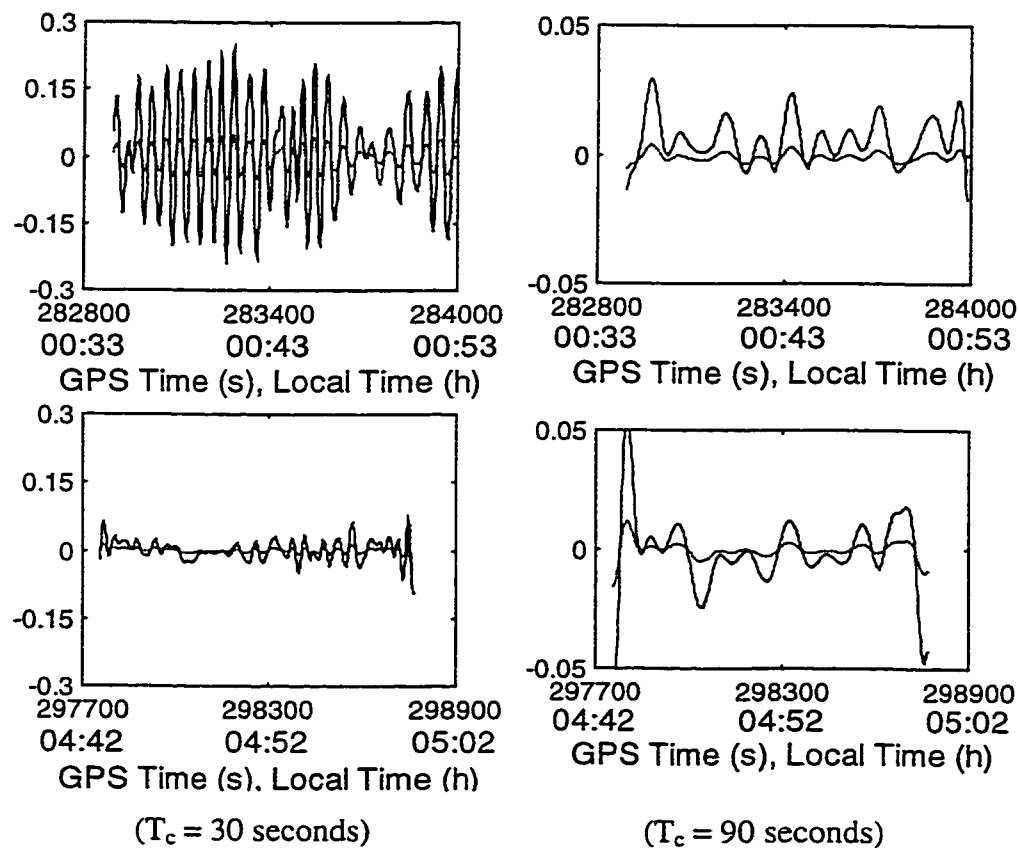
**Figure 2.5:** North Misalignment Factor and East DGPS Acceleration Error Factor, N-S and E-W Flight Lines, (RISG - dotted)
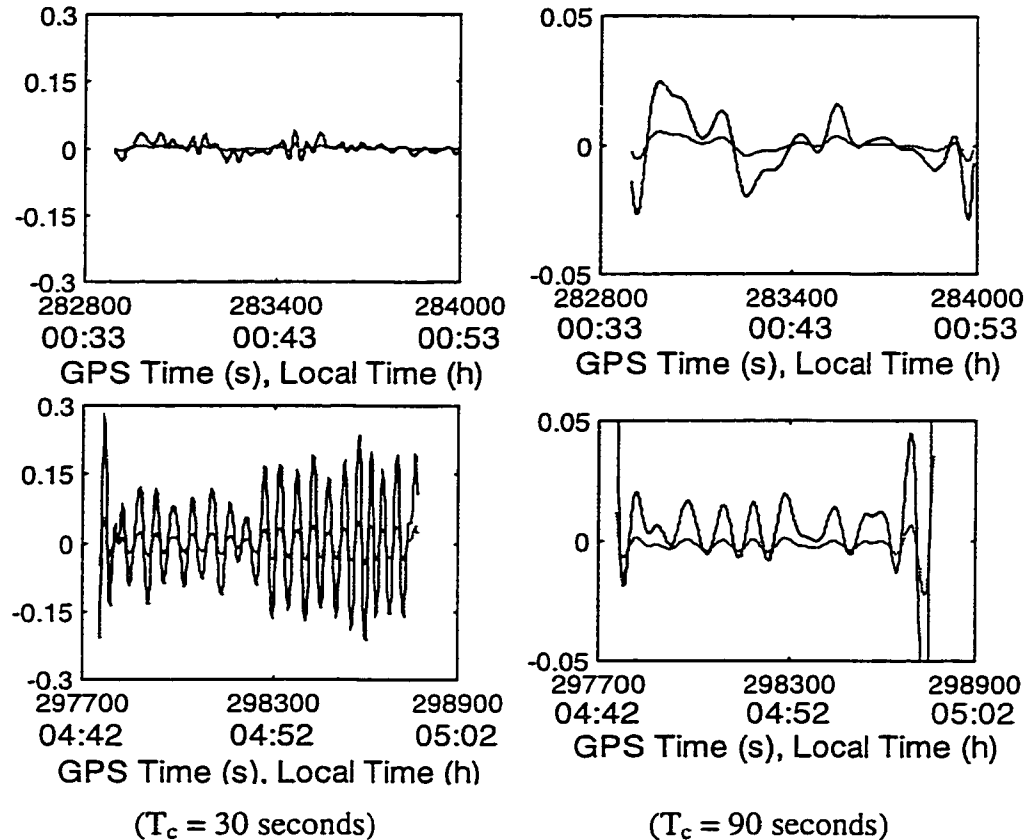
**Figure 2.6:** East Misalignment Factor and North DPGS Acceleration Error Factor, N-S and E-W Flight Lines, (RISG - dotted)

In Figure 2.5 the modifying factors are much larger for the top flight line than the bottom, while in Figure 2.6 the opposite is the case. This is due to the fact that the top flight line is north-south while the bottom is east-west, and therefore, the modifying factors displayed depend upon flight line direction. By examining the figures it is evident that a high degree of correlation exists between the north misalignment and east DGPS error and the east misalignment and north DPGS error. The correlation coefficients for both cases over ten flight lines examined are 0.99. In fact, using the rule-of-thumb that 1" of misalignment corresponds to 5 mGal, and therefore dividing the SISG factors by 5, the SISG and RISG modifying factors in Figures 2.5 and 2.6 are for all practical purposes identical.

However, identical modifying factors does not mean that the errors due to misalignment and DGPS horizontal acceleration error will be the same. Their

contribution will be dependent upon the nature of these error sources themselves. DGPS acceleration errors are presented in section 3.2.2, and are found to be predominantly high frequency in nature. INS attitude errors can be approximated by the formula (Schwarz and Li, 1996):

$$\varepsilon^l = \varepsilon_o^l + \int_{t_1}^{t_2} R_b^l(t) H \omega_{ib}^b(t) dt \tag{2.16}$$

where the first term represents initial misalignment errors, and the second term represents integrated gyro errors. Therefore, the structure of the misalignment errors is quite complicated and consists of a slow varying component (Schuler oscillation of initial misalignment) and a faster changing component that is caused by the interaction of aircraft motion with the gyro errors. These gyro errors include non-orthogonality, scale factors, drift, correlated random errors, quantizer errors and noise. Siouris (1993), Savage (1978) or Li and Schwarz (1994) should be consulted for a more detailed discussion of gyro error sources. Therefore, although the modifying factors are the same it is doubtful that the error terms due to misalignment and horizontal DPGS acceleration errors will be similar. However, a degree of correlation should exist between the two error sources. GPS velocity is used to determine DGPS acceleration and, in addition, GPS velocity updates to the INS Kalman filter provide a mechanism for estimating inertial system misalignment, Škaloud (1995). Thus, errors in DGPS velocity will have an effect on the accuracy of both the INS misalignment estimation and DGPS acceleration.

In order to try to quantify the expected error budget for both the RISG and SISG approach, realistic values for each of the first-order errors in equation (2.8) and (2.10) have been chosen. Accelerometer errors include both the bias and noise of the accelerometer, and therefore a value of 50 mGal has been chosen for all three accelerometer errors ($df_x$, $df_y$, $df_z$). The time synchronization error was chosen as 3 milliseconds. The DGPS acceleration errors were set to 5 mGal at 30 seconds and 1.5 mGal at 90 seconds. Finally, the misalignment errors were given a value of 10 arcseconds. Based on experience, these values would be close to those expected for a

strapdown INS/DGPS airborne gravity system. These error values were used along with the error factors computed in Figures 2.1 to 2.6 to provide an error budget for the RISG and SISG approaches at both 30 and 90 second filtering periods. The error budget is displayed in Table 2.2.

| Error Term | RISG Error Budget (mGal) | | SISG Error Budget (mGal) | |
|---|---|---|---|---|
| | 30 seconds | 90 seconds | 30 seconds | 90 seconds |
| X-accelerometer ($df_x$) | 0.25 | 0.25 | 2.5 | 0.25 |
| Y-accelerometer ($df_y$) | 2.5 | 2.5 | 2.5 | 2.5 |
| Z-accelerometer ($df_z$) | 50 | 50 | 50 | 50 |
| Synchronization (dT) | 4.5 | 0.6 | 4.5 | 0.6 |
| East GPS Accel ($d\dot{v}_e$) | 0.5 | 0.03 | 0.0 | 0.0 |
| North GPS Accel ($d\dot{v}_n$) | 0.5 | 0.03 | 0.0 | 0.0 |
| Up GPS Accel ($d\dot{v}_u$) | 5.0 | 1.5 | 5.0 | 1.5 |
| East Misalignment ($\varepsilon_E$) | 0.0 | 0.0 | 1.5 | 0.2 |
| North Misalignment ($\varepsilon_N$) | 0.0 | 0.0 | 1.5 | 0.2 |
| Total (with Z-accel) | 50.52 | 50.09 | 50.62 | 50.09 |
| Total (without Z-accel) | 7.22 | 2.99 | 7.90 | 3.00 |

**Table 2.2:** Error Budget for the RISG and SISG Approaches to Airborne Gravity

The values in the table should be considered conservative. The magnitudes of the individual errors were chosen conservatively. In addition, the maximum values of the modifying factors in Figures 2.1 to 2.6 were used to calculate the error budget. The total error budget is given both with the z-accelerometer included and neglected. This is due to the fact that the majority of the z-accelerometer error (i.e. > 99.5%) would simply be a bias in the results.

Table 2.2 clearly shows that the performance of RISG is theoretically better than that of the SISG method, especially below the phugoid period. This is promising because the RISG approach is obviously more attractive from an economic standpoint. The SISG method requires an entire strapdown inertial system, while the RISG method only requires a triad of three orthogonal accelerometers, at a fraction of the cost of a strapdown

system. However, previous investigations have clearly shown that results obtained using the SISG method are consistently better than those obtained using the RISG method, see for example Wei and Schwarz (1998) and Schwarz and Glennie (1998). This contradicts the findings discussed above. An explanation for the poorer results using the RISG method may be found in one of the simplifications used in the derivation of the RISG formula. In order to obtain equation (2.5) the deflections of the vertical were neglected, i.e. $\alpha_u$ (l-frame) was assumed to equal $\alpha_h$ (local astronomic frame). However, in actuality, $\alpha_h$ is given by

$$\alpha_h = \begin{bmatrix} \xi & \eta & 1 \end{bmatrix} \cdot \begin{bmatrix} \alpha_e \\ \alpha_n \\ \alpha_u \end{bmatrix}, \qquad (2.17)$$

where $\xi, \eta$ are the deflections of the vertical. Note that a small angle approximation has been assumed in equation (2.17). Typical values for the deflections of the vertical are approximately 10". During a flight line, at a 30 second filtering period, the horizontal accelerations experienced by the aircraft are approximately 0.5 m/s$^2$ and 0.1 m/s$^2$ in the along track and cross track directions respectively. Using these values, an error of 3 mGal in $\alpha_h$ would result due to neglecting the deflections. At a 90 second filtering period the horizontal aircraft accelerations are approximately 0.1 m/s$^2$ in both directions. This translates into introducing a 1 mGal error by ignoring the deflections. These errors are significant and may partially explain the poorer operational results obtained using the RISG method and reported in previous investigations. The tests described in both Wei and Schwarz (1998) and Schwarz and Glennie (1998) were flown in mountainous regions where large deflections of the vertical could be expected.

This detailed examination has shown that there are some small differences between errors in the RISG and SISG approaches. Overall, however, the errors between the two approaches will be quite similar. Therefore, a comparison of the two different solutions will only be a good consistency check on the data processing, while an

averaging of the two solutions will most likely not increase the accuracy of the results. This point will be examined further in section 6.1.

## 2.4 Data Processing Technique

In order to determine gravity disturbances using strapdown INS/DGPS a method of processing the raw INS and DGPS data collected is required. The processing of this data currently occurs in three distinct steps. In the first step the attitude, position and velocity of the airborne gravity system is calculated by integrating the inertial measurements with the DGPS carrier phase and phase rate measurements. The integration is done in the software package KINGSPAD (Kinematic Geodetic System for Position and Attitude Determination). This is an existing software package that was developed at the University of Calgary. KINGSPAD utilizes a decentralized Kalman filter to integrate the INS and DGPS measurements. Through this integrated approach the accelerometer biases and drift rates of the INS can be estimated and corrected for before gravity estimation. The inertial system is also used to detect and correct GPS cycle slips. The attitude of the system is used to transform the specific force estimates from the b-frame to the l-frame for the SISG approach. The algorithm for processing the raw INS data and the error model applied for the INS are well documented and can be found in Wei and Schwarz (1990), Siouris (1993) and Britting (1971), for example. The algorithm applied and the general error model are briefly repeated in the Appendix for completeness.

In the second step, GPS position and velocity information are used to derive an estimate of the aircraft acceleration using the software package GPSACC. This software package utilizes a low-pass differentiating finite impulse response (FIR) filter to determine GPS acceleration. A discussion of various differentiating filters and differentiating techniques for GPS acceleration determination can be found in Bruton et al. (1999). The GPS position and velocity is also used to estimate the Coriolis acceleration correction, which is given by the second term on the right hand side of equation (2.4). Additionally, since the origin of the INS and GPS measurements cannot

physically be located at the same point, a difference in acceleration due to this lever-arm offset must be calculated. The lever-arm velocity difference between the INS and GPS measurement origins is given in Knickmeyer (1990) as

$$v_{INS}^l - v_{GPS}^l = \Omega_{be}^l R_b^l l^b \qquad (2.18)$$

where

$\Omega_{be}^l$      is a skew-symmetric matrix of the angular velocity between the b-frame and the e-frame given in the l-frame,

$R_b^l$      is a rotation matrix from the b-frame to the l-frame, and

$l^b$      is the position difference between the INS and GPS measurement origins in the INS b-frame.

During installation of the INS/DGPS system into the aircraft a total station is used to measure the $l^b$ vector. The lever-arm velocity difference is computed and output by KINGSPAD. A differentiating FIR filter is then used to compute a lever-arm acceleration correction.

Finally, in the third step, an estimate of the gravity disturbance is obtained by differencing the INS specific force measurements and the GPS accelerations, and applying the corrections due to Coriolis and lever-arm offset acceleration. This is accomplished using the software package SIGD (Strapdown Inertial Gravity Determination). The package SIGD can output gravity disturbance estimates using either the RISG or SISG approaches according to equations (2.5) and (2.2), respectively. To reduce measurement noise the resulting gravity disturbances are then low-pass filtered to the desired cut-off frequency using a finite impulse response (FIR) filter. A summary of the data processing procedure to determine gravity disturbances at flight level from the raw INS and DGPS measurements is given in Figure 2.7.
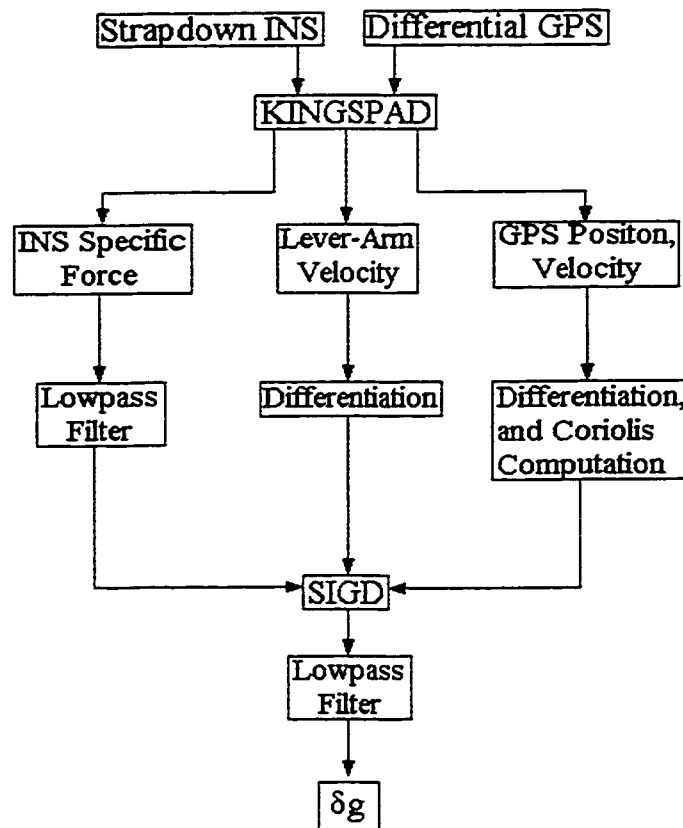
**Figure 2.7:** Data Flow for Gravity Disturbance Determination

The choice of a cut-off frequency for the final FIR filtering of the airborne gravity disturbance estimates is not a trivial one. Several factors must be considered such as: flight height, atmospheric turbulence, expected gravity field variation, the type of inertial system used, and the quality of the DGPS accelerations. The optimal filtering period is a tradeoff between the removal of measurement noise and an over-smoothing of the estimates, and therefore, will vary between airborne gravity flights (see section 5.3).

Figure 2.8 is presented in order to give an idea of the typical filtering periods used with a strapdown INS/DGPS airborne gravity system. The figure shows the spectrum of gravity disturbances at flight level along with the INS/DGPS system disturbance estimation residuals for two flight tests undertaken in September of 1996 (see section 3.3).
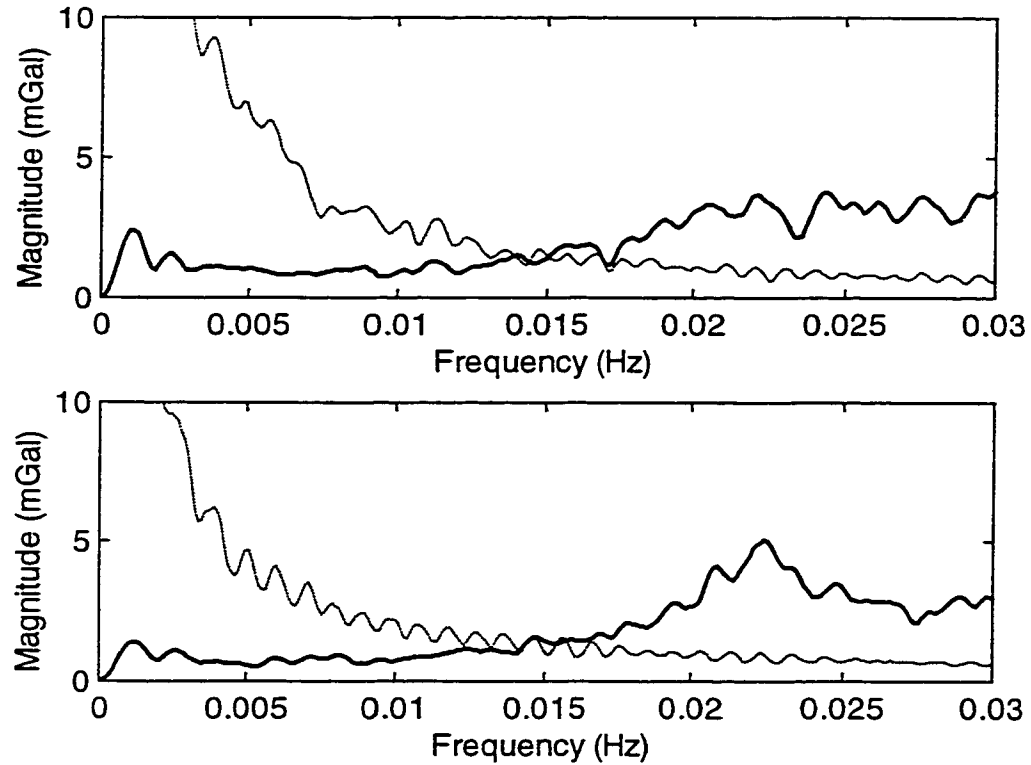
**Figure 2.8:** Spectrum of Gravity Disturbances at Flight Level (Dotted) and Airborne Strapdown INS/DGPS Disturbance Estimation Residuals (Solid), for Two Flight Tests

Figure 2.8 shows that for the two flight tests of the strapdown INS/DGPS system the signal to noise ratio drops below one at a frequency of approximately 0.015 Hz (67 second period). However, the signal to noise ratio is very close to one between approximately 0.01 and 0.02 Hz. For the purposes of this dissertation cut-off frequencies in and around this frequency band have been selected. The cut-off frequencies that will be used are 0.0333, 0.01667, 0.01111 and 0.008333 Hz, which correspond to the 1/e response times of 30, 60, 90, and 120 seconds respectively.

# CHAPTER 3

## Prototype System and Flight Test Description

In this chapter the hardware configuration of the prototype strapdown airborne gravity system developed at the University of Calgary is introduced and described. An indication of expected performance accuracy for both the DGPS and INS sub-systems is given. Expected INS acceleration errors are given by analyzing a static data set for the INS. The DGPS sub-system errors are quantified by examining acceleration differences between different master-remote receiver combinations from a flight test. A detailed description of the flight tests carried out in September 1996 and June 1998 is presented. The June 1998 test was flown alongside a modified LaCoste and Romberg (LCR) air/sea gravimeter. Therefore, the principle of operation of the LCR, along with current performance results are also presented.

## 3.1 Prototype System Hardware Description

The hardware used to determine gravity disturbances by strapdown INS/DGPS has three main components: a strapdown INS, GPS master and remote stations, and a data acquisition system. The prototype system developed at the University of Calgary utilizes a Honeywell LASEREF III (LRF III) navigation grade strapdown inertial system. The Honeywell system contains QA 2000 accelerometers and GG1342 ring laser gyroscopes. In addition to the Honeywell INS, which should be considered the current operational system (and will be referred to as the prototype system hereafter), a flight test has also been conducted with the Litton 101 Flagship, which is another navigation grade strapdown inertial system. The Litton 101 (LTN-101) contains undithered zero-lock ring laser gyroscopes, and A4 force rebalance accelerometers, both developed by Litton. Typical sensor performance specifications of navigation grade strapdown inertial navigation systems are given in Table 3.1.

| PERFORMANCE PARAMETER | CLASS II 1.0 nmi./h |
|---|---|
| Gyro Bias Uncertainty (deg/h) | 0.003 |
| Gyro Random Noise (deg/$\sqrt{h}$ ) | 0.001 |
| Gyro Scale-Factor Uncertainty (ppm) | 1.0 |
| Accelerometer Bias Uncertainty (mg) | 10-25 |
| Accelerometer Scale-Factor Uncertainty (ppm) | 25-50 |
| Accelerometer Alignment Uncertainty (sec) | 5 |
| $\sigma_{position}$ | 0.5 m with ZUPTs every 3 minutes |
| $\sigma_{accel}$ | • net bias < 50 mGal<br>• short term bias < 3 mGal |

**Table 3.1:** Sensor Performance for Navigation Grade Strapdown Inertial Systems

Various types of GPS receivers have been used with the prototype airborne gravity system. The major requirements for GPS receivers are low noise and high reliability. In order to increase the reliability of the system multiple reference stations are used on the ground in the flight area, and at least two receivers are located on the airplane. The receiver should have the ability to output a PPS (pulse-per-second) to be used in synchronizing the INS and GPS data streams to a common time basis (GPS time). In Wei and Schwarz (1998) a higher GPS data rate (10 Hertz) did not significantly improve gravity estimation results, and therefore the ability of the receiver to output at a 1 or 2 Hertz data rate is currently sufficient. Dual frequency observations are not a requirement, as the long-term effect of the ionosphere causes negligible errors in GPS determined accelerations. In addition, the amplification of noise caused by the dual frequency ionosphere-free or wide-lane observables is undesirable for precise acceleration determination. In previous tests, the types of GPS receivers utilized include Trimble 4000 SSE and SSI, Ashtech Z-12, and NovAtel GPSCard. No significant difference in performance has been observed for these different receivers.

The data acquisition system in the plane consists of a PC with data logging software developed at the University of Calgary to collect and synchronize INS and GPS data. The PC is able to collect the 50 Hertz raw inertial data, the GPS phase and phase rate measurements, and the PPS output which is used to reset the computer clock to synchronize the INS and GPS time frames. The inertial data is collected through a special

high speed ARINC interface board installed in the computer. The GPS and PPS data are collected into the PC using the existing computer serial ports.

### 3.1.1 Advantages of Strapdown INS/DPGS Combination

There are several advantages to using a strapdown INS/DGPS system as opposed to other methods of airborne gravity determination, e.g. a modified Lacoste and Romberg (LCR) air/sea gravimeter. Firstly, the strapdown INS can be purchased as an off-the-shelf unit and does not require expensive modifications for airborne gravity field determination. Secondly, the strapdown INS/DGPS combination is not restricted to gravity disturbance estimation. It can be used for any application that requires position and attitude of a moving platform, for example, photogrammetry without ground control; see Škaloud (1995) and (1999). Additionally, in general, the strapdown INS/DGPS combination has the advantage of smaller size, lower power requirements, increased reliability, and perhaps most importantly, a significantly lower cost. Typically, a high accuracy navigation grade strapdown INS costs approximately $150K U.S., whereas a LCR gravimeter may exceed $500K U.S. with the required modifications for airborne gravimetry.

## 3.2 Estimated Sensor Performance

### 3.2.1 Accelerometer Noise

An examination of equations (2.8) and (2.10) shows that the vertical accelerometer error will directly affect the accuracy of the estimated gravity disturbances. Therefore, in an effort to determine the resolution of the vertical accelerometers of the two tested strapdown inertial systems, a static data set was examined for each system. The results from these static lab tests represent the noise levels of the two systems under ideal conditions. The raw vertical accelerometer measurements were low pass filtered to typical airborne gravity cut-off filter periods of 30, 60, 90, and 120 seconds. The RMS

values of the vertical accelerometer residuals, after removal of a linear bias, at the four filtering periods ($T_c$) are given in Table 3.2.

| INS | 30 sec | 60 sec | 90 sec | 120 sec |
|-----|--------|--------|--------|---------|
| LRF III | 1.9 | 1.6 | 1.5 | 1.4 |
| LTN101 | 4.3 | 3.1 | 2.6 | 2.2 |

**Table 3.2**: RMS of Z-Accelerometer Noise in Static Tests,
Linear Bias Removed (mGal)

The results for the QA 2000 accelerometers in the LRF III are considerably better than those for the A4 accelerometers in the LTN 101. This is not necessarily a reflection of the inherent sensor accuracy, the differences may be due to a better solution of the quantization problem for the QA 2000 accelerometers.

Ideally, the error spectra of the accelerometers should resemble white noise. Figures 3.1 and 3.2 give the error spectra of the INS accelerometers. There are several spikes that appear in the spectra. Particularly troublesome are the very low frequency spikes that appear for both the LRF III and the LTN-101. An examination of several static data sets has confirmed that the error spectrums shown in Figures 3.1 and 3.2 seem to be consistent for both systems.
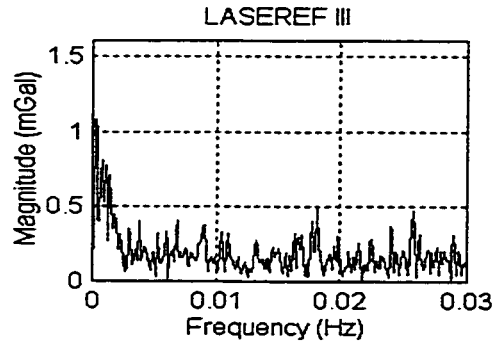


**Figure 3.1**: LRF III Z-Accel Residual Spectrum,
Linear Bias Removed ($T_c$ = 30 sec)

LITTON 101
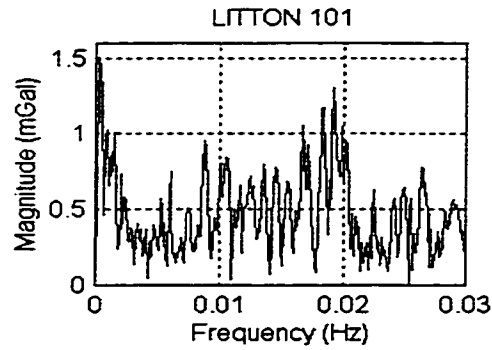


**Figure 3.2**: LTN-101 Z-Accel Residual Spectrum,
Linear Bias Removed ($T_c$ = 30 sec)

### 3.2.2 GPS Acceleration Errors

The errors in GPS determined vertical acceleration will have a direct effect on the
accuracy of the gravity disturbance estimates determined using the SISG and RISG
approaches. This can be verified by examining equations (2.8) and (2.10). To assess the
errors in GPS vertical acceleration two different master-remote DGPS pairs from a flight
test were used to determine accelerations, and the results were compared. The RMS
values of the differences are given in Table 3.3, and a spectrum of the residual differences
is given in Figure 3.3.

| $T_c$ | 30 sec | 60 sec | 90 sec | 120 sec |
|---|---|---|---|---|
| RMS diff | 7.1 | 2.3 | 1.1 | 0.7 |

**Table 3.3**: RMS Acceleration Differences (mGal), Different Master-Remote DGPS Pairs
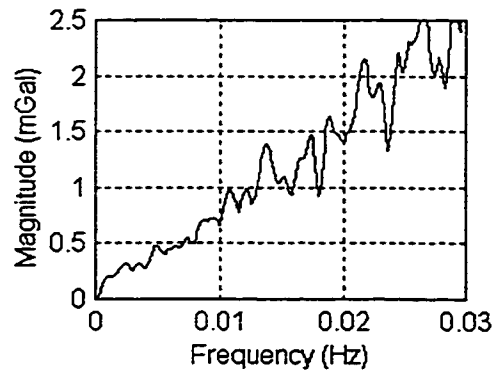


**Figure 3.3**: Spectrum of Acceleration Differences,
Different Master-Remote Receiver Pairs ($T_c$ = 30 sec)

It should be noted that the numbers given might be considered as optimistic for the GPS acceleration error budget because common mode errors will exist for the two acceleration determinations. This is due to the fact that the remote receivers in the airplane were on a zero baseline and would therefore have the same errors due to multipath and atmospheric effects. However, the accuracy of GPS acceleration estimation presented in other analyses that made use of a precise independent reference for the determination of GPS acceleration errors seem to be fairly consistent with the results reported here. In Zhang and Schwarz (1996) an Anorad precision motion table was used to examine multipath errors, and in Wei and Schwarz (1995) the vertical DGPS acceleration was compared to that derived from a Laser Range Finder. These previous analyses have also shown that multipath errors at the remote antenna are high frequency in nature (due to aircraft motion) and generally of smaller magnitude than the measurement noise, and that atmospheric errors generally contribute less than 0.1 mGal of error. Therefore, the numbers given can be considered representative of the GPS acceleration error budget despite the existence of common mode errors due to the zero baseline on the aircraft. For additional analyses of DGPS acceleration accuracy, the interested reader is referred to Jekeli and Garcia (1997), Brozena et al. (1989) and Van Dierendonck et al. (1994).

### 3.3 September 1996 Flight Test

3.3.1 Test Purpose

A first test of the prototype system discussed in section 3.1 and 3.2 was performed in June 1995 by the University of Calgary. The test was designed to analyze the short-term accuracy and repeatability of gravity disturbance determination by the strapdown INS/DGPS system. Test results showed that the short-term accuracy and repeatability was at the level of 2 to 4 mGal. For a more in-depth analysis of the June 1995 flight test refer to Wei and Schwarz (1998). Based on these promising results a more extensive test

of the concept was flown in September 1996. The test was used to obtain a data set which covered a 100 km by 100 km area to assess the long term accuracy and repeatability of the system, to evaluate the performance of different strapdown inertial systems, and to explore the possibilities for geoid and vertical gradient of gravity determination.

## 3.3.2 Test Description

The following test description closely mirrors that which was given in Glennie and Schwarz (1997) and (1999). For the September 1996 test, two different navigation grade strapdown inertial systems were used: the Honeywell LASEREF III, and the Litton 101 Flagship. Two GPS receivers are required as a minimum (one on the airplane and one on a known ground station) to use DGPS to determine vehicle position, velocity and acceleration. To increase reliability the airplane, a Cessna Conquest, was equipped with two receivers on a zero baseline: an Ashtech Z-12 and a Trimble 4000SSI. Four ground stations were also set up in the flight area using an Ashtech Z-12, a Trimble 4000SSI, a Trimble 4000SSE, and a NovAtel GPSCard.

Airborne testing of the above hardware was carried out on September 9, 10 and 11 of 1996 in Alberta, Canada, over the Rocky Mountains. This area was chosen because of the high variability of the gravity field, and the availability of dense ground gravity values to determine an upward continued reference for the flights (see section 3.4). Figures 3.4 and 3.5 show contour plots of the topography in the flight area and the gravity disturbances upward continued to 4350 metres, respectively. The height of terrain in the area varied from 800 metres to 3600 metres. Statistics for the upward continued gravity disturbances at the two flight heights used in the September 1996 test are given in Table 3.4.
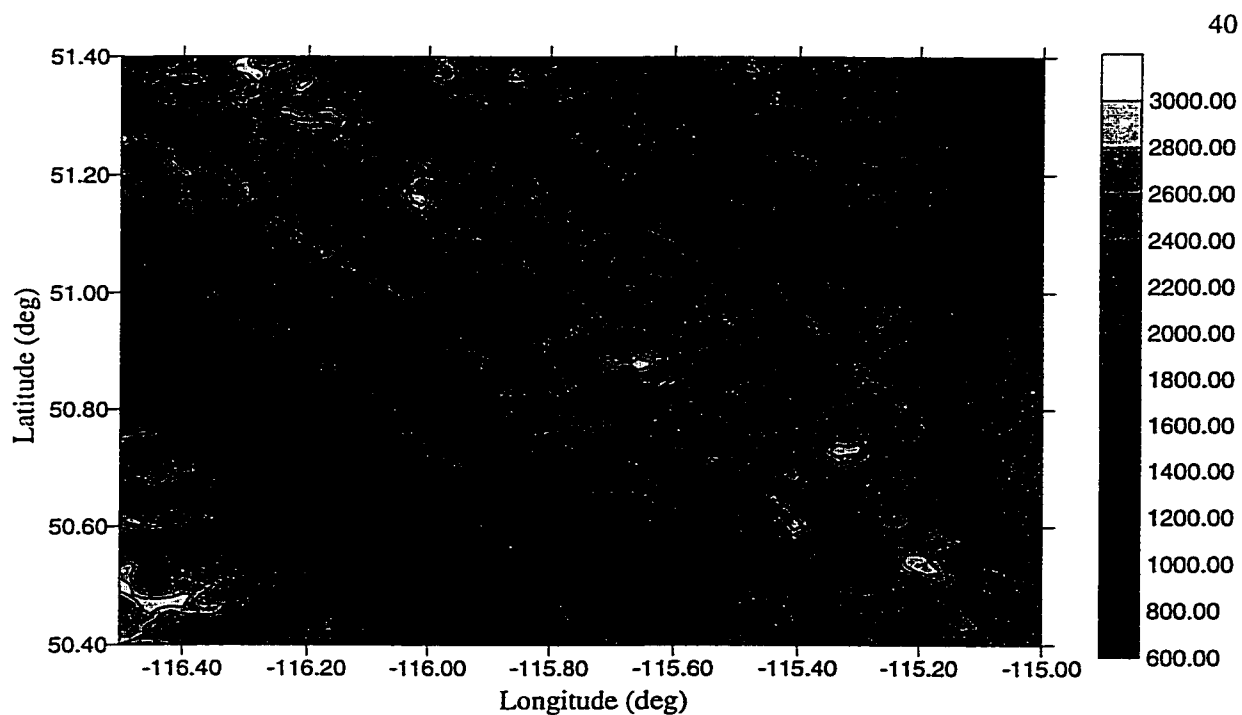
**Figure 3.4:** Topography in Area of September Flight Test (heights in metres)
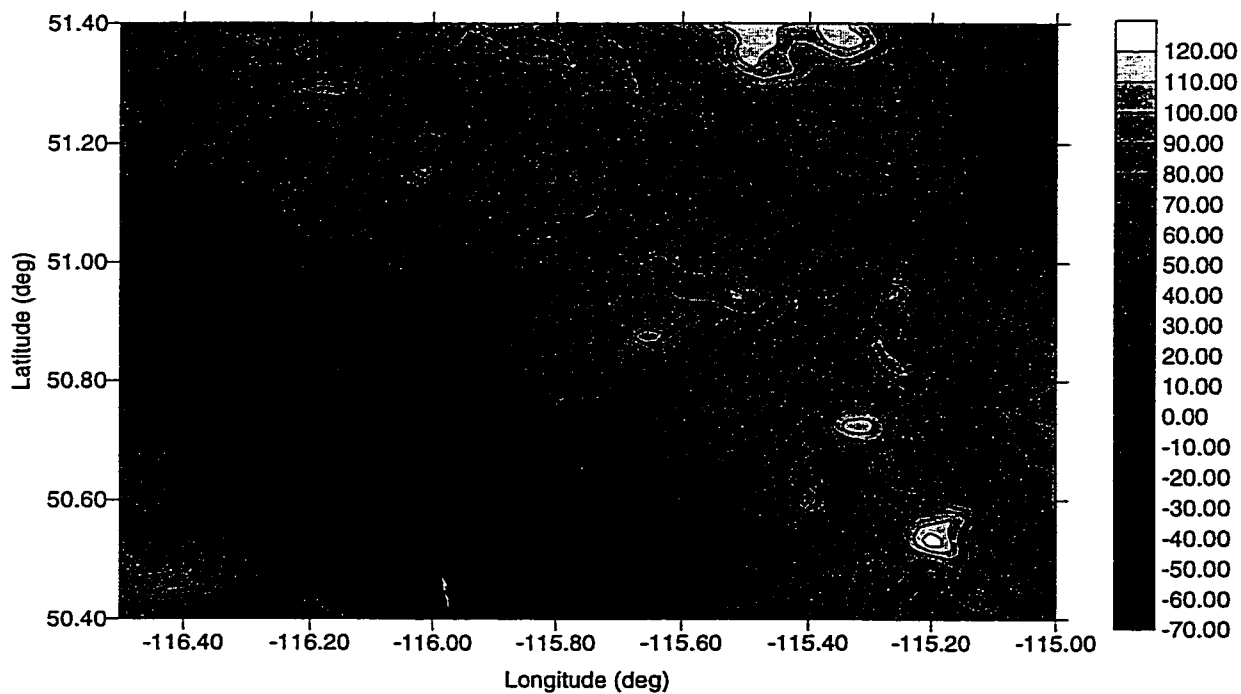


**Figure 3.5:** Gravity Disturbances (in mGal) in Flight Area at h = 4350 metres

| Height (m) | Average | $\sigma$ | Max. | Min |
|---|---|---|---|---|
| 4350 | 37.0 | 39.3 | 126.4 | -62.7 |
| 7300 | 35.5 | 33.5 | 102.0 | -43.1 |

**Table 3.4:**Statistics of Upward Continued Gravity Disturbances (mGal)
September 1996 Test

It should be noted that the flight area represents an extreme case with respect to gravity field variations, and this should be taken into account when comparing results of this test to results achieved in areas with less gravity variation.

The first flight (Day 1) was flown at an average height of 4350 metres in east-west direction, the second (Day 2) at the same height in north-south direction, and the last (Day 3) at an average height of 7300 metres, again in east-west direction. All flights covered the same 100 km by 100 km area. The first two days of testing were used to examine the effect of flight direction on the determination of gravity disturbances, and to provide a grid of disturbances for investigations into airborne geoid determination. The third flight at a higher altitude was performed to assess the system's ability to determine the vertical gradients of gravity by combining results from Day 1 and Day 3 and to explore the effect of flight height on the accuracy of disturbance determination. All flights were done at night between 12 am and 6 am local time to minimize the effect of air turbulence. Average flight velocity for all three tests was 360 km/h. GPS master stations were located at the Calgary Airport (NovAtel GPSCard), Banff (Trimble 4000SSI, Ashtech Z-12), and Invermere (Trimble 4000SSE). More than one base station was deployed to provide redundancy and to explore the possibility of using multiple base stations for gravity disturbance estimation. Figure 3.6 shows the flight pattern for Days 1 and 3 along with the location of the master stations. Figure 3.7 shows the flight pattern for Day 2. The last two flight lines for each day which run perpendicular to the first eleven flight lines were flown to be used as a possible method to correct for the expected linear drift of the system gravity disturbance estimates. Note that the word drift is used to characterize a linear time dependence of the results, but does not necessarily mean that the effect is a system error.
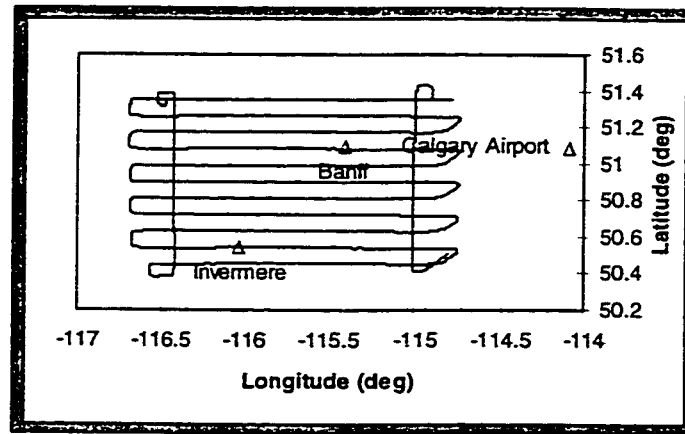
**Figure 3.6:** Flight Pattern, Days 1 and 3
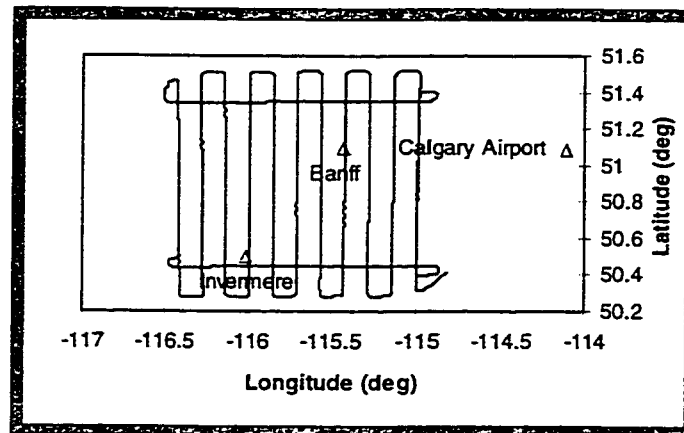


**Figure 3.7:** Flight Pattern, Day 2

### 3.3.3 Upward Continued Reference

The area of the September 1996 flight test was chosen primarily because it was well covered by ground gravity values and a detailed DEM, thus allowing the computation of an accurate upward continued reference for the flight lines. Details concerning the method of computation used for upward continuation can be found in Argeseanu (1995). Figure 3.8 shows the locations of the ground gravity measurements used in the computations. The test area covered by the flights has been shaded.
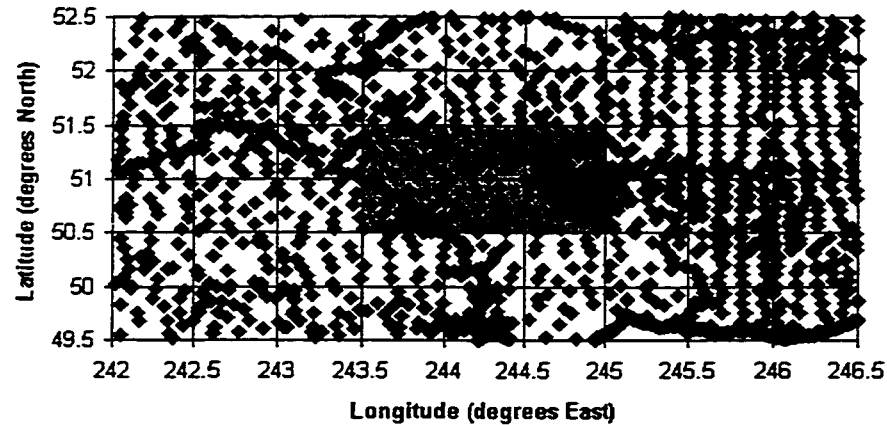
**Figure 3.8:** Location of Ground Gravity Measurements used in Reference Computation (Shaded Region is Airborne Test Location)

There were 1912 gravity measurements used in the upward continuation with an average spacing of 8 km. In addition, point elevations on a 1 km by 1 km grid were also available for the entire area. For a small portion of the flight area (bottom right of the shaded region) the point gravity anomalies have an average spacing of 3 km, and a 100 m by 100 m DEM was available. A Poisson integral approach was used to do the upward continuation. Considering the data used, and the uncertainties in the global geopotential model, the accuracy of the upward continued reference is likely not better than 2 mGal for the whole area, and 1.5 mGal for the more densely covered area, Schwarz and Glennie (1998).

## 3.4 June 1998 Flight Test Description

The University of Calgary, in cooperation with the Danish National Survey and Cadastre (KMS), undertook an airborne gravity test on June 6, 8, and 9 of 1998 in the Disko Bay area off the west coast of Greenland. The major purpose of this flight test was a comparison of existing airborne gravity measurement systems. The area where the flights took place is shown inside the black box in Figure 3.9.
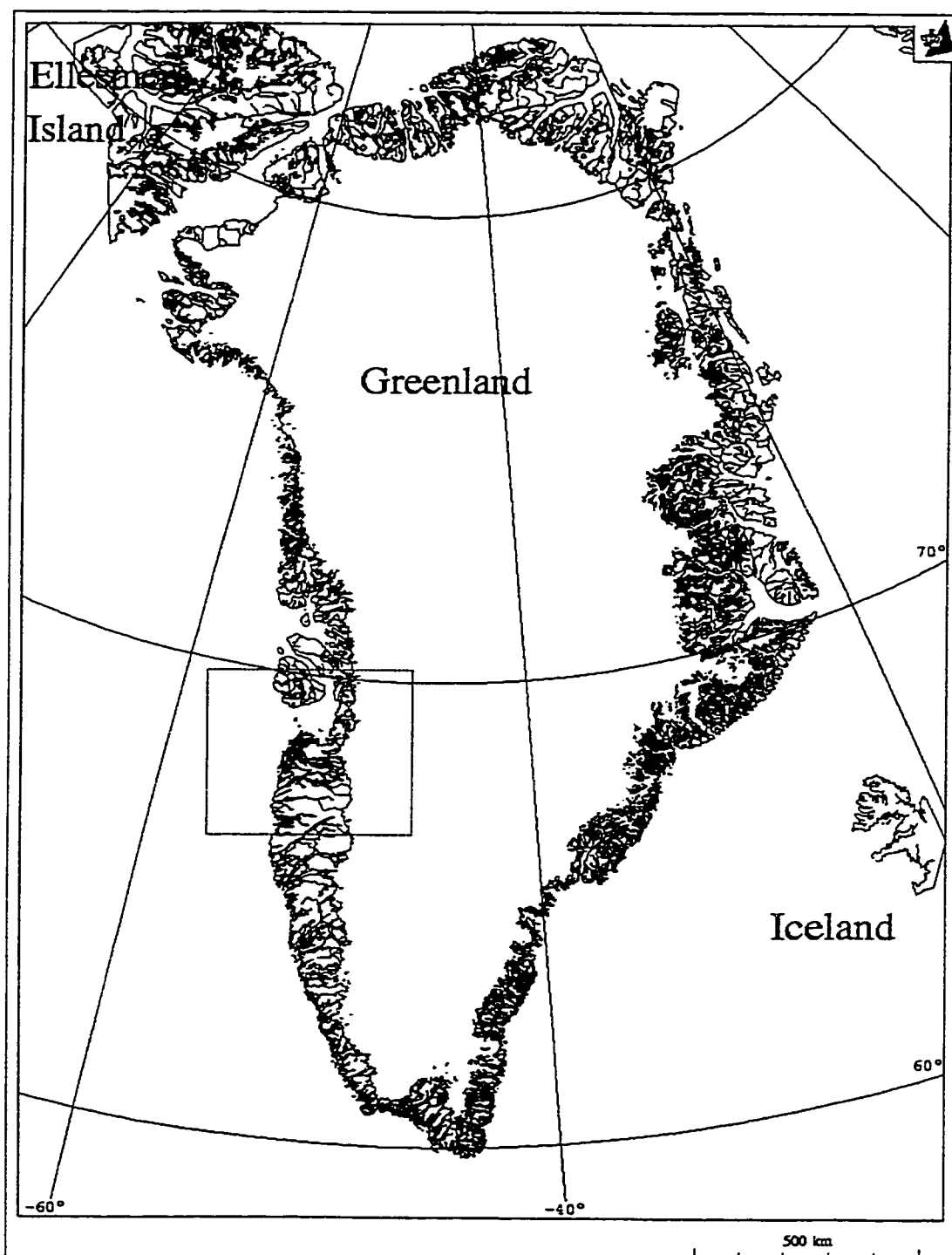
**Figure 3.9**: Greenland, Flight Test Area (Fig 3.10) is shown Enclosed in Black Box

For the June 1998 test three airborne gravity systems were flown: the Honeywell
Laseref III strapdown INS/DGPS system, a LaCoste and Romberg (LCR) modified 'S'

type air/sea gravimeter, and an orthogonal triad of QA 3000 Q-Flex accelerometers. The LCR gravimeter is owned by the University of Bergen, Norway, and previously had been successfully flown in campaigns for the AGMASCO (Airborne Geoid Mapping System for Coastal Oceanography) project. For details on the AGMASCO project see Hehl et al. (1997) and Bastos et al. (1998). The Q-Flex triad was developed by Dr. G. Boedecker at the Bavarian Academy of Sciences, Munich, in cooperation with the AGMASCO project. For information on the QA-3000 accelerometers, see Foote and Grindeland (1992).

The three independent systems were mounted in a Twin Otter airplane. Two dual frequency GPS antennae were mounted on the fuselage of the aircraft. The front antenna was attached to a Trimble 4000 SSI receiver, while the rear antenna signal was split between another Trimble 4000 SSI and an Ashtech Z-XII receiver. The Ashtech receiver was required to provide time synchronization for the strapdown INS system. Three days of testing were undertaken. The flight patterns for the three days are shown in Figure 3.10.



**Figure 3.10:** Flight Lines and Master Station Locations (*), June 1998

For the first flight (June 6th) master GPS stations were located at Kangerlussuaq and Ilulisat (see Figure 3.10). Data for the Q-Flex unit was not collected on the first day. For June 8th and 9th, master GPS stations were located at Kangerlussuaq, Ilulisat and Aasiaat. The master stations at Kangerlussuaq and Aasiaat were equipped with Trimble 4000 SSI receivers while the Ilulisat site was occupied with an Ashtech Z-Surveyor receiver. All flights were performed during the afternoon (local time) over the ocean. Average flight heights were approximately 300 metres, with an average flight velocity of approximately 70 m/s. To provide an independent reference, four flight lines were flown over top of existing shipborne gravity data profiles, one on June 6, one on June 8, and two on June 9. The accuracy of the ship data is expected to be approximately 1 mGal or better (Rene Forsberg, pers. comm.).

## 3.5 Comparison of the LCR Gravimeter with the Strapdown INS System

The following overview of the airborne gravity measurement method of the modified LaCoste and Romberg (LCR) air/sea gravimeter focuses on those aspects that are important when comparing it to a SISG or RISG system. For a more detailed description of the LCR gravimeter the reader is referred to Valliant (1992) or LaCoste and Romberg (1998).

The modified LCR air/sea gravimeter is a highly damped spring gravity sensor mounted on a two-axes stabilized platform. The major difference between the use of this platform system and the strapdown algorithm discussed in Chapter 2 is the maintenance of a direction in space (i.e. orientation). For the strapdown system the relationship between the b-frame and the l-frame is computed by numerically integrating the output of the gyroscopes. For a platform system, alignment with the l-frame is realized mechanically by using the output of horizontal accelerometers and gyroscopes in a feedback loop. The feedback loop normally has a user selectable damping period of 4 to 18 minutes, Valliant (1992). In general, the longer the damping period, the greater the reduction in error due to horizontal accelerations.

In addition to having entirely different methods of orientation control, the prototype strapdown INS system and the LCR gravimeter also use significantly different methods of vertical acceleration determination. The Honeywell Laseref III strapdown INS contains QA 2000 accelerometers. These accelerometers measure acceleration using quartz flexure suspension technology. Essentially, acceleration is measured by the displacement of a proof mass that is pendulously supported with only one degree of freedom. The acceleration sensed is proportional to the restoring force required to keep the proof mass in the null position. More details on the principle behind the QA accelerometer can be found in Foote and Grindeland (1992).

The vertical acceleration sensed by the LCR gravimeter is based upon the zero-length spring principle. The general principle is displayed in Figure 3.11.
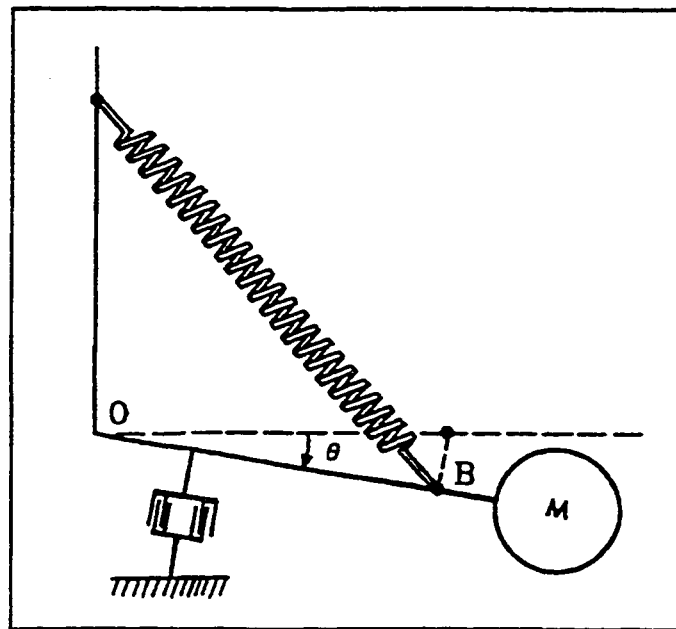


**Figure 3.11:** Zero-Length Spring System, after Valliant (1992)

The beam of the system is overdamped, and acceleration is determined by a combination of spring tension S, and beam velocity $v_b$, using the equation (Olesen et al., 1997):

$$f_u = S + Kv_b \tag{3.1}$$

where K is a scale factor which is determined by laboratory calibration. The beam is kept roughly at the center of its dynamic range (null position) by adjustment of the spring tension. The spring tension can be automatically adjusted or manually set by the user. More details on the zero-length spring gravimeter can be found in Valliant (1992) or LaCoste (1988).

In principle, equation (2.2) for the SISG determination of gravity disturbances applies to the LCR meter as well. However, differences arise in the gravity disturbance estimation due to differences in the nature of attitude control and measurement of vertical acceleration. The formula to determine gravity disturbances by the LCR gravimeter is given as:

$$\delta g = f_u - \dot{v}_u + \left( \frac{v_e}{R_n + h} + 2\omega_e \cos\varphi \right) v_e + \frac{v_n^2}{R_m + h} - \gamma + c_{cc} + c_{tilt} \qquad (3.2)$$

where,

$c_{cc}$ \qquad is the cross-coupling correction and corrections due to beam position, and

$c_{tilt}$ \qquad is a correction due to platform misalignment.

All other terms in equation (3.1) have been previously defined (see section 2.1.1). The cross-coupling errors of the LCR meter arise due to the method of vertical acceleration measurement employed. Essentially, the horizontal accelerations experienced by the platform cross-couple into the vertical acceleration output whenever the vertical accelerometer beam is not in the null position. The formula for the cross-coupling correction is given in Valliant (1992) as:

$$c_{cc} = a_1 v_b^2 + a_2 (f_y p_b) + a_3 (f_x v_b) + a_4 (f_y v_b) + a_5 (f_x^2 v_b), \qquad (3.3)$$

where,

$a_1, a_2 \cdots a_5$ \qquad are statistically or empirically determined coefficients,

$v_b$ \qquad is the beam velocity,

$p_b$         is the beam position, and

$f_x$, $f_y$       are the cross-track and longitudinal accelerometer measurements.

The general method used to determine the coefficients is described in Valliant (1992). Typical values for the cross-coupling correction, after low-pass filtering (normally to $T_c = 200$ s), are 1 to 5 mGal, although it can be as high as 25 mGal in higher dynamics (Arne Olesen, pers. comm.).

The tilt correction is necessary due to the method of platform stabilization. As a result of the damped horizontal feedback applied in the LCR meter the platform may become significantly off-level, especially right after turns (i.e. periods of higher horizontal accelerations). This misalignment can be estimated by comparing the horizontal accelerometer output to DGPS determined horizontal accelerations using the formula (Olesen et al., 1997):

$$c_{tilt} = \frac{f_x^2 + f_y^2 - \alpha_e^2 - \alpha_n^2}{2g}, \tag{3.4}$$

where all terms have been previously defined.

In order to compare the error sources for the LCR gravimeter and strapdown inertial gravimetry a first order error linearization of equation (3.2) is performed, giving:

$$
\begin{aligned}
d\delta g = df_u - d\dot{v}_u + \frac{f_x}{g}df_x + \frac{f_y}{g}df_y - \frac{\alpha_e}{g}d\alpha_e - \frac{\alpha_n}{g}d\alpha_n + \\
\left(a_3 v_b + 2a_5 f_x v_b\right)df_x + \left(a_2 p_b + a_4 v_b\right)df_y + \\
\left(2a_1 v_b + a_3 f_x + a_4 f_y + a_5 f_x^2\right)dv_b + \left(a_2 f_y\right)dp_b - \\
v_b^2 da_1 + f_y p_b da_2 + f_x v_b da_3 + f_y v_b da_4 + f_x^2 v_b da_5
\end{aligned}
\tag{3.5}
$$

where

$da_1$, $da_2 \cdots da_5$   are errors in the coefficients,

$dv_b$           is the beam velocity error, and

$dp_b$           is the beam position error.

All other terms have been previously defined. Assuming DGPS position and velocity information, the errors in Eötvös and normal gravity computations will be negligible Schwarz and Wei (1994), and therefore, these errors have been omitted from equation (3.5). By examining equation (3.5) it is immediately evident that the errors in the first line of the error model are very similar to those of the RISG method (equation 2.10). It is important to note that the horizontal accelerometers of the platform system are of lower quality than the vertical one, and therefore, horizontal accelerometer errors are a significant source of gravity disturbance error for the LCR system. In examining the other errors in equation (3.5), it is difficult to relate them to either the RISG or SISG approach to strapdown airborne gravity. Of the remaining terms in equation (3.5) the most significant appear to be due to errors in beam velocity and errors in determining the cross coupling coefficients. Unfortunately, the author was unable to locate any sources of information that gave expected errors for the beam velocity or cross-coupling coefficient determination. It should also be noted that a time synchronization error has not been included in equation (3.5). In principle, the term due to time synchronization error should be identical between the SISG approach and the LCR gravimeter. However, the actual synchronization error (i.e. value of dT) would be system dependent.

The strapdown INS system and the LCR gravimeter system have significant differences in orientation maintenance and acceleration measurement techniques. These differences are made evident by trying to relate the error models of the two approaches. Therefore, a flight test with the two systems operating side-by-side allows a unique opportunity to compare the two methods for consistency, and additionally to try to detect and eliminate design specific errors in each system. The June 1998 test represents the first time that these two systems have been flown side-by-side for comparison purposes.

### 3.5.1 Operational Results with LCR Gravimeter

It is difficult to quantify the error budget for gravity disturbance estimation using any airborne gravity system. This is mainly due to the fact that the accuracy of the

disturbance estimates is not just function of the gravity sensor used. It also depends on such factors as the flight conditions under which the disturbances were estimated (specifically aircraft flight height and speed), the method of filtering used, and the source of estimated vehicle acceleration. Therefore, rather than trying to quantify the estimation accuracy with the LCR gravimeter, flight test results reported in other sources will be given (along with the information source).

The first operational airborne gravity results using an LCR gravimeter were realized by the Naval Research Laboratory (NRL) for the Greenland Aerogeophysics Project (GAP). This project was the first successful gravity survey of continental extent, see Brozena (1992) for a project description. A large stable military aircraft (P-3 Orion) was flown at flight speeds between 370 and 450 km/h at a flight height of approximately 4 km. DGPS was used for acceleration determination. Low-pass filtering of the data using 2 to 3 minute averaging times yielded an RMS accuracy of 3-5 mGal by comparison at crossover points, and 5 mGal when compared with sparse upward continued surface data. For more details see Brozena and Peters (1994) and Forsberg and Kenyon (1994). More recent flights performed by the NRL in Artic survey campaigns (carried out from 1992 to the present) have shown improved results over those reported for the GAP project. The improvements are due to a number of factors: full GPS constellation, improved GPS receivers, shorter DGPS baselines, better operational procedures, and improvements in data processing and filtering methods. In general, the Artic missions have given internal consistancy estimates (crossover point analysis) in the 2 to 3 mGal range, Brozena et al. (1997). In the 1996 Arctic survey a limited area was flown which contained regular high-quality surface gravity measurements made on the ice. The NRL airborne estimates agreed with these surface measurements at approximately the 2 mGal RMS level, Childers et al. (1997). The flight parameters for the Arctic surveys are similar to those given for the GAP project above.

In addition to the large regional surveys reported above the NRL also performed a test in March 1997 that attempted to improve the resolution and accuracy of the gravity estimates from their LCR system. The March 1997 test flight was performed off the coast of San Diego in conjunction with the US Navy's Ocean Survey Program. These flights

were carried out using the Orion P-3 aircraft and were flown at approximately 300 km/h at a height of 300 m above the ocean. Lines were flown repeatedly over top of existing shipboard gravity measurements. Preliminary analysis of the data, given in Childers et al. (1997), has shown that a comparison of the multiply flown lines with the average value along track has given an RMS agreement at the level of 1.3 to 2.0 mGal.

The Geodynamics and Geodesy Laboratory of the Institute of Geodesy and Photogrammetry of the ETH Zurich, in cooperation with LaCoste and Romberg Gravity Meters Inc., undertook an airborne gravity survey of Switzerland during November and December of 1992. The survey was performed using a Twin-Otter aircraft at an altitude of 5200 metres and a flight speed of 240 km/h. DGPS was used for aircraft acceleration determination. The flight results showed crossing point differences between flight lines varying from 1 to 30 mGal. A comparison with an upward continued reference grid showed a RMS difference of 11.1 mGal. A poor GPS constellation (at date of survey GPS did not have a full constellation) and the fact that the GPS and gravimeter data could only be synchronized to 0.5 seconds seems to be the limiting factors in these results. Further details of the Switzerland mission can be found in Klingele et al. (1996) and (1995), and Klingele and Halliday (1995).

Airborne gravimetry results with the LCR gravimeter were also obtained as part of the AGMASCO project. Results have been presented for the Skagerrak campaign of the project flown in September 1996. The Skagerrak area is located between the northern part of Denmark and southern Norway. The survey was performed using a Dornier 228 aircraft at a flight altitude of 350 metres and a flight speed of 220 km/h. For this test both DGPS and laser altimetry were used to determine aircraft acceleration. Low-pass filtering of the data using 200 second averaging times yielded crossover point differences of approximately 2.3 mGal. A comparison with an upward continued reference yielded differences of approximately 3.5 mGal. It is felt (Olesen et al., 1997) that the larger deviation with respect to the reference is due to insufficient ground gravity spacing for computation of the reference. Another test of the AGMASCO system was carried out in October of 1997 in the Azores, however results from this test were not available at the time of writing. The flight conditions for the Skagerrak campaign are very close to those

of the June 1998 test. In addition, the data was collected using the same LCR gravimeter, and also processed by KMS. Therefore, assuming no significant data processing scheme changes, the expected accuracy of the June 1998 LCR gravimeter estimates should be 2 to 3 mGal (the accuracy given for the Skagerrak campaign).

# CHAPTER 4
## Accelerometer Bias Estimation and Compensation

In this chapter, problems with the long-term drift of the strapdown INS/DGPS gravity disturbance estimates are examined. The drift of the disturbance estimates from the September 1996 flight test are presented. Methods of modeling this drift in the INS Kalman filter are then investigated. It will be shown that modeling of the changes in the accelerometer bias through the INS filter for the current prototype system ais inadequate, and therefore, a crossover adjustment is presented as an initial step to reference the airborne gravity estimates to the absolute gravity field.

## 4.1 Long-Term Drift of Gravity Disturbance Estimates

Airborne gravity is an effective tool for measuring relative changes in the gravity field. However, in order for these relative measurements to be meaningful they must be self-consistent, i.e. measurements taken at the same location at different times should give the same value. This may not be easy to accomplish due to the fact that the strapdown inertial gravity estimates may drift over time due to non-linearities or long-term errors in either the specific force or GPS acceleration determinations. The word drift is used here to characterize a time dependence of the results.

Results of the first flight test of the prototype strapdown INS/DGPS system performed in June 1995 had suggested that the long-term drift of the INS/DGPS gravity disturbance estimates was stable and linear. This is an ideal drift situation because in order to correct for this effect, in theory, only one crossover point (point where two flight lines intersect) must be flown. From this crossover point the difference in disturbances can be used to estimate the linear drift. Obviously, for a more reliable estimation and to average the effects of measurement noise, a number of crossover points should be used to determine the linear drift.

The second flight test in September 1996 was flown in part to verify the drift results obtained in the June 1995 test over a much longer flight time. The flight patterns

were chosen in such a way that the last two flight lines were flown perpendicular to the first eleven to provide crossover points to account for the expected linear drift of the gravity disturbance estimates (see Figures 3.6 and 3.7). An analysis of this data has shown that the drift is not linear over the longer time period. Figures 4.1, 4.2 and 4.3 display the long-term drift of the prototype system estimates for Days 1, 2, and 3, respectively. The graphs in the figures are gravity estimates minus upward continued reference for the 14 flight lines each day. The gaps in the graphed lines denote the turns between the individual flight lines. It should be noted that no Kalman filtering scheme has been used to estimate accelerometer biases in these graphs and therefore the results represent the change in the "raw" gravity estimation error.
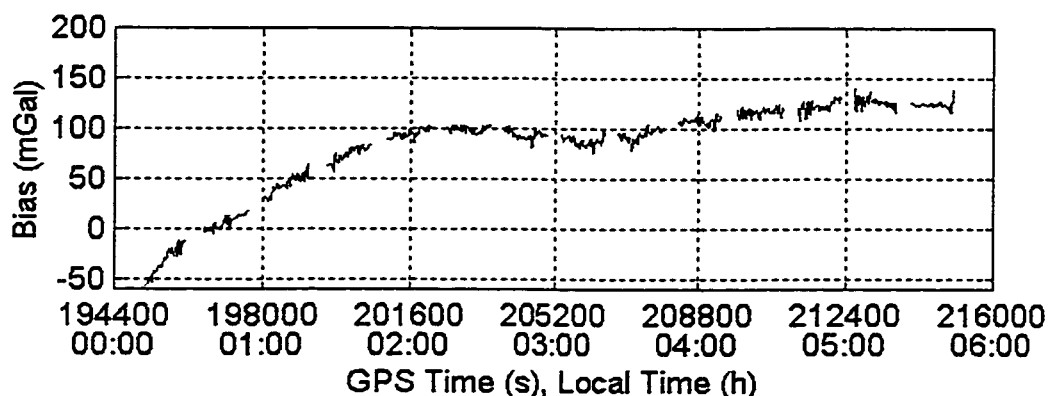
**Figure 4.1:** Bias of Prototype System Disturbance Estimate, Day 1 ($T_c$ = 90 sec)
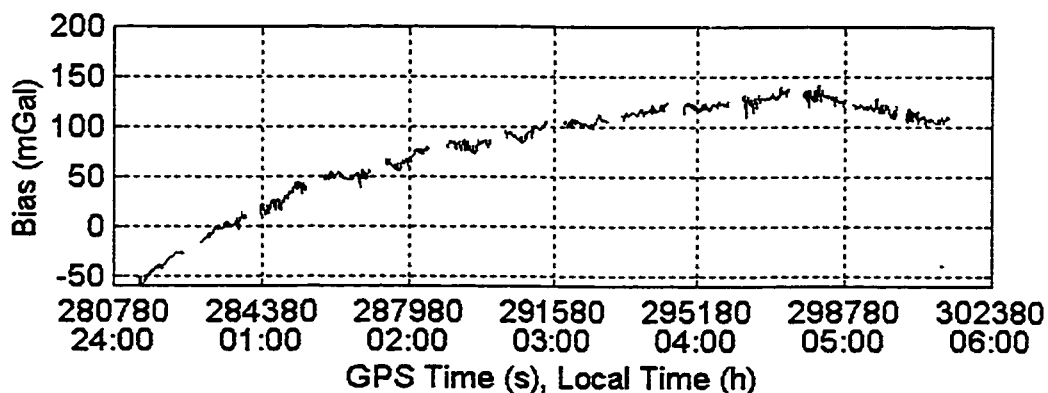
**Figure 4.2:** Bias of Prototype System Disturbance Estimate, Day 2 ($T_c$ = 90 sec)
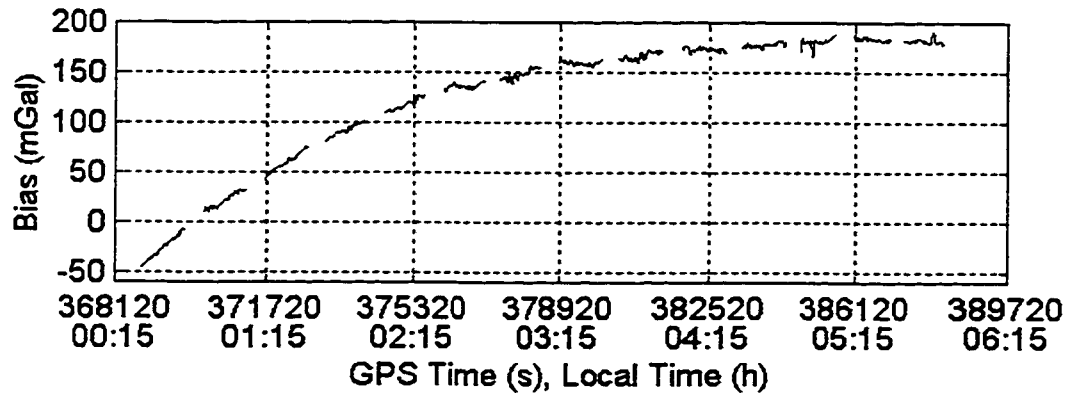
**Figure 4.3:** Bias of Prototype System Disturbance Estimate, Day 3 ($T_c$ = 90 sec)

All three figures clearly show that the bias is more or less linear over a time period of approximately 2 hours at the beginning of the flight. However, over the full flight period of 5.5 hours the biases are no longer linear. They take on more of a 3$^{rd}$ order polynomial shape. In order to ensure that the above effect was not due to flight dynamics several static data sets with the LRF III were collected. The long-term bias of the up specific force (1-frame) measurements for two of the static tests is displayed in Figures 4.4 and 4.5. The figures for the two static tests show a similar bias behaviour to that of the airborne gravity tests. Therefore, it would appear that the non-linear biases encountered in the September 1996 airborne gravity tests were not due to dynamic effects.
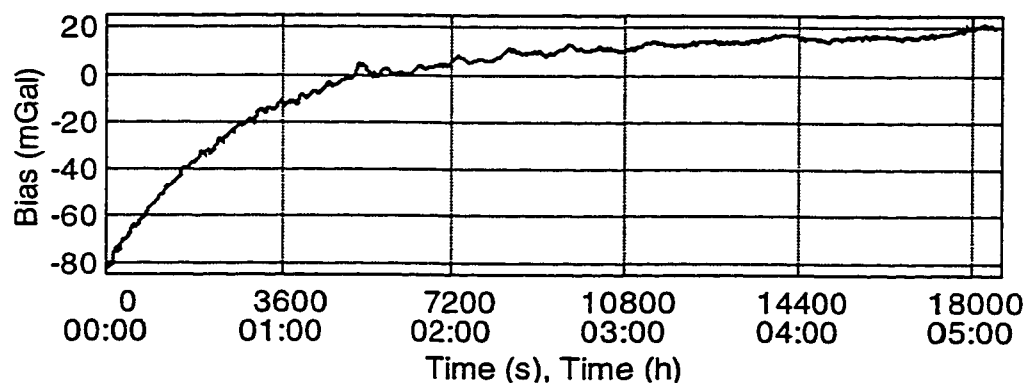


**Figure 4.4:** Bias of Up Acceleration, Static Test #1 ($T_c$ = 90 sec)
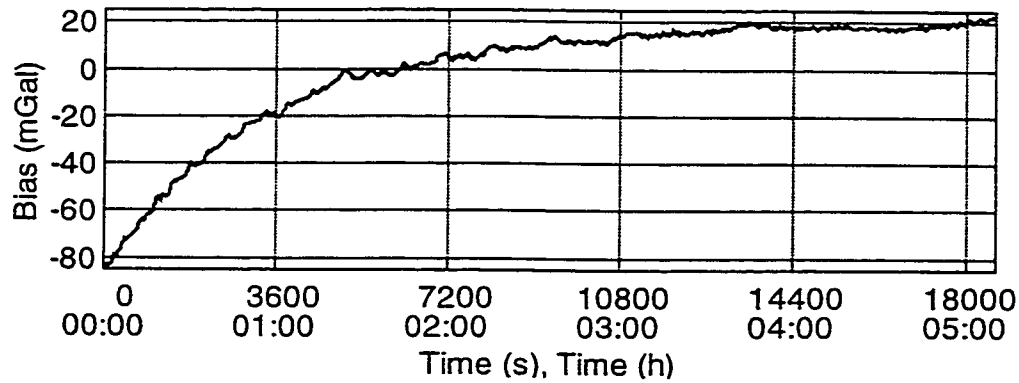
**Figure 4.5:** Bias of Up Acceleration, Static Test #2 ($T_c = 90$ sec)

The most likely reason for the fairly steep drift of the accelerometer bias for the first couple of hours is due to an accelerometer temperature dependency. This could be due to an incorrect thermal model for the accelerometer, or a malfunctioning accelerometer temperature probe. After the system reaches a normal operating temperature the bias is noticeably more stable. Therefore, it would appear that the initial steep ramp of the accelerometer bias could be avoided by allowing the inertial system to run for a couple of hours before takeoff. This may be impractical in some airplanes due to the fact that the engines need to be running to provide power for the inertial system. However, this would not be a problem assuming that an external power supply is available.

Even after a warm-up period of a couple of hours the accelerometer bias still cannot be considered linear for the purposes of airborne gravity. There are significant deviations from a linear drift in both the airborne and static data sets. However, the airborne data shows more significant deviations from linearity. It may be possible to model the drift of the accelerometer biases in the Kalman filter used to process the INS measurements. GPS position and velocity updates give information to the Kalman filter that allows the estimation of accelerometer errors. However, a model must be found for the accelerometer biases which accurately describes their behaviour. In the following section, different models for the accelerometer bias will be investigated.

## 4.2 Modeling the Accelerometer Bias

### 4.2.1 First-Order Gauss-Markov Model for Accelerometer Bias

For the Kalman filtering of INS data (Appendix) a first-order Gauss-Markov process is normally used to model the time changes in the accelerometer bias states. A first-order Gauss-Markov process is completely described by its autocorrelation function, which is given as (Gelb, 1974):

$$\varphi_{xx}(\tau) = \sigma^2 e^{-\beta\tau} \qquad (4.1)$$

where $\beta$ is the inverse of the correlation time. The correlation time is the point where the normalized autocorrelation function takes on the value of $1/e$.

In order to investigate whether a Gauss-Markov model is a reasonable approximation of the actual accelerometer bias states an autocorrelation function was generated for each of the drifts depicted in Figures 4.1 to 4.3. These autocorrelation functions, along with the autocorrelation function of a Gauss-Markov process with a correlation time of 10000 seconds, are displayed in Figure 4.6.
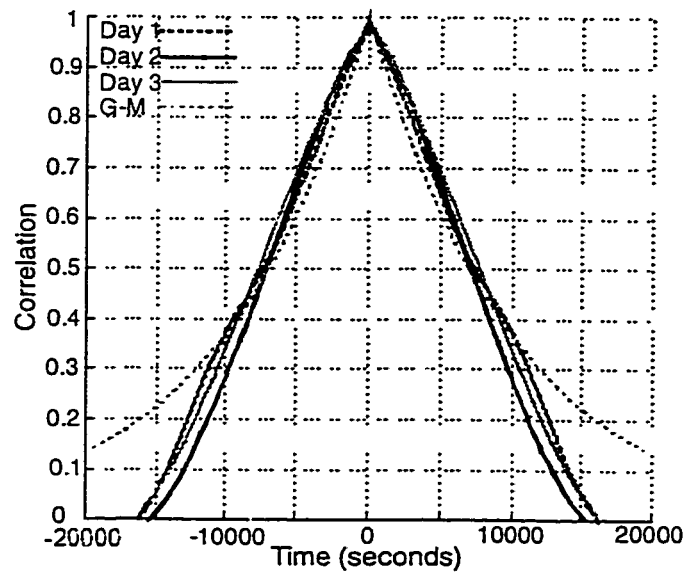


**Figure 4.6:** Autocorrelation Functions of Gravity Disturbance Estimation Drifts and First-Order Gauss-Markov Process ($1/\beta$ = 10000 seconds)

It should be noted that the gravity drift depicted in Figures 4.1 to 4.3 is theoretically a combination of biases due to all three accelerometers. However, because the strapdown inertial system was mounted with the b-frame aligned closely with the l-frame, the majority of the long-term bias is due to the z-accelerometer. Therefore, using the gravity disturbance bias to determine the z-accelerometer behaviour is still valid. If the IMU was mounted in such a way that the body and local-level frames were not approximately parallel, then the above assumption could not be made.

Figure 4.6 shows that the Gauss-Markov process does not provide a reasonable approximation of the actual accelerometer bias behaviour. This is especially true for the tails of the Gauss-Markov process. The figure clearly shows that the actual long-term drifts are much more linear than that expected by the Gauss-Markov model. In order to verify this analysis the September 1996 data was reprocessed using a first-order Gauss Markov model of the accelerometer states. The 1/e points for the actual biases in Figure 4.6 are 10097, 8806 and 9552 seconds for Days 1, 2 and 3 respectively. Therefore, for the actual raw data processing, an average correlation time of 9500 seconds was used for the Gauss-Markov model of the accelerometer biases.

In terms of accelerometer bias estimation, there are four important input parameters for the Kalman filter which influence the filter's ability to determine the bias states. These four parameters are the initial variance of the bias state ($\sigma_a^2$), the spectral density of the accelerometer bias ($q_a$), the variance of the GPS position and velocity updates and the GPS update interval. In order to determine the optimum values for each of these parameters a trial and error approach was utilized. This approach is normally called "filter tuning." The data was processed several times, each time varying the above parameters until a combination of the best short-term accuracy of the gravity estimates and long-term bias estimation was obtained. Figures 4.7 to 4.9 display the long-term drift of the system gravity disturbance estimate after the application of a first order Gauss-Markov model with a "tuned" Kalman filter. Note the difference in scale between Figures 4.1 to 4.3 and 4.7 to 4.9.
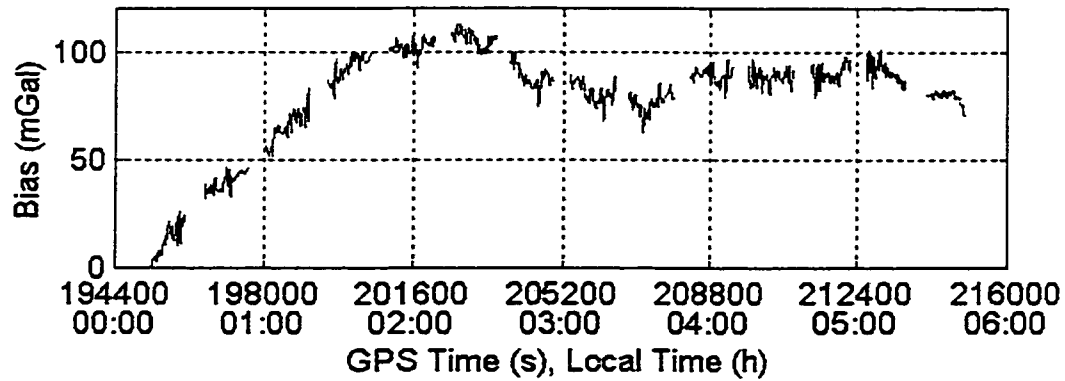
**Figure 4.7:** Drift of System Disturbance Estimate, Day 1 ($T_c$ = 90 sec) Accelerometer Bias Modeled as First Order Gauss-Markov
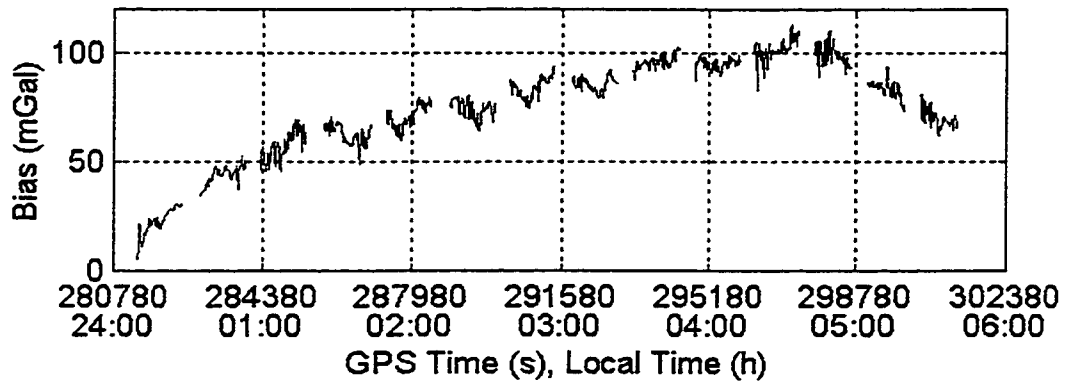


**Figure 4.8:** Drift of System Disturbance Estimate, Day 2 ($T_c$ = 90 sec) Accelerometer Bias Modeled as First Order Gauss-Markov
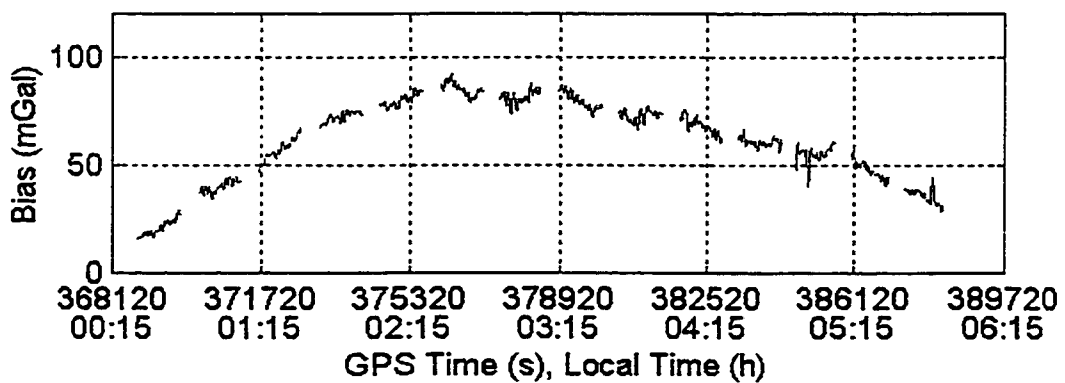


**Figure 4.9:** Drift of System Disturbance Estimate, Day 3 ($T_c$ = 90 sec) Accelerometer Bias Modeled as First Order Gauss-Markov

Comparing Figures 4.7-4.9 to 4.1-4.3 it is apparent that the Gauss-Markov model was only able to effectively estimate a portion of the long-term drift of the accelerometer bias. The short-term drift in the gravity disturbance estimates is nearly identical between the raw and estimated bias cases. This therefore confirms that the Gauss-Markov model of the accelerometer biases is not adequate, and therefore, other models must be investigated.

## 4.2.2 Polynomial Fit of Accelerometer Bias

As mentioned previously, the accelerometer drifts in Figures 4.1 to 4.3 appears to display a polynomial behaviour overlaid with shorter-term deviations. Therefore, it may be possible to model this drift with a combination polynomial fit and short-term error model. However, the short-term error behaviour for the static and kinematic tests should be consistent so that a proper error model can be chosen. In order to examine the short-term error behaviour of the accelerometer drift a $3^{rd}$ order polynomial was removed from each of the drifts in Figures 4.1 to 4.4. Each drift had a separate polynomial fit to it. The resulting residual drifts are displayed in Figures 4.10 to 4.13. Note that only one static data set is presented due to the similarities between the two static accelerometer drift patterns in Figures 4.4 and 4.5.
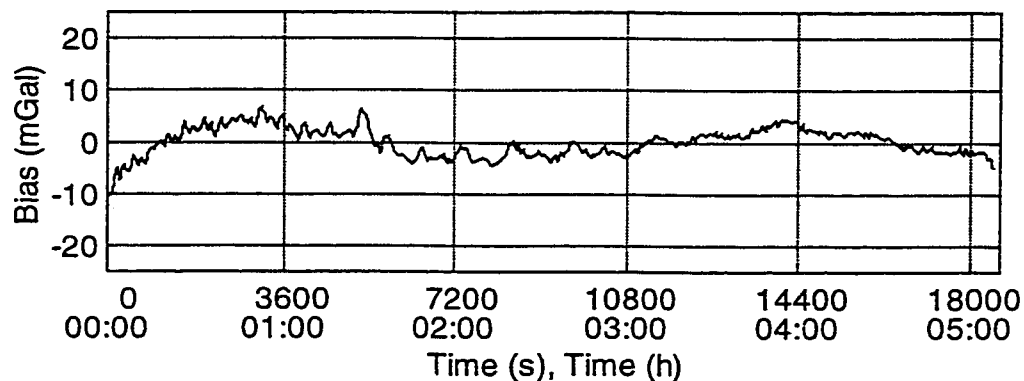


Figure 4.10: Static Test #1, Drift of Up Acceleration, $3^{rd}$ order Polynomial Removed ($T_c = 90$ sec)
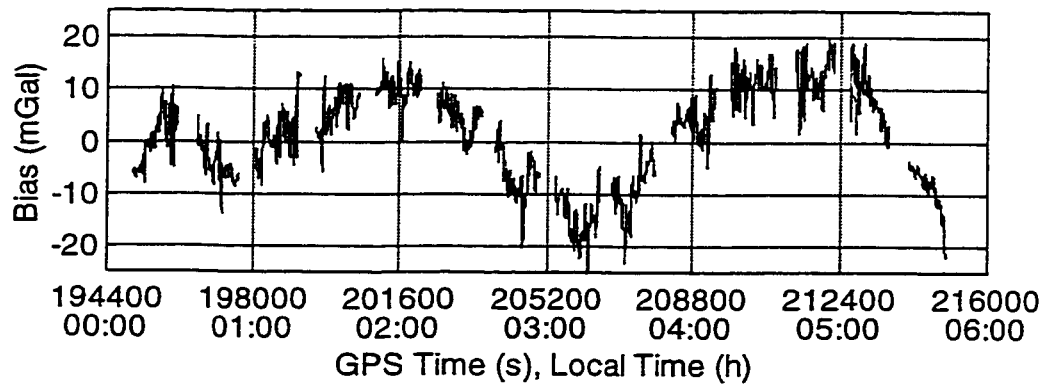
**Figure 4.11:** Day 1, Drift of System Disturbance Estimate, 3rd order Polynomial Removed ($T_c = 90$ sec)
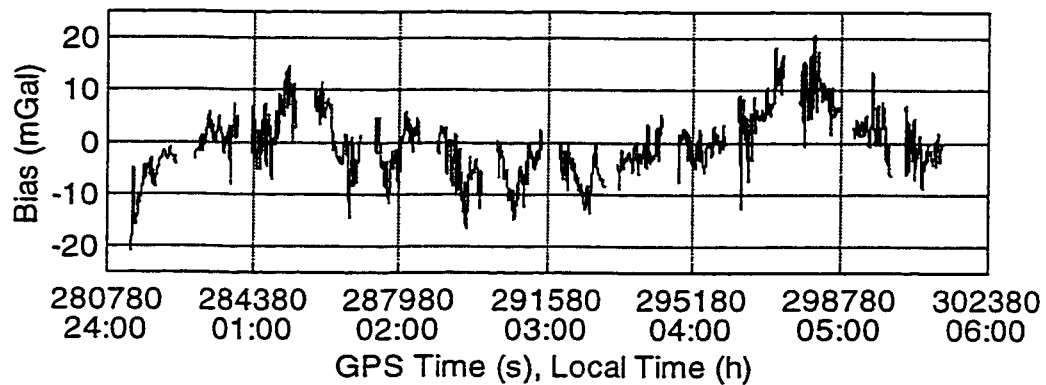


**Figure 4.12:** Day 2, Drift of System Disturbance Estimate, 3rd order Polynomial Removed ($T_c = 90$ sec)
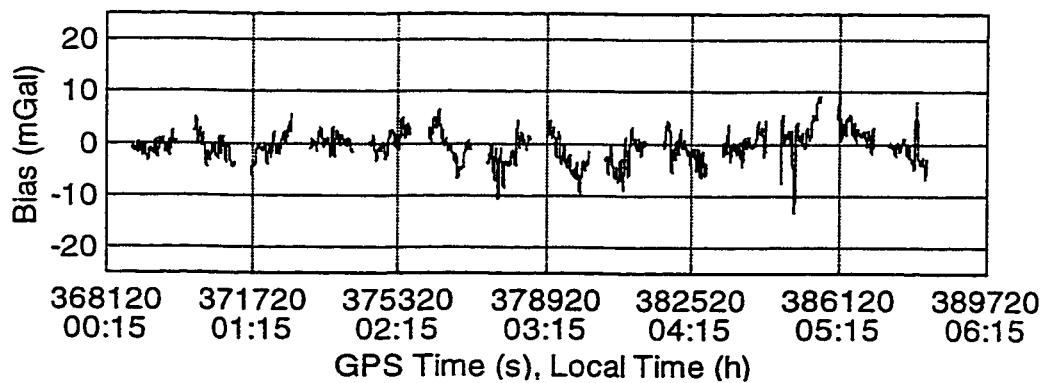


**Figure 4.13:** Day 3, Drift of System Disturbance Estimate, 3rd order Polynomial Removed ($T_c = 90$ sec)

After the removal of a 3rd order polynomial the residual biases for all four figures are quite small, generally below 20 mGal. However, these residual errors are still not

small enough to be neglected. The four figures also show that the drift pattern does not appear to be similar from test to test. The static drift and the drift for Day 1 show significant correlation times, approximately 1000 seconds for the static test, and 1500 seconds for Day 1. However, the drifts for Day 2 and Day 3 do not show any significant time correlation. The difference in behaviour is troubling because it means that it is unlikely a model could be chosen to suitably estimate the change in the accelerometer bias for all situations.

Despite the differences in the accelerometer bias characteristics for the three days of testing an attempt was made to model the residual bias errors. The raw z-accelerometer measurements first had the $3^{rd}$ order polynomial bias removed. The data was then reprocessed using two different models for the accelerometer bias state: a first-order Gauss-Markov model, and a random walk model. For each bias model the three days of data was processed several times in an attempt to tune the filter to successfully estimate the above residual accelerometer errors. Unfortunately, neither of the models allowed a successful estimation of the above drifts. In all attempts the resulting residual bias remained practically the same, or was made worse by the Kalman filter estimation.

## 4.2.3 Iterative Estimation of Accelerometer Bias

For a strapdown INS airborne gravity system the gravity disturbances and the accelerometer bias states are both low frequency phenomena. In the mechanization of the INS raw measurements a value for gravity is required (see equation A.1). A normal gravity model is used for this computation and therefore the gravity disturbances are neglected during the mechanization. Thus, it can be expected that to a certain extent the gravity disturbance information and the accelerometer bias will overlap in the frequency band of interest. This may be the cause of some of the residual accelerometer errors that are presented in Figures 4.11 to 4.13. In order to deal with this information overlap an iterative technique to better separate accelerometer biases and gravity disturbances has been proposed; see Schwarz and Li (1996). In the first step, the data is processed using the methods presented in the Appendix, i.e. using a normal gravity model. This allows an

initial estimation of the gravity disturbances. In the second step, these initial disturbance estimates are added to the normal gravity model used during mechanization, and the data is then reprocessed. It is hoped that the addition of the disturbances, to give a more accurate representation of gravity field effects in the flight area, will allow a better estimation of accelerometer biases, and therefore better gravity disturbance estimates in the second step. In theory, the iteration continues until the difference between the current gravity estimates and the previous estimates is below a certain threshold (say 1 mGal).

In order to evaluate the potential of the above iterative technique a slightly modified approach was implemented. Instead of feeding back the actual system gravity disturbance estimates the upward continued reference values were used in the mechanization. This approach should give the best performance that could be expected of the iterative procedure, since the reference represents the best performance that could be expected of the system gravity disturbance estimation. After the removal of a $3^{rd}$ order polynomial both a first-order Gauss-Markov model and a random walk model for the accelerometer bias states were attempted. The Kalman filter was re-tuned after the introduction of the gravity disturbance information to the INS mechanization equations.

The addition of the gravity disturbances to the mechanization gravity model caused only a minor change (a max. of 6 mGal) in the long-term accelerometer bias error. The residual biases from the iterative technique are not presented because they are nearly indistinguishable from the drifts presented in Figures 4.11 to 4.13. The drift is still not linear, which was the result desired. It should also be noted that the agreement with the upward continued reference for the individual flight lines did not improve for any of the flight tests. This shows that the short-term accelerometer bias estimation was not changed significantly by the introduction of the gravity disturbances to the INS mechanization.

## 4.2.4 General Conclusions on Accelerometer Bias

Based on the analysis presented in sections 4.2.2 and 4.2.3 it would appear that the residual biases displayed in Figures 4.10 to 4.13 are near the noise level of

accelerometer bias estimation for the prototype system using DGPS position and velocity estimates. To support the argument that the noise level of accelerometer bias estimation has been reached an examination of the estimation equations for the INS errors is required. Equation (A.5) gives the error model utilized in the Kalman filtering of the INS data. GPS position and velocity information are used to update the INS Kalman filter. By examining equation (A.5) it is apparent that the main information regarding accelerometer bias estimation will be contained in the GPS velocity updates. The state equations for velocity errors are given as:

$$\delta \dot{v}^e = -F^e \varepsilon^e + N^e \delta r^e - 2\Omega_{ie}^e \delta v^e + R_b^e b \qquad (4.2)$$

where all terms have been previously defined. Given frequent DGPS position and velocity updates the velocity state errors due to position and velocity errors will be small and random, and can be safely neglected (Škaloud, 1995), and therefore the error state equation reduces to:

$$\delta \dot{v}^e = -F^e \varepsilon^e + R_b^e b . \qquad (4.3)$$

Velocity errors are thus mainly affected by accelerometer biases and inertial system misalignment. Accelerometer bias estimation is therefore limited by the accuracy with which inertial system misalignment can be estimated, and also by the amount of correlation observed between misalignment errors and accelerometer bias states. For the Honeywell Laseref III used in the September 1996 test the resolution of the gyroscope measurements is 2.5 arcseconds. Using the rule of thumb that 1 arcsecond of misalignment corresponds to 5 mGal of error, the noise level of misalignment estimation is 12.5 mGal. This noise level seems to be consistent with the level of the accelerometer biases displayed in Figures 4.10 to 4.13. Therefore, it would appear that the accelerometer bias estimation of the current filtering procedure is at or near the estimation resolution level.

The bias stability of the accelerometers in the LRF III system is not sufficient for airborne gravity field determination. The accelerometers used in the LRF III prototype system were Allied Signal Q-Flex model QA 2000-010. The specifications for bias and scale factor stability for this and other Allied Signal QA accelerometer models are given in Table 4.1.

| | 2000-010 | 2000-020 | 2000-030 | 3000-010 | 3000-020 | 3000-030 |
|---|---|---|---|---|---|---|
| Bias Stability (μg) | 550 | 220 | 160 | 125 | 80 | 40 |
| Scale Factor Stability (ppm) | 600 | 500 | 310 | 250 | 160 | 80 |

**Table 4.1:** Allied Signal Q-Flex Quartz Accelerometer (QA) Specifications by Model (values listed are maximum)

The bias and scale factor stability of the model 2000-010 accelerometers in the prototype system are significantly worse than those of the other listed accelerometers. The poor performance specifications for the 2000-010 accelerometers are most likely the cause of the large temperature drift and non-linear bias behaviour of the gravity disturbance estimates from the prototype system. The model 3000-020 accelerometers, for example, show a factor of seven improvement for bias stability and a factor of four improvement for scale factor stability. Figure 4.14 shows static data from a QA 3000 accelerometer over a 12 hour period. The statistics of the residual accelerometer measurements are also given on the graph.
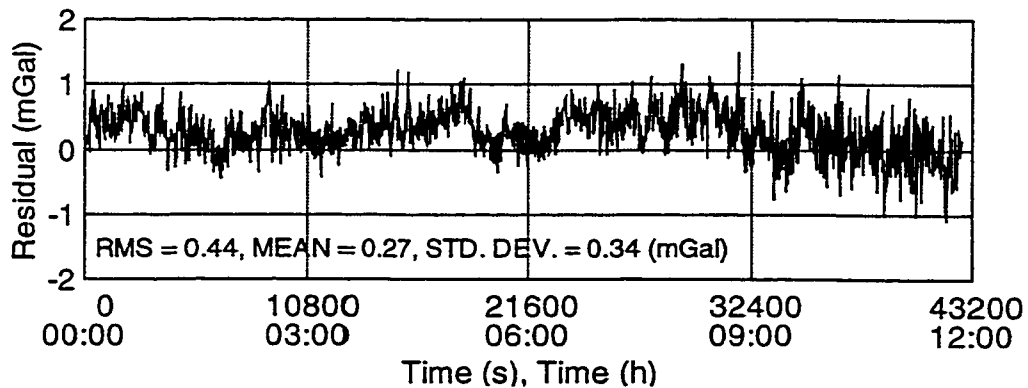


**Figure 4.14:** Static Data from QA 3000 Accelerometer (T$_c$ = 16 sec)

The bias stability displayed in Figure 4.14 for a QA 3000 accelerometer is far better than that of the QA 2000 in the LRF III (compare to Figures 4.4 and 4.5). In addition, the static noise level of the QA 3000 is also lower (compare to Table 3.2). It is likely that with the use of these more stable accelerometers the drift of the disturbance estimates would be linear. However, this would obviously have to be verified with the examination of dynamic data sets using these accelerometers.

## 4.3 Crossover Adjustment

The results of the accelerometer bias modeling presented in sections 4.2 were disappointing. They showed that the z-accelerometer bias cannot be estimated with sufficient accuracy by the Kalman filter from GPS position and velocity updates. As a result, the drift of the prototype system estimates is not linear. There are two methods of alleviating this problem. As mentioned in section 4.2.4, the first possibility is to acquire a set of accelerometers that have better bias stability than the QA 2000 accelerometers used in the prototype system. The development of a system with higher quality accelerometers is currently underway at the University of Calgary. The second possibility is to develop a post-processing adjustment method that attempts to make the system gravity disturbance estimates self-consistent; i.e. measurements taken at the same location at different times give the same value.

For the purposes of this dissertation an initial step towards the realization of an adjustment method that accounts for the non-linear drift was developed and tested. The adjustment was based on the use of crossover point differences in gravity disturbance estimates between flight lines. Each flight line used in the crossover adjustment is considered to have a separate slope and bias term. Therefore, a minimum of 2*n crossover points are required, where n is the number of flight lines. The crossover point differences are processed using a parametric least squares adjustment. More information on least squares adjustment techniques can be found in Leick (1995). The measurement model for the adjustment is given as:

$$\Delta \delta g = s_i \Delta t_i + s_j \Delta t_j + b_i + b_j \qquad (4.4)$$

where,

$\Delta\delta g$      is the difference in disturbance estimates between flight lines at the crossover point,

$s_i, s_j, b_i, b_j$      are the slopes and biases of flight lines i and j respectively, and

$\Delta t_i, \Delta t_j$      are the time differences between the start of the flight line and the time of the current crossover point.

The program CROSOVER has been written in C to automatically compute crossover point differences between input flight lines, form the measurement equations for the adjustment, perform the adjustment, and then apply the calculated slope and bias terms to the original flight line data. The result of the adjustment is a set of self-consistent gravity disturbance estimates.

The crossover adjustment has been applied to the flight data for Days 1 and 2 of the September 1996 test for both the RISG and SISG estimates at four filtering periods. Note that a $3^{rd}$ order polynomial bias was first removed from the gravity estimates, and therefore the data used in the crossover adjustment has the drift patterns given in Figures 4.11 and 4.12. Alternatively, the $3^{rd}$ order fit could have also been built into the crossover adjustment mathematical model. For the SISG results eleven flight lines were used from each day for a total of 121 crossover points and 44 unknowns (slope and bias for each line). For the RISG data the first three flight lines of Day 2 were removed due to poor results (see section 5.1.1.2). Therefore, for the RISG adjustment there were a total of 88 crossover points and 38 unknowns. The RMS and maximum values of the crossover point residuals after the application of the adjustment are given in Table 4.2.

| Diff | SISG | | | | RISG | | | |
|------|--------|--------|--------|---------|--------|--------|--------|---------|
| (mGal) | 30 sec | 60 sec | 90 sec | 120 sec | 30 sec | 60 sec | 90 sec | 120 sec |
| RMS | 10.7 | 3.2 | 2.3 | 2.6 | 11.7 | 3.9 | 3.4 | 3.5 |
| Max. | 28.4 | 8.2 | 6.2 | 6.9 | 29.3 | 13.7 | 10.1 | 10.7 |

**Table 4.2:** Residual Crossover Point Differences After Adjustment, LRF III, Days 1 & 2

The table shows that after the removal of a slope and bias from each flight line the agreement at the crossover points is quite good. A more detailed discussion of the residual crossover point differences is delayed until Chapter 5.

After the crossover adjustment the airborne data is self-consistent. However, the biases with respect to the actual absolute gravity disturbances have not been completely removed. Figures 4.15 and 4.16 give the bias in the system disturbance estimates after the crossover adjustment. Note that only eleven flight lines are displayed in these figures because only eleven flight lines for each day were used in the crossover adjustment.
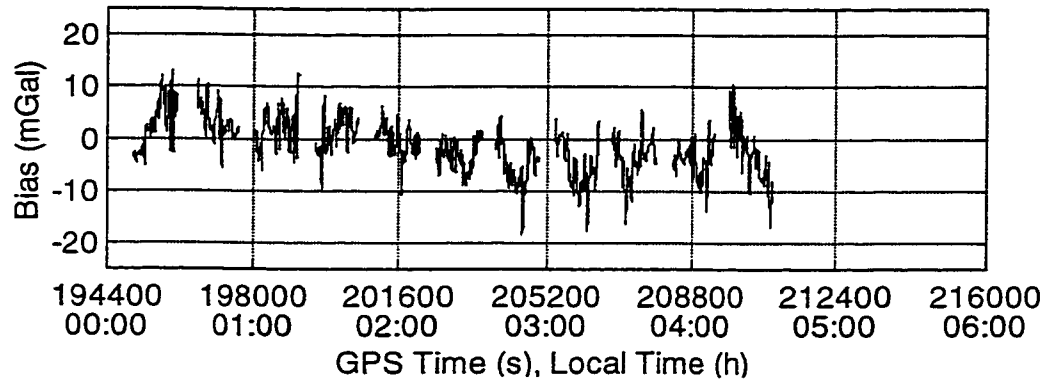


**Figure 4.15:** Day 1, Bias of System Disturbance Estimate after Crossover Adjustment ($T_c = 90$ sec)
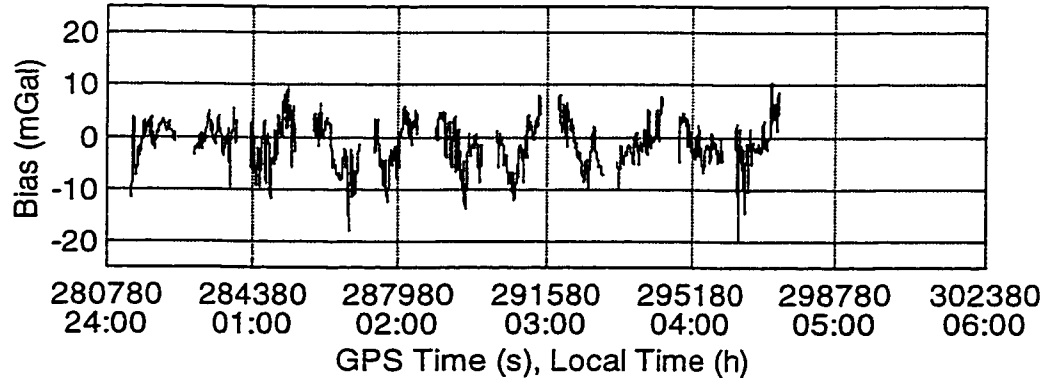


**Figure 4.16:** Day 2, Bias of System Disturbance Estimate after Crossover Adjustment ($T_c = 90$ sec)

The biases depicted in Figures 4.15 and 4.16 generally vary between ±10 mGal. However, they still do not appear to be centered around zero; small linear drifts are still visible for some of the flight lines. It should be emphasized that the crossover adjustment method presented represents only an initial attempt to compensate for the long-term drift of the strapdown INS/DGPS airborne gravity disturbance estimates. No attempt has been made to refer the self-consistent relative gravity disturbances to the absolute gravity field.

Future developments should concentrate on optimal merging of all data sources available for the flight area. Examples of additional data sources include geopotential models, ground gravity measurements, digital elevation models, orthometric heights, and satellite altimetry over oceans. Algorithms should be developed which use these other sources of absolute gravity information in order to refer the more accurate relative measurements of the airborne gravity system to the absolute gravity reference. Software for the optimal combination of all these data sources have not yet been developed, and therefore this is an area in which further theoretical and practical development must take place.

Finally, it should be briefly mentioned that the number of crossover points used in the September 1996 crossover adjustment described above was quite high, and gave more than adequate redundancy to compute the biases for each of the flight lines. Acquiring this many crossover points would be quite costly for production flights of airborne gravity systems. It is therefore recommended that the number of crossover points flown should be tailored to the individual airborne gravity system. In general, the more stable the accelerometer biases, the less crossover points required. The choice of the optimal number of crossover points will also rely on operator experience as to how much redundancy is needed to ensure satisfactory adjustment results.

## 4.4 Long-Term Accelerometer Drift of Litton 101

The above analysis of long-term accelerometer bias estimation has focused on the Laseref III strapdown INS/DGPS airborne gravity system developed by the University of Calgary. However, for the September 1996 test a Litton 101 strapdown inertial system was also used. The raw accelerometer bias of the LTN 101 system for Day 1 and Day 3 is presented in Figures 4.17 and 4.18. The last three flight lines of Day 3, and all of Day 2 are not presented due to logging computer malfunctions.
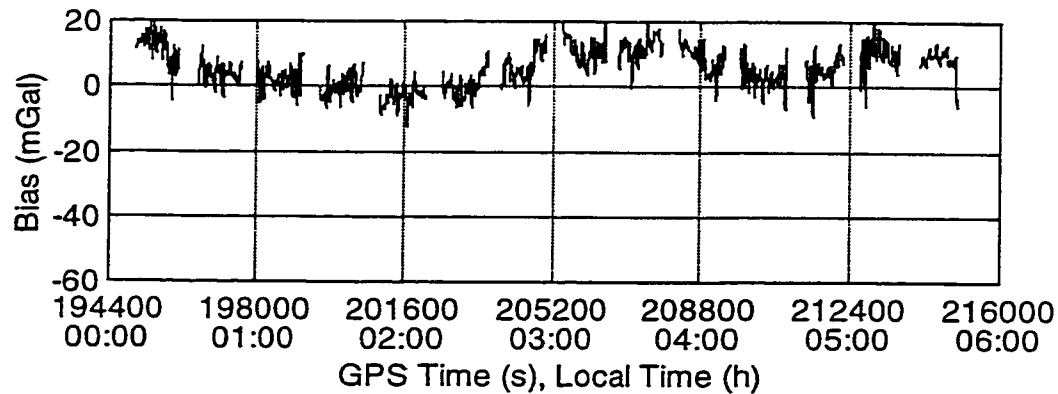
**Figure 4.17:** Bias of LTN 101 System Disturbance Estimate, Day 1 ($T_c = 90$ sec)
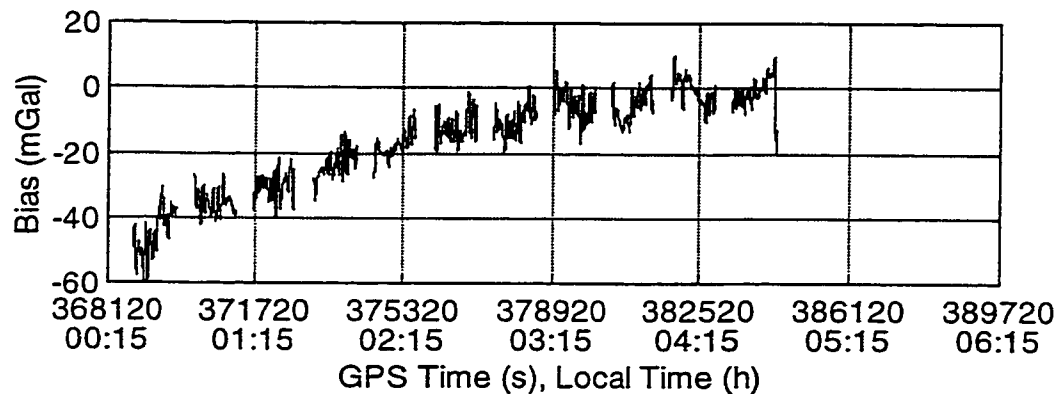


**Figure 4.18:** Bias of LTN 101 System Disturbance Estimate, Day 3 ($T_c = 90$ sec)

Figure 4.17 and 4.18 do not show a polynomial drift for the LTN 101 disturbance estimates, as the LRF III did. There is very little long-term trend in the Day 1 bias, and the bias for Day 3 shows a fairly linear trend. However, like the LRF III, the short-term error behaviour of the LTN 101 bias is non-linear. It should be noted that attempts to model the short-term errors of the LTN 101 accelerometer biases were also unsuccessful. Thus, it appears that the A4 accelerometers in the Litton 101, like the QA 2000-010 accelerometers in the LRF III, lack the bias stability required for airborne gravity. Unfortunately, specifications on the A4 accelerometer were not available from the manufacturer for comparison purposes.

# CHAPTER 5

## Flight Test Results

In the following, results of the two flight tests in September 1996 and June 1998 will be presented and discussed. The details of both flight tests are given in Chapter 3. Preliminary results of the September 1996 test have been published in Glennie and Schwarz (1997) and (1999) and Schwarz and Glennie (1998). They will be used in the following without specific reference to these papers.

## 5.1 September 1996 Flight Test Results

The flight test in September 1996 was flown with two strapdown inertial systems over the same 100 km by 100 km area which had dense ground gravity coverage. As a consequence of the in-flight information collected the results can be analyzed in three different ways. Firstly, the individual system estimates can be compared with an upward continued reference. Secondly, the two strapdown INS estimates can be inter-compared, and thirdly, crossover points can be analyzed to determine the long-term repeatability of the system. All three days of data will be presented for the analysis of the results. It should be noted that, following the discussion in Chapter 4, a linear bias has been removed when comparing gravity disturbance estimates to each other or to the reference to remove the long-term drift problems of the strapdown inertial systems.

### 5.1.1 System Comparison with Upward Continued Reference

#### 5.1.1.1 Day 1 Comparison with Reference

Tables 5.1 and 5.2 give the results of comparisons between the upward continued reference and the LRF III and LTN 101 sub-systems respectively for Day 1 of the flight test. The results are presented for 14 flight lines, which are shown in Figure 3.6. The

values given are the RMS of the differences between the system estimate and the upward continued reference in mGal. The last two columns of the tables give the average RMS values and standard deviations for all 14 flight lines. The standard deviations were computed using an accuracy of approximately 1.5 mGal for the reference. Comparison results are given for both the SISG and RISG approach at four filtering periods.

| FLIGHT | SISG RMS (mGal) | | | | RISG RMS (mGal) | | | |
|---|---|---|---|---|---|---|---|---|
| LINE # | 30 sec | 60 sec | 90 sec | 120 sec | 30 sec | 60 sec | 90 sec | 120 sec |
| 1 | 11.8 | 2.9 | 2.8 | 3.4 | 13.6 | 4.3 | 4.1 | 4.4 |
| 2 | 12.3 | 2.8 | 2.3 | 2.7 | 12.7 | 3.8 | 3.1 | 3.4 |
| 3 | 14.3 | 4.7 | 3.4 | 3.4 | 14.3 | 4.7 | 3.3 | 4.0 |
| 4 | 11.1 | 3.7 | 2.9 | 2.8 | 12.7 | 4.3 | 3.9 | 4.0 |
| 4 | 10.3 | 2.9 | 2.8 | 3.2 | 10.4 | 3.0 | 3.1 | 3.4 |
| 6 | 7.4 | 2.8 | 2.8 | 3.2 | 8.6 | 3.2 | 3.0 | 3.4 |
| 7 | 8.9 | 4.2 | 4.2 | 4.8 | 8.9 | 4.1 | 4.1 | 4.8 |
| 8 | 10.0 | 4.3 | 3.7 | 4.1 | 11.7 | 4.9 | 4.4 | 4.9 |
| 9 | 10.9 | 4.4 | 4.0 | 4.4 | 11.0 | 4.1 | 3.3 | 4.1 |
| 10 | 9.3 | 3.4 | 3.1 | 3.1 | 10.4 | 4.2 | 3.8 | 4.0 |
| 11 | 11.0 | 4.4 | 3.3 | 3.4 | 12.6 | 6.4 | 4.6 | 6.1 |
| 12 | 13.6 | 4.1 | 3.7 | 4.8 | 13.9 | 4.6 | 4.7 | 4.6 |
| 13 | 11.0 | 3.4 | 3.1 | 3.8 | 12.8 | 4.0 | 4.6 | 4.0 |
| 14 | 11.2 | 3.2 | 2.1 | 1.9 | 13.3 | 4.2 | 3.4 | 4.8 |
| AVG(14) | 10.9 | 3.8 | 3.2 | 3.4 | 11.9 | 4.6 | 4.1 | 4.6 |
| σ | 10.8 | 3.4 | 2.8 | 3.2 | 11.9 | 4.3 | 3.8 | 4.3 |

**Table 5.1:** Day 1, LRF III Comparison with Reference, RMS Residuals (mGal)

| FLIGHT | SISG RMS (mGal) | | | | RISG RMS (mGal) | | | |
|---|---|---|---|---|---|---|---|---|
| LINE # | 30 sec | 60 sec | 90 sec | 120 sec | 30 sec | 60 sec | 90 sec | 120 sec |
| 1 | 29.8 | 6.7 | 3.6 | 3.4 | 29.3 | 6.7 | 4.6 | 4.8 |
| 2 | 31.9 | 7.2 | 2.8 | 3.0 | 31.2 | 7.3 | 3.1 | 3.1 |
| 3 | 24.6 | 6.9 | 3.4 | 2.9 | 24.4 | 6.7 | 3.2 | 3.2 |
| 4 | 29.6 | 4.2 | 2.9 | 3.0 | 27.3 | 4.9 | 3.3 | 3.3 |
| 4 | 26.3 | 4.6 | 2.8 | 3.1 | 24.6 | 4.7 | 3.2 | 3.4 |
| 6 | 14.6 | 3.4 | 3.0 | 3.4 | 13.9 | 3.4 | 3.0 | 3.4 |
| 7 | 18.6 | 4.8 | 4.1 | 4.6 | 17.6 | 4.0 | 4.2 | 4.7 |
| 8 | 16.0 | 4.3 | 3.6 | 3.3 | 14.8 | 4.4 | 3.6 | 3.6 |
| 9 | 14.4 | 4.0 | 3.4 | 4.0 | 14.2 | 3.9 | 3.2 | 4.0 |
| 10 | 17.9 | 3.2 | 2.9 | 3.1 | 18.1 | 4.0 | 3.4 | 3.4 |
| 11 | 14.6 | 4.4 | 3.7 | 4.4 | 14.4 | 4.9 | 3.6 | 3.7 |
| 12 | 17.9 | 4.1 | 3.4 | 4.8 | 17.4 | 4.1 | 4.4 | 4.1 |
| 13 | 26.4 | 4.4 | 4.3 | 4.0 | 26.0 | 4.7 | 4.4 | 4.0 |
| 14 | 19.6 | 3.8 | 3.1 | 2.8 | 18.6 | 4.8 | 3.4 | 2.8 |
| AVG(14) | 21.7 | 4.1 | 3.4 | 3.6 | 20.9 | 4.2 | 3.7 | 3.8 |
| σ | 21.6 | 4.9 | 3.0 | 3.3 | 20.9 | 4.0 | 3.4 | 3.4 |

**Table 5.2:** Day 1, LTN 101 Comparison with Reference, RMS Residuals (mGal)

To give a visual idea of the excellent agreement between the system estimates and upward continued reference Figure 5.1 is presented. It shows SISG profiles for both inertial systems on two typical flight lines for Day 1. The residual pattern displayed in the figure is similar for the two inertial systems.
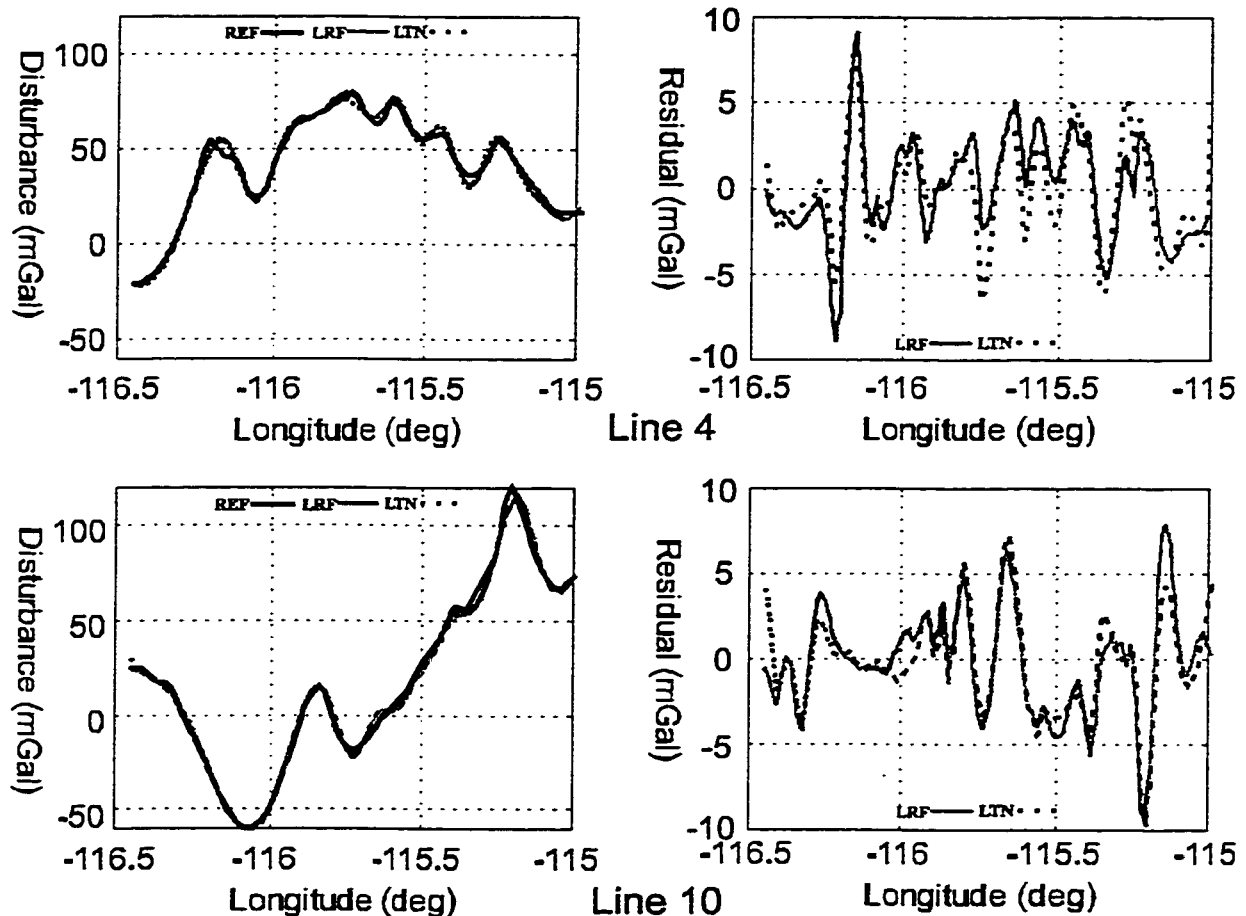


**Figure 5.1:** Day 1, Flight Lines 4 and 10, LRF III and LTN 101 SISG Profiles (left) and Residuals ($T_c = 90$ sec)

Table 5.1 shows that the RMS agreement of the LRF III with the upward continued reference is about 3.2 mGal for the SISG results when using an averaging time of 90 seconds. The LTN 101 performance is slightly worse, with a best RMS agreement for the SISG results of 3.4 mGal. This was to be expected based on the noise levels of the z-accelerometers for the two systems (section 3.2.1). The corresponding best standard deviations are 2.8 and 3.0 mGal for the LRF III and LTN 101 systems respectively. For

both systems the SISG results are consistently better than the RISG results. For the LRF III the SISG results are significantly better, approximately 20% to 30%, while for the LTN 101 the improvement is less (about 4% to 10%). An average spectrum of the residuals for all fourteen flight lines for both systems' SISG and RISG estimates are shown in Figure 5.2. Particularly troublesome in all the spectral plots is the peak of approximately 2 mGal at 0.001 Hz.
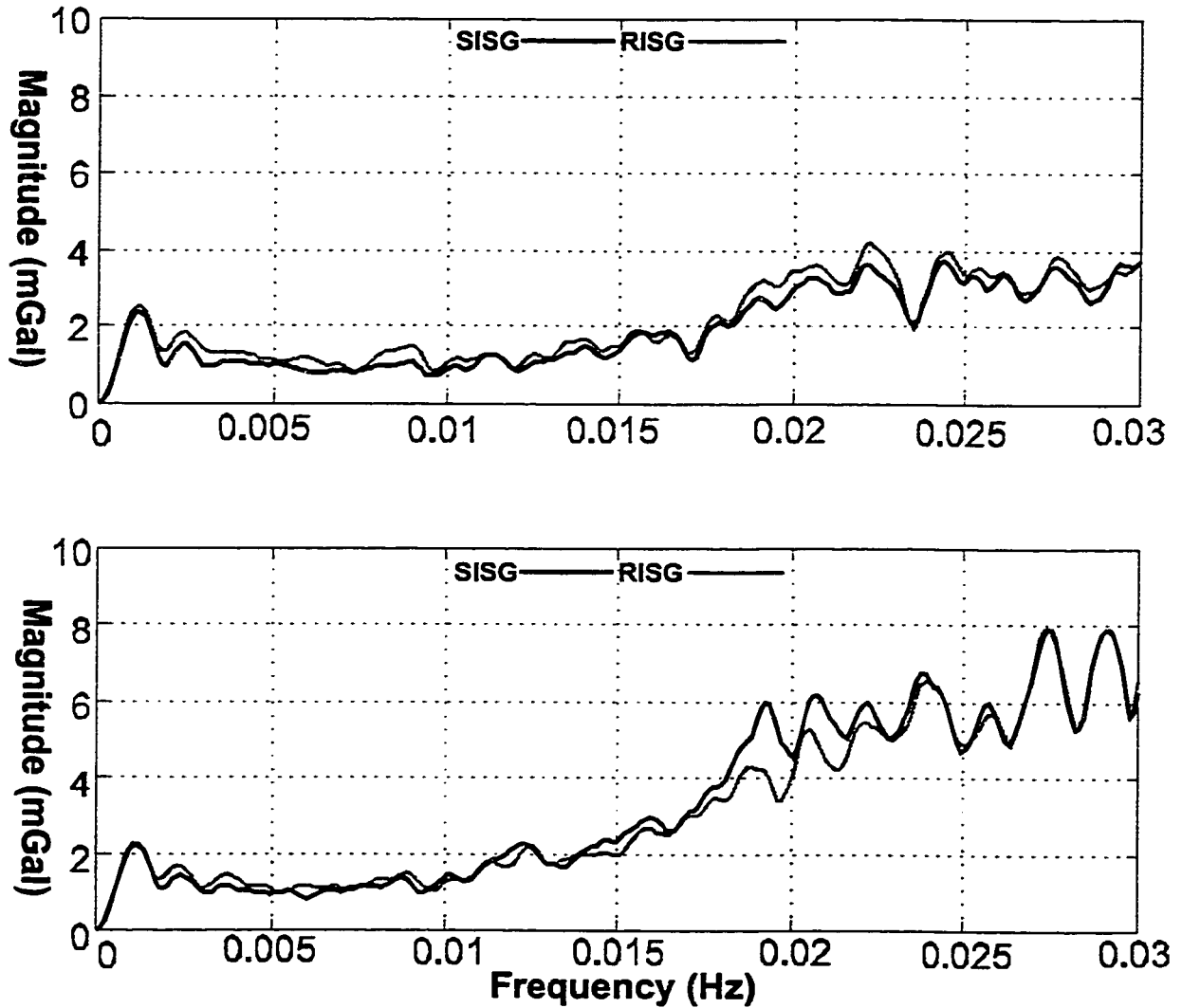
Figure 5.2: LRF III (top) and LTN 101 (bottom) Day 1 Average Spectrum of SISG and RISG Residuals, Linear Bias Removed ($T_c$ = 30 sec)

The four residual spectrums in Figure 5.2 are fairly flat to approximately f = 0.017 Hz where the residual spectrums noticeably increase; the increase is more dramatic for the LTN 101. This sudden increase in the residual spectrum may be explained by a phenomenon known as phugoid motion. Phugoid motion is a natural oscillation of an aircraft at a certain frequency due to the action of a symmetric disturbance on the aircraft. An example of a symmetric disturbance would be an up-gust of wind. The motion is predominantly sinusoidal, with variation in aircraft height and forward speed. The period of the phugoid oscillation is approximately given by the formula (Babister, 1980):

$$T_{ph} = \frac{\sqrt{2}\pi}{g} v \qquad (5.1)$$

where g = 9.81 m/s$^2$ (gravity) and v is the horizontal aircraft velocity. By inserting the average horizontal velocity for the September test of 100 m/s into equation (5.1) a phugoid period of 44 seconds is obtained. This period corresponds to a frequency of 0.022 Hz, which is close to the location of the residual spectrum increase.

Since phugoid oscillation results in aircraft motion it should theoretically cancel out when the INS and GPS accelerations are differenced because both systems sense aircraft motion. However, the response of the INS and GPS systems to phugoid motion appears to differ, and therefore the noise level for all frequencies larger than the phugoid frequency is higher. This would explain the poor results obtained for both systems at a filtering period of 30 seconds, which is well above the phugoid frequency. The proximity of the phugoid frequency to the 60 second cut-off may also partly explain the poorer results at this filtering period.

Currently, there is not a clear explanation why the response of the two sub-systems to the phugoid oscillation differs. The residual phugoid error appears to be dependent on the inertial system used. This can be verified by examining Figure 5.2, and noting that the increase in residuals near the phugoid frequency is much more pronounced for the LTN 101 than for the LRF III. The same DGPS accelerations were used in the generation of all four spectral plots in Figure 5.2, and therefore, the difference in residuals

cannot be explained by DGPS errors. The difference in response could be due to the higher noise level of the LTN 101 accelerometers. Salychev and Schwarz (1995) suggest that the differing response to phugoid motion may be due to non-linearities of the accelerometer scale factors, although this has not been verified. A detailed discussion of phugoid motion can be found in Babister (1980) and Bryson (1994) for example.

### 5.1.1.2 Day 2 Comparison with Reference

Tables 5.3 and 5.4 give the results of a comparison between the upward continued reference and the LRF III and LTN 101 for Day 2 of the flight test. Again, the values quoted are RMS differences (in mGal) for the fourteen flight lines (see Figure 3.7). The standard deviations were computed using an accuracy of 1.5 mGal for the reference. Note that only RISG data is available for the LTN 101. The logging computer collecting the LTN 101 data malfunctioned in the first flight line of the Day 2 test. Consequently, the INS and computer had to be reset in-flight, and as a result, there was no static data to align the LTN 101. Therefore, the raw accelerometer outputs of the LTN 101 could only be used to compute RISG gravity disturbance estimates for the $2^{nd}$ to $14^{th}$ flight lines.

| FLIGHT | SISG RMS (mGal) | | | | RISG RMS (mGal) | | | |
|---|---|---|---|---|---|---|---|---|
| LINE # | 30 sec | 60 sec | 90 sec | 120 sec | 30 sec | 60 sec | 90 sec | 120 sec |
| 1 | 11.8 | 2.4 | 2.2 | 1.9 | 14.1 | 9.4 | 8.1 | 7.6 |
| 2 | 9.2 | 2.9 | 2.7 | 3.1 | 28.0 | 22.3 | 19.2 | 17.6 |
| 3 | 12.4 | 4.4 | 3.9 | 4.4 | 17.4 | 11.0 | 9.7 | 8.6 |
| 4 | 9.7 | 3.7 | 3.3 | 3.6 | 11.7 | 4.7 | 4.4 | 6.4 |
| 4 | 12.2 | 4.4 | 3.6 | 3.8 | 12.8 | 4.2 | 4.4 | 4.4 |
| 6 | 12.9 | 4.4 | 3.6 | 3.9 | 14.0 | 4.4 | 4.9 | 4.7 |
| 7 | 14.8 | 3.9 | 3.6 | 3.6 | 14.9 | 4.2 | 3.7 | 4.1 |
| 8 | 6.9 | 3.4 | 3.1 | 3.3 | 7.6 | 4.6 | 4.3 | 4.3 |
| 9 | 8.4 | 2.7 | 2.2 | 2.7 | 8.4 | 3.1 | 3.1 | 3.2 |
| 10 | 8.7 | 3.1 | 2.2 | 2.4 | 8.8 | 3.6 | 2.8 | 3.1 |
| 11 | 9.1 | 3.7 | 3.6 | 4.7 | 10.4 | 4.6 | 4.9 | 4.6 |
| 12 | 14.0 | 4.3 | 3.7 | 3.7 | 14.6 | 4.4 | 4.1 | 4.0 |
| 13 | 11.1 | 4.7 | 3.2 | 3.0 | 11.6 | 6.6 | 4.6 | 4.1 |
| 14 | 13.2 | 3.6 | 3.1 | 3.4 | 14.0 | 4.7 | 4.3 | 4.0 |
| AVG(14) | 11.1 | 3.9 | 3.1 | 3.4 | 13.7 | 6.9 | 6.0 | 4.9 |
| σ | 11.0 | 3.6 | 2.8 | 3.1 | 13.6 | 6.7 | 4.8 | 4.7 |
| AVG(11) | | | | | 11.9 | 4.9 | 4.3 | 4.4 |
| σ | | | | | 11.8 | 4.6 | 4.0 | 4.2 |

**Table 5.3:** Day 2, LRF III Comparison with Reference, RMS Residuals (mGal)

By examining Table 5.3 it is noted that the RISG results for the LRF III are significantly worse for the first three flight lines compared to lines four through fourteen. Therefore, in the last four lines of the table the average RMS and standard deviations have been computed for all fourteen flight lines and for the last eleven flight lines to remove the outlying results. A discussion of the possible reasons for these outliers is given in section 6.2.

| FLIGHT | RISG RMS (mGal) | | | |
|---|---|---|---|---|
| LINE # | 30 sec | 60 sec | 90 sec | 120 sec |
| 1 | | | | |
| 2 | 44.6 | 23.9 | 20.4 | 18.9 |
| 3 | 48.7 | 13.3 | 11.6 | 10.6 |
| 4 | 48.4 | 6.6 | 4.3 | 4.6 |
| 4 | 47.4 | 8.6 | 4.8 | 4.1 |
| 6 | 47.6 | 8.4 | 4.3 | 4.4 |
| 7 | 44.1 | 6.3 | 4.9 | 4.7 |
| 8 | 42.3 | 11.4 | 7.2 | 6.4 |
| 9 | 120.7 | 14.4 | 10.0 | 7.7 |
| 10 | 86.8 | 12.6 | 4.4 | 4.4 |
| 11 | 90.7 | 17.0 | 11.0 | 10.3 |
| 12 | 419.9 | 271.4 | 213.6 | 176.2 |
| 13 | 48.1 | 14.0 | 6.8 | 4.3 |
| 14 | 36.1 | 11.3 | 6.1 | 4.3 |
| Avg(12) | 62.2 | 12.4 | 8.3 | 7.4 |
| $\sigma$ | 62.2 | 12.3 | 8.2 | 7.3 |
| Avg(9) | 60.3 | 10.4 | 6.2 | 4.4 |
| $\sigma$ | 60.3 | 10.4 | 6.0 | 4.3 |

**Table 5.4:** Day 2, LTN 101 Comparison with Reference, RMS Residuals (mGal)

In Table 5.4 the data for flight line 12 is obviously an outlier. In addition the data for flight lines 2, 3 and 11 show significantly higher RMS residuals than the other lines. Therefore, the average RMS values and standard deviations have been computed for 12 flight lines (with no line 12) and for 9 flight lines (with no lines 2, 3, 11, 12) in Table 5.4.

The SISG results for the LRF III given in Table 5.3 are consistent with the results obtained for Day 1 of the test (Table 5.1). They confirm that the best RMS agreement of the LRF III with the upward continued reference is at the three mGal level. The RISG results (ignoring the first three flight lines) are also consistent with the results from Day 1. The consistency of the results is significant because it shows that the level of accuracy

obtained does not seem to be affected by flight line direction. Day 1 flight lines were east-west, while Day 2 had north-south flight lines.

The RISG results for the LTN 101 for Day 2 are significantly worse then for Day 1, even after removal of the four outlying flight lines. The poor results may be explained by the reset of the inertial system in flight. The LTN 101 requires a period of static alignment for operation. However, during the alignment period it still outputs raw accelerometer and gyro measurements. This allows for post-mission alignment and data analysis. After the reset, because the airplane was in flight, the LTN 101 was not able to statically align itself. Therefore, the poorer results could be explained by a difference in the raw output of the LTN 101. The output after a successful static alignment may be slightly better than the raw output obtained when the LTN is attempting to align. Unfortunately, the LTN 101 was returned to its owner before this theory could be verified.

### 5.1.1.3 Day 3 Comparison with Reference

The final flight test of September of 1996 was flown at an average elevation of approximately 7274 metres, or 3000 metres higher than the flights for Day 1 and 2. This higher test was flown to determine the capability of the system to determine the vertical gradients of gravity. Additionally, the higher flight allowed an evaluation of the system's performance with a smoother gravity field (at flight height) and under conditions of less atmospheric turbulence. Tables 5.5 and 5.6 show the SISG and RISG results for both the LRF III and LTN 101 respectively. The values quoted are RMS differences (in mGal) between the system estimates and the upward continued reference. To compute the standard deviations, an accuracy of 1.5 mGal was assumed for the upward continued reference. Note that no data was available for the LTN 101 for the last three flight lines due to logging computer problems.

| FLIGHT | SISG | | | | RISG | | | |
|--------|------|------|------|-------|------|------|------|-------|
| LINE # | 30 sec | 60 sec | 90 sec | 120 sec | 30 sec | 60 sec | 90 sec | 120 sec |
| 1 | 9.6 | 2.2 | 1.2 | 1.2 | 11.8 | 4.7 | 4.4 | 4.2 |
| 2 | 7.9 | 2.4 | 1.8 | 1.4 | 8.3 | 3.1 | 2.3 | 1.8 |
| 3 | 10.6 | 1.9 | 1.4 | 1.3 | 10.4 | 2.2 | 1.8 | 1.6 |
| 4 | 9.9 | 2.4 | 1.3 | 1.1 | 10.8 | 2.9 | 2.2 | 1.9 |
| 4 | 10.0 | 2.2 | 1.6 | 1.4 | 10.1 | 2.4 | 2.1 | 2.0 |
| 6 | 8.7 | 2.9 | 2.3 | 2.2 | 9.6 | 2.9 | 2.3 | 2.4 |
| 7 | 11.3 | 3.9 | 2.6 | 2.1 | 11.9 | 4.3 | 3.1 | 2.4 |
| 8 | 13.8 | 2.6 | 1.9 | 1.7 | 14.7 | 3.2 | 2.4 | 2.3 |
| 9 | 10.9 | 3.4 | 2.4 | 2.2 | 10.7 | 3.2 | 2.0 | 1.8 |
| 10 | 10.2 | 4.1 | 2.0 | 1.6 | 11.0 | 4.6 | 2.2 | 1.9 |
| 11 | 8.8 | 2.3 | 1.8 | 1.4 | 9.0 | 2.8 | 2.3 | 2.4 |
| 12 | 13.3 | 4.8 | 3.7 | 3.1 | 14.1 | 4.3 | 4.4 | 4.3 |
| 13 | 7.6 | 2.4 | 1.4 | 2.4 | 7.4 | 2.6 | 2.0 | 2.7 |
| 14 | 8.4 | 3.4 | 2.6 | 2.4 | 8.8 | 4.2 | 3.9 | 3.6 |
| AVG(14) | 10.1 | 2.9 | 2.0 | 1.8 | 10.6 | 3.4 | 2.8 | 2.6 |
| σ | 10.0 | 2.4 | 1.4 | 1.1 | 10.4 | 3.2 | 2.4 | 2.1 |

**Table 5.5:** Day 3, LRF III Comparison with Reference, RMS Residuals (mGal)

| FLIGHT | SISG | | | | RISG | | | |
|--------|------|------|------|-------|------|------|------|-------|
| LINE # | 30 sec | 60 sec | 90 sec | 120 sec | 30 sec | 60 sec | 90 sec | 120 sec |
| 1 | 32.8 | 14.9 | 4.1 | 3.6 | 34.1 | 17.1 | 6.6 | 4.6 |
| 2 | 28.8 | 6.3 | 3.3 | 2.0 | 29.6 | 6.9 | 3.8 | 3.1 |
| 3 | 63.4 | 12.1 | 3.9 | 2.3 | 64.1 | 12.1 | 4.6 | 2.9 |
| 4 | 79.4 | 11.1 | 3.4 | 1.8 | 79.4 | 11.0 | 3.3 | 1.9 |
| 4 | 61.8 | 10.1 | 3.0 | 2.4 | 62.1 | 10.0 | 3.1 | 2.4 |
| 6 | 44.7 | 7.9 | 4.0 | 2.6 | 44.2 | 8.1 | 4.7 | 2.9 |
| 7 | 47.2 | 10.7 | 4.0 | 2.6 | 63.2 | 11.2 | 4.3 | 2.9 |
| 8 | 64.4 | 11.2 | 4.1 | 2.6 | 63.2 | 11.2 | 4.3 | 2.9 |
| 9 | 46.6 | 9.4 | 4.1 | 3.3 | 47.3 | 9.4 | 3.9 | 2.9 |
| 10 | 47.4 | 7.2 | 3.2 | 2.4 | 48.0 | 6.9 | 3.8 | 2.4 |
| 11 | 40.2 | 8.2 | 4.3 | 3.4 | 41.3 | 8.8 | 9.2 | 6.4 |
| 12 | | | | | | | | |
| 13 | | | | | | | | |
| 14 | | | | | | | | |
| AVG(11) | 42.4 | 9.9 | 3.8 | 2.7 | 42.9 | 10.2 | 4.8 | 3.3 |
| σ | 42.4 | 9.8 | 3.4 | 2.2 | 42.9 | 10.1 | 4.4 | 3.0 |

**Table 5.6:** Day 3, LTN 101 Comparison with Reference, RMS Residuals (mGal)

The results for the LRF III show a best RMS difference with the reference of 1.8 mGal for the SISG results using a 120 second filter. The LTN 101 results are again slightly worse than the LRF III, with a best RMS agreement of 2.7 mGal for the SISG results. The corresponding best standard deviations are 1.1 and 2.2 mGal for the LRF III

and LTN 101 systems, respectively. The SISG results are significantly better than the RISG results for both systems, about 40 % better for the LRF III and 24 % better for the LTN 101. The agreement with the reference for this higher flight is noticeably better than the agreement for the two lower flights. This is to be expected since the gravity field is smoother at a higher flight height. In order to quantify the effect of gravity field variation on disturbance estimation Table 5.7 is presented. It gives the standardized errors for the LRF III for all three days of testing in September of 1996. Note that the gravity field variation statistics are given in Table 3.4.

| Flight Test | LRF III | | | |
| | SISG | | RISG | |
| | 90 sec | 120 sec | 90 sec | 120 sec |
|---|---|---|---|---|
| Day 1 | 0.071 | 0.081 | 0.097 | 0.109 |
| Day 2 | 0.071 | 0.079 | 0.102 | 0.107 |
| Day 3 | 0.042 | 0.033 | 0.072 | 0.063 |

**Table 5.7:** Standardized Errors ($\frac{\sigma_{error}}{\sigma_{gravity\ variation}}$), LRF III, September 1996

Table 5.7 clearly shows that the smoother variation of the gravity field does not account for all of the improvement in the gravity estimates. The rest of the improvement is likely due to the decreased effects of atmospheric turbulence on aircraft motion at the higher elevation. The decreased turbulence will result in significantly smaller and smoother aircraft accelerations. Following the discussion of the SISG and RISG error models in Chapter 2, it is noted that smaller aircraft accelerations decrease the gravity disturbance estimation errors.

It should be noted that the best results for Day 1 and Day 2 were obtained for a 90 second filter period, while the best results for Day 3 were obtained using a 120 second filter period. This shows that a filtering period cannot be blindly chosen. It should be decided upon based on factors such as flight height, gravity field variation, the type of inertial system and the quality of the DGPS accelerations. The optimal filtering period is therefore a tradeoff between removal of measurement noise and an over-smoothing of the results (see section 5.3).

In order to give a visual representation of the system estimates agreement with the reference for Day 3 two representative flight profiles are displayed in Figure 5.3. It should be noted that these two flight lines are in approximately the same horizontal location as the two flight lines given in Figure 5.1 (for Day 1). Therefore, the smoothness of the gravity field at the higher flight elevation can clearly be observed by comparing the two figures.
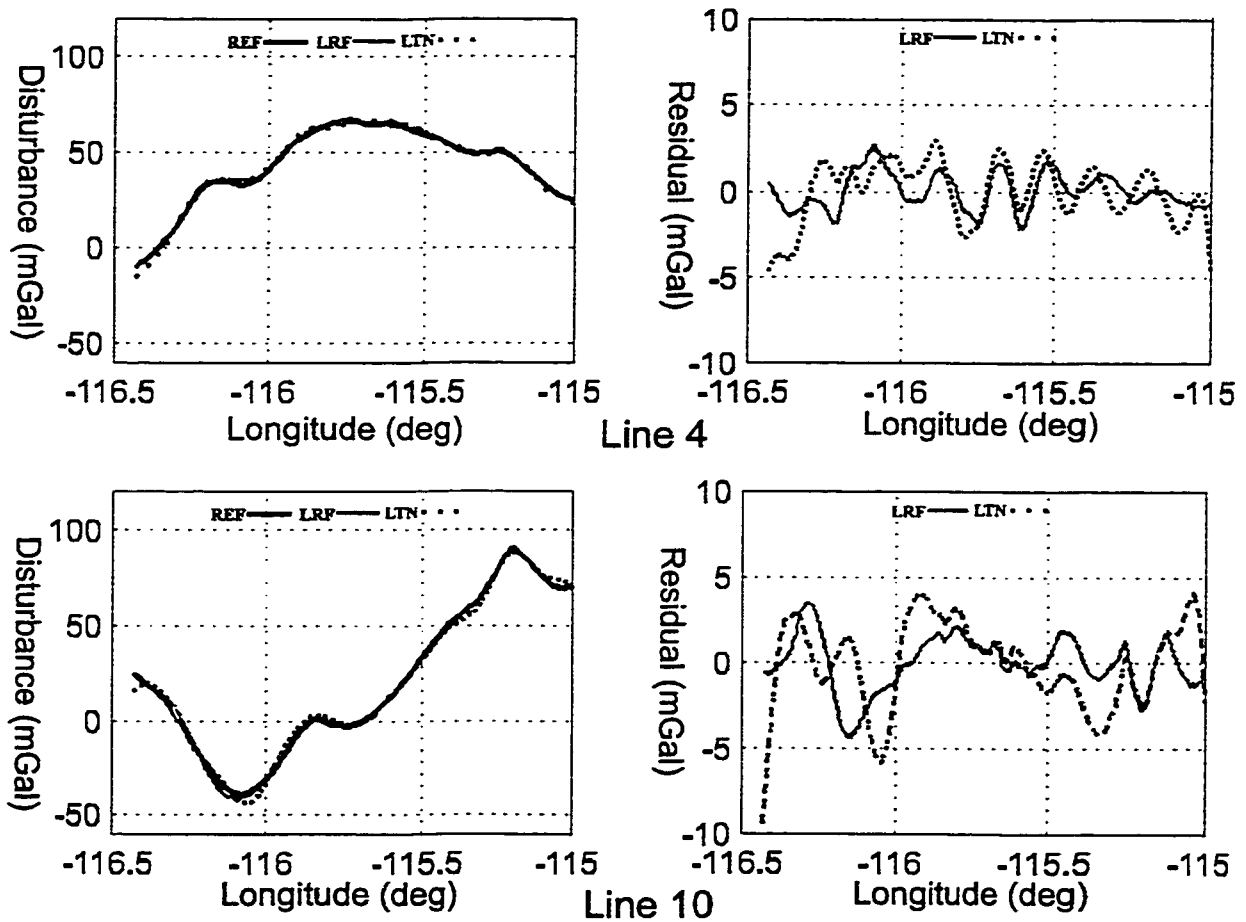


**Figure 5.3:** Day 3, Flight Lines 4 and 10, LRF III and LTN 101 SISG Profiles and Residuals ($T_c = 120$ sec)

The LTN 101 results for Day 3 are significantly worse than those for the LRF III. In addition the LTN 101 results do not show the same level of improvement as the LRF III results due to a higher flight elevation. In fact, the LTN 101 results are significantly worse (by almost a factor of 2) at the higher flight elevation for the 30 and 60 second

filtering periods. This result is quite puzzling. However, an examination of the raw INS data from Day 3 for the LTN 101 has shown an unusually large number of time jumps and data gaps. Therefore, the larger errors may be due to data logging problems. As was mentioned earlier, the University of Calgary had only a limited amount of time with the LTN 101, and therefore, the logging software developed was not fully tested.

## 5.1.2 Inter-comparison of System Estimates

### 5.1.2.1 Day 1 Inter-comparison

Because two inertial systems were flown side-by-side in the September test, an inter-comparison of results obtained with each system can be undertaken. This inter-comparison provides a unique opportunity to isolate error sources that are inertial system specific. In addition, flying the inertial systems side-by-side gives an opportunity to determine improvements that may be possible by utilizing a multiple sensor configuration. This will be discussed in Chapter 6.

Table 5.8 displays the results of a comparison between gravity estimates of the LRF III and LTN 101 for Day 1 of the test.

| FLIGHT LINE # | SISG (LRF) v. SISG (LTN) | | | | RISG (LRF) v. RISG (LTN) | | | |
|---|---|---|---|---|---|---|---|---|
| | 30 sec | 60 sec | 90 sec | 120 sec | 30 sec | 60 sec | 90 sec | 120 sec |
| 1 | 38.0 | 7.0 | 3.4 | 2.4 | 39.0 | 6.6 | 3.1 | 2.1 |
| 2 | 38.3 | 7.4 | 2.2 | 2.2 | 38.4 | 7.4 | 2.0 | 1.6 |
| 3 | 28.3 | 7.2 | 2.7 | 1.9 | 28.1 | 6.9 | 2.3 | 1.8 |
| 4 | 31.9 | 4.7 | 1.9 | 1.8 | 29.6 | 4.2 | 2.1 | 1.7 |
| 4 | 32.4 | 4.4 | 2.3 | 1.6 | 31.7 | 4.0 | 1.9 | 1.3 |
| 6 | 18.0 | 3.8 | 2.7 | 2.4 | 18.6 | 3.3 | 2.4 | 2.4 |
| 7 | 24.6 | 3.7 | 1.9 | 1.4 | 24.3 | 3.6 | 1.8 | 1.4 |
| 8 | 19.6 | 3.9 | 1.9 | 2.3 | 19.8 | 4.1 | 2.0 | 2.1 |
| 9 | 18.0 | 4.0 | 2.8 | 1.9 | 19.0 | 3.1 | 2.3 | 1.7 |
| 10 | 21.8 | 2.4 | 1.6 | 1.4 | 23.2 | 2.8 | 2.0 | 1.4 |
| 11 | 18.2 | 4.4 | 2.7 | 3.0 | 19.4 | 6.2 | 4.4 | 4.8 |
| 12 | 19.1 | 4.3 | 2.6 | 2.1 | 18.2 | 4.7 | 3.3 | 2.3 |
| 13 | 32.8 | 6.2 | 3.2 | 2.8 | 33.1 | 6.4 | 3.4 | 2.4 |
| 14 | 22.4 | 3.4 | 1.9 | 2.1 | 22.1 | 3.4 | 3.4 | 4.4 |
| AVG(14) | 26.0 | 4.8 | 2.4 | 2.1 | 26.1 | 4.8 | 2.7 | 2.3 |
| σ | 18.4 | 3.4 | 1.7 | 1.4 | 18.4 | 3.4 | 1.9 | 1.6 |

**Table 5.8:** Day 1, LRF v. LTN Residual Differences (mGal), Different DGPS Combination

Note that a different master-remote GPS receiver pair was used with each inertial system. Therefore, the RMS values given in Table 5.8 should reflect the errors of both inertial systems, DGPS acceleration errors, and errors in the computation of the relative lever-arm correction. Because the RMS of the differences was computed, the values are divided by $\sqrt{2}$ to obtain the standard deviation ($\sigma$ in the table) for one measuring system (INS/DGPS combination). An average spectrum of the residuals for the system inter-comparison for all flight lines is given in Figure 5.4.
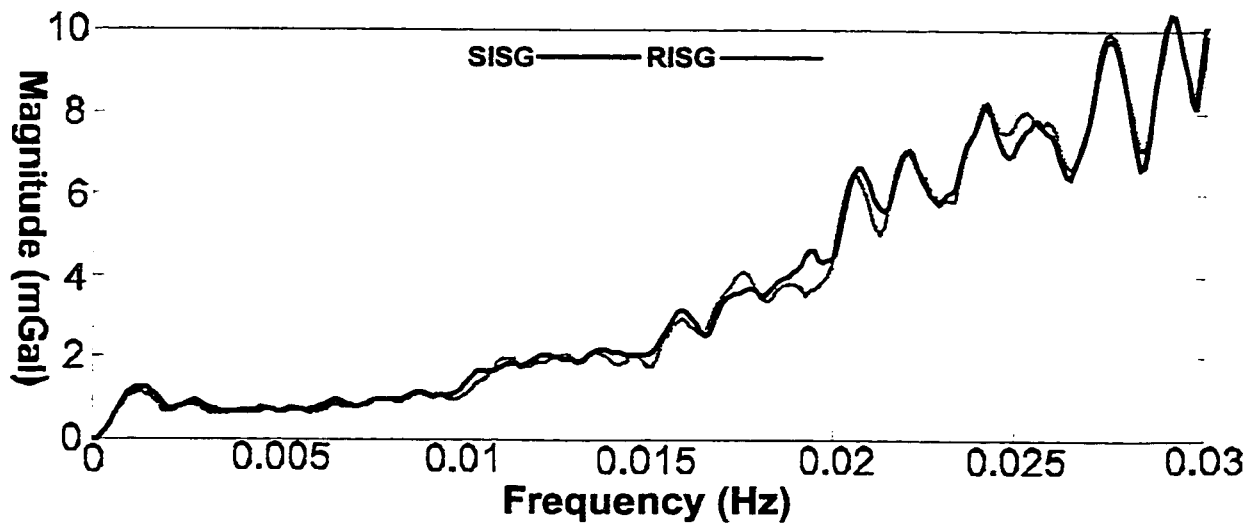


**Figure 5.4:** Day 1, Spectrum of Differences, LRF III v LTN 101 ($T_c = 30$ sec)

An analysis of the errors in the relative lever-arm correction has shown that this error is negligible compared to the RMS differences quoted in Table 5.8 for the respective filtering times. For example, for a 90 second filtering period, the error will be less than 0.2 mGal RMS for the test's flight hardware configuration. Therefore, the standard deviation values in Table 5.8 represent the combined INS and DGPS errors for one measuring system (assuming both are of the same accuracy).

The standard deviations of the differences given in Table 5.8 for the 90 and 120 second filtering periods are considerably better than the $\sigma$ values given in Tables 5.1 and 5.2 for the comparison of the individual system estimates with the upward continued reference. The improvement is approximately 44% and 34% respectively for the 120 and

90 second filters. The agreement of 1.4 mGal at 120 seconds and 1.7 mGal at 90 seconds for the SISG results corresponds approximately to the noise level of the accelerometers.

A possible explanation for the better system comparison agreement compared to the individual agreement with the reference is that the upward continued reference and the system gravity disturbance estimates have not had the same filtering methods applied to them. Therefore, the reference may contain information that has a higher frequency content than the low-pass filtered estimates. In addition, due to the fact that low-pass filters deviate from ideal filters, some distortion may have been introduced into the estimate through the filtering process. To test this explanation of the discrepancies, the upward continued reference was filtered to the various cut-off periods using the same low-pass filters that were applied to the gravity disturbance estimates. Table 5.9 gives average RMS and σ values for all fourteen flight lines for a comparison between the LRF III system estimate and an identically low-pass filtered upward continued reference.

| Diff | SISG | | | | RISG | | | |
|---|---|---|---|---|---|---|---|---|
| (mGal) | 30 sec | 60 sec | 90 sec | 120 sec | 30 sec | 60 sec | 90 sec | 120 sec |
| RMS | 10.9 | 3.7 | 2.8 | 2.4 | 11.9 | 4.4 | 3.8 | 3.7 |
| σ | 10.8 | 3.4 | 2.3 | 1.9 | 11.9 | 4.2 | 3.4 | 3.4 |

**Table 5.9:** Day 1, Average of Fourteen Flight Lines, RMS Difference Between LRF III and Upward Continued Reference (mGal), both Filtered to the Same Period using Identical Low-pass Filters

The values given in Table 5.9 agree more closely with the values given in Table 5.8, especially for the SISG results for the 90 and 120 second filtering periods. However, for the 30 and 60 second filtering periods the results in Table 5.9 are nearly identical to those in Table 5.1, i.e. the RMS values from the comparison with the unfiltered upward continued reference. This indicates that the reference contains information to a frequency between 60 and 90 seconds (0.0167 and 0.0111 Hz). This is confirmed by examining Figure 5.5, that shows a spectrum of the upward continued reference for Day 1.
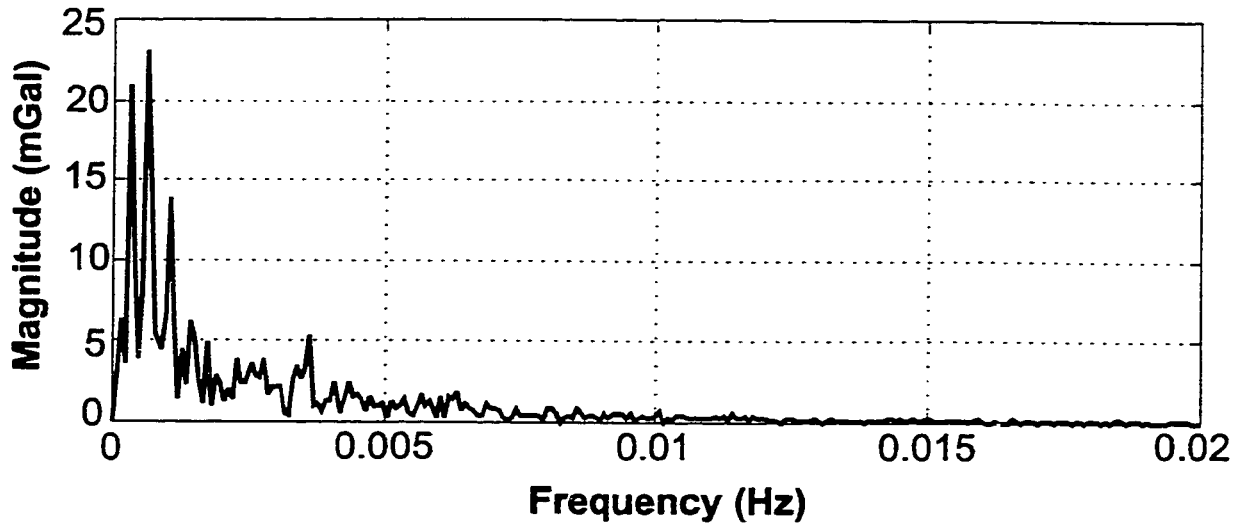
**Figure 5.5:** Spectrum of Upward Continued Reference, Day 1

Filtering the upward continued reference does not account for all of the differences between Tables 5.1 and 5.2 and Table 5.8, however. There are still some differences that are not accounted for. An examination of Figure 5.2 shows a common peak in the residual spectrum for both inertial systems of over 2.0 mGal at a frequency of approximately 0.001 Hz. However, this peak is for the most part removed when the two system estimates are differenced (Figure 5.4). This indicates two possible sources of the low frequency error: systematic errors in the data processing which affects both systems in the same way, or errors in the upward continued reference. It is currently not possible to state with certainty which is the cause of the error. However, an exhaustive examination of the data processing algorithm design has been undertaken without detecting a cause for such an error, and therefore, an error in the upward continued reference seems to be the more likely cause.

In the high frequency spectrum, i.e. at 30 and 60 second filter lengths, the difference between the two inertial systems shows the same error as the difference between one of the systems and the upward continued reference. An examination of the residual spectrum of the differences between the inertial system estimates in Figure 5.4 shows a noticeable increase in the spectrum at approximately the phugoid motion period (0.022 Hz). It should be noted that although Figure 5.4 was generated using different

master-remote pairs for each sub-system the same pattern can be observed when differencing between the two inertial systems using identical DGPS accelerations. Therefore, the increase in the error spectrum near the phugoid period seems to be caused by a difference in the high frequency response of the inertial systems to the phugoid oscillation.

### 5.1.2.2 Day 2 Inter-Comparison

For the LTN 101 on Day 2 only RISG results are available due to a logging computer malfunction, and therefore only a comparison of RISG results between the two systems on Day 2 is possible. The results of the comparison are displayed in Table 5.10. Again, since the RMS of the differences is computed it must be divided by $\sqrt{2}$ to get the standard deviation for one inertial system.

| FLIGHT | RISG (LRF) v. RISG (LTN) | | | |
|--------|--------|--------|--------|---------|
| LINE # | 30 sec | 60 sec | 90 sec | 120 sec |
| 1 | | | | |
| 2 | 44.1 | 8.0 | 4.4 | 3.9 |
| 3 | 70.0 | 10.2 | 4.3 | 3.8 |
| 4 | 44.7 | 9.7 | 3.9 | 2.3 |
| 4 | 46.8 | 8.4 | 4.4 | 2.8 |
| 6 | 40.8 | 6.8 | 3.7 | 3.3 |
| 7 | 64.4 | 7.6 | 3.4 | 3.0 |
| 8 | 47.3 | 12.2 | 7.0 | 4.4 |
| 9 | 127.7 | 14.6 | 9.2 | 6.4 |
| 10 | 92.6 | 14.7 | 6.1 | 4.4 |
| 11 | 191.3 | 63.8 | 34.6 | 24.4 |
| 12 | 421.6 | 272.4 | 214.4 | 174.8 |
| 13 | 46.9 | 20.1 | 6.1 | 3.4 |
| 14 | 39.7 | 12.4 | 7.4 | 4.6 |
| Avg(11) | 66.1 | 11.4 | 4.6 | 4.1 |
| σ | 46.8 | 8.0 | 3.9 | 2.9 |

**Table 5.10:** Day 2, LRF v. LTN Residual Differences (mGal), Same DGPS Combination

In Table 5.10 flight lines 11 and 12 have been omitted from the calculation of average RMS and σ values. The large differences for these lines appears to be caused by errors in the LTN 101 estimate. This can be verified by examining Table 5.4 which

shows the LTN 101 comparison with the upward continued reference. In general, the comparison of the RISG results for Day 2 does not show the same level of agreement as those for Day 1. The larger discrepancy is caused by larger errors in the LTN 101 estimates, as can be verified by examining Table 5.4. The possible reason for the higher noise level of the LTN 101 results for Day 2 has been discussed in section 5.1.1.2.

Despite the higher level of disagreement between the RISG results for the two systems on Day 2 an interesting observation can still be made. For both the LRF III and the LTN 101 the RISG results when compared to the upward continued reference for flight lines 2 and 3 are quite poor (see Tables 5.3 and 5.4). However, the inter-comparison of the two systems for these flight lines shows good agreement. Since the two system estimates were computed using the same DGPS acceleration it can be argued that the DGPS acceleration error has been eliminated by differencing. However, no combination of master-remote receiver pairs provided significantly different accelerations for these two flight lines. In addition, the SISG results for these two flight lines are good for the LRF III (Table 5.3). This result is puzzling because if the error is due to erroneous DGPS acceleration it should also affect the SISG results, unless the error is only in the horizontal GPS acceleration. An error that affects only horizontal GPS acceleration and not vertical acceleration is highly unlikely due to the high correlation between coordinates in a DGPS solution. A more detailed examination of these results, as well as suggestions for possible sources of the error, will be given in section 6.2.

### 5.1.2.3 Day 3 Inter-Comparison

A comparison of the RISG and SISG results for the LRF III and LTN 101 for Day 3 of the September 1996 flight test is presented in Table 5.11. Flight lines 12, 13 and 14 are omitted because no data was available for the LTN 101. The last two lines give the average RMS values and standard deviations for the remaining eleven flight lines. Because the RMS of the differences was computed the values must be divided by $\sqrt{2}$ to get the standard deviation for one inertial system.

| FLIGHT | SISG (LRF) v. SISG (LTN) | | | | RISG (LRF) v. RISG (LTN) | | | |
|--------|--------|--------|--------|---------|--------|--------|--------|---------|
| LINE # | 30 sec | 60 sec | 90 sec | 120 sec | 30 sec | 60 sec | 90 sec | 120 sec |
| 1 | 36.2 | 16.2 | 4.9 | 3.1 | 36.7 | 16.4 | 4.8 | 3.0 |
| 2 | 31.4 | 6.4 | 3.4 | 1.8 | 32.2 | 6.9 | 3.6 | 2.4 |
| 3 | 71.4 | 12.4 | 4.1 | 2.0 | 71.8 | 12.4 | 4.4 | 2.1 |
| 4 | 84.1 | 12.4 | 3.2 | 1.4 | 84.3 | 12.0 | 3.7 | 2.1 |
| 4 | 66.3 | 11.0 | 2.9 | 2.1 | 66.9 | 10.8 | 2.8 | 2.2 |
| 6 | 46.8 | 7.8 | 4.3 | 3.0 | 46.3 | 7.9 | 4.9 | 3.8 |
| 7 | 44.6 | 10.4 | 3.6 | 1.8 | 44.6 | 10.7 | 3.7 | 2.4 |
| 8 | 66.3 | 11.6 | 3.4 | 1.8 | 64.8 | 11.9 | 4.4 | 2.8 |
| 9 | 49.4 | 9.1 | 3.2 | 2.3 | 60.6 | 9.2 | 3.4 | 2.6 |
| 10 | 49.4 | 6.7 | 2.9 | 2.4 | 40.1 | 6.6 | 4.0 | 2.6 |
| 11 | 43.4 | 7.9 | 4.0 | 3.1 | 44.0 | 9.2 | 9.8 | 7.9 |
| 12 | | | | | | | | |
| 13 | | | | | | | | |
| 14 | | | | | | | | |
| AVG(11) | 44.4 | 10.2 | 3.6 | 2.3 | 44.9 | 10.4 | 4.4 | 3.1 |
| σ | 39.3 | 7.2 | 2.6 | 1.6 | 39.6 | 7.3 | 3.2 | 2.2 |

**Table 5.11:** Day 3: LRF v. LTN Residual Difference (mGal), Same DGPS Combination

The system agreement in Table 5.11 is slightly worse than the agreement for Day 1 (Table 5.7). This is despite the fact that the flight was at a higher elevation (less turbulence) and the same DGPS combination was used to create Table 5.10 (Table 5.7 used different DGPS pairs). The poorer agreement for Day 3 seems to be mostly due to problems with the LTN 101 estimates. These problems are discussed in section 5.1.1.3.

## 5.1.3 Crossover Point Comparison

The final method of evaluating the September 1996 test is to compare gravity estimates at crossover points. Crossover points between Day 1 and Day 2 can be analyzed because these two flight tests were performed at approximately the same elevation. The results give an estimate of the long-term repeatability of the system estimates. A detailed description of the adjustment performed for crossover point analysis can be found in section 4.3. The first eleven flight lines from Day 1 and Day 2 were used for the LRF III to form 121 crossover points. For the RISG results the first three flight lines of Day 2 are omitted for a total of 88 crossover points. The RISG and

SISG results for the crossover point comparison are presented in Table 5.12. Because the RMS of the differences was computed the values aree divided by $\sqrt{2}$ to get the standard deviation ($\sigma$) for one estimate.

| Diff | SISG | | | | RISG | | | |
|------|--------|--------|--------|---------|--------|--------|--------|---------|
| (mGal) | 30 sec | 60 sec | 90 sec | 120 sec | 30 sec | 60 sec | 90 sec | 120 sec |
| RMS | 10.7 | 3.2 | 2.3 | 2.6 | 11.7 | 3.9 | 3.4 | 3.4 |
| $\sigma$ | 7.6 | 2.3 | 1.6 | 1.8 | 8.3 | 2.8 | 2.4 | 2.4 |

**Table 5.12:** Crossover Point Comparisons (mGal), LRF III, Day 1 and Day 2

For the SISG results the standard deviations are 1.6 and 1.8 mGal for the 90 and 120 second filtering periods respectively. The RISG results again are slightly worse. The crossover adjustment results indicate that 90 seconds is the optimal filtering period for these flight conditions. The 120 second filter appears to over-smooth the resulting estimates. These results correspond quite closely to the combined expected noise levels of the LRF III accelerometers and the DGPS accelerations that were presented in section 3.2.

## 5.2 June 1998 Flight Test Results

Three days of testing were performed in June 1998. Three independent gravity estimation systems were flown, the U of C LRF III strapdown inertial system, the Lacoste and Romberg S-99 air/sea gravimeter, and an orthogonal triad of QA 3000 accelerometers. Unfortunately, the accelerometer triad was not operational during the flight tests, and therefore, results will only be presented for the Lacoste and Romberg and LRF III systems. Additionally, on the third day of testing a brief power problem in the airplane caused a malfunction of the strapdown INS data-logging computer. As a result, there is no strapdown inertial data available for the third day.

A total of five flight lines were flown for the first two days of testing. These lines will be denoted by A, B, C (June 6th) and F and G1 (June 8th); see Figure 3.10. Flight

lines A and G1 were partly flown over top of existing shipborne gravity profiles, and therefore an independent reference is available for these lines.

In order to provide a common basis of comparison for the two system estimates similar filtering operations must be applied to each. The data processing scheme for the LCR gravimeter utilized by KMS filters the final gravity estimates with a second order Butterworth filter to a frequency of 0.005 Hz, or a period of 200 seconds (Arne Olesen, pers. comm.). Therefore, the LRF III gravity estimates were also low-pass filtered to the same cut-off frequency. It should be noted that the identical filter was not used, only the same cut-off frequency. Therefore, distortion due to transfer function differences between the two filters may also cause discrepancies in the results. However, it is expected that this effect will be negligible compared to the overall system errors.

The same DGPS position estimates were used to determine aircraft kinematic acceleration for both systems. Obviously, the position estimates must be differentiated twice to determine acceleration. KMS utilizes a first-order Taylor Series central difference approximation to differentiate the data (Arne Olesen, pers. comm.). The U of C acceleration estimate is computed using a low-pass FIR differentiating filter. Bruton et al. (1999) describe and compare these two methods of differentiation. The conclusion in this reference is that these two methods of differentiation are nearly equivalent for the frequency band of interest in airborne gravity.

Therefore, differences in the relative estimates between the LCR and the LRF III systems should represent the combined noise levels of the two systems' specific force estimates plus any differences due to lever arm effects. In order to compensate for the lever-arm effect the offset between the LCR and LRF III was used along with the strapdown INS angular velocities to compute a lever arm velocity (see equation 2.14). This velocity was then differentiated to compute a relative lever-arm acceleration that was subsequently low-pass filtered to 200 seconds. The filtered lever-arm acceleration corrections were then applied to the LRF III data. Figure 5.6 shows the magnitude of this lever-arm correction for flight line F.
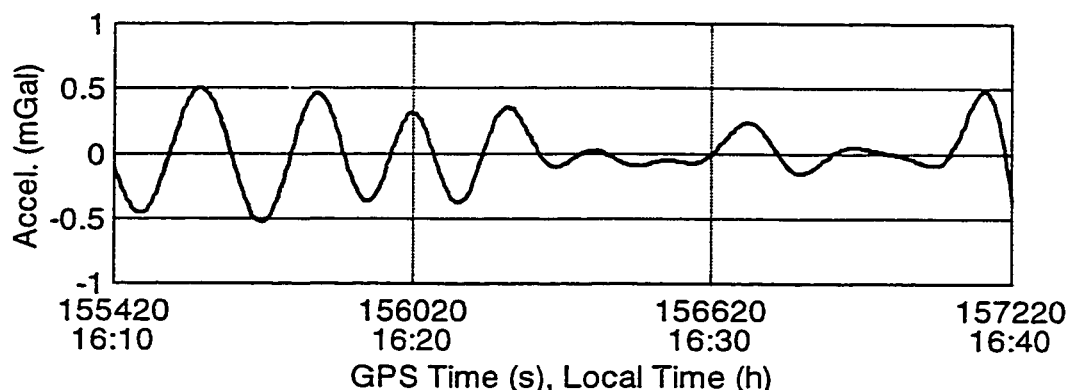
**Figure 5.6:** Relative Lever-Arm Acceleration, Flight Line F ($T_c$ = 200 sec)

The results of the comparison between the LCR and the LRF III estimates are displayed in Table 5.13. All five flight lines are shown, along with comparisons for both the RISG and SISG approaches using the LRF III data. The RMS of the differences was computed, and therefore, these values are divided by $\sqrt{2}$ to get an idea of the standard deviation ($\sigma$) for each measuring unit. It should also be noted that a linear bias has been removed between the two system estimates. The linear biases have a slope of approximately 0.01 mGal/s.

| Flight | LCR v. SISG | | LCR v. RISG | |
|--------|------|------|------|------|
| Line | RMS | $\sigma$ | RMS | $\sigma$ |
| A | 2.4 | 1.7 | 2.9 | 2.0 |
| B | 3.0 | 2.1 | 3.6 | 2.4 |
| C | 1.4 | 1.1 | 1.9 | 1.4 |
| F | 7.7 | 4.4 | 19.1 | 13.4 |
| G1 | 4.0 | 2.9 | 14.0 | 9.9 |

**Table 5.13:** Comparison of LCR and LRF III Gravity Estimates, in mGal ($T_c$ = 200 sec)

Two of the lines flown during the Greenland test (A and G1) were partly along existing shipborne gravity profiles. This allowed an independent check of the individual system estimates. The results of the comparison between the system estimates and the shipborne gravity are displayed in Table 5.14. Plots showing the individual system estimates and the reference are displayed in Figure 5.7, 5.8, and 5.9 for flight lines A, F and G1 respectively.

| Flight | LCR | LRF III | |
| Line | | SISG | RISG |
| A | 1.7 | 2.0 | 2.7 |
| G1 | 2.3 | 3.8 | 16.0 |

**Table 5.14:** Comparison of LCR and LRF III with Reference, in mGal ($T_c = 200$ sec)
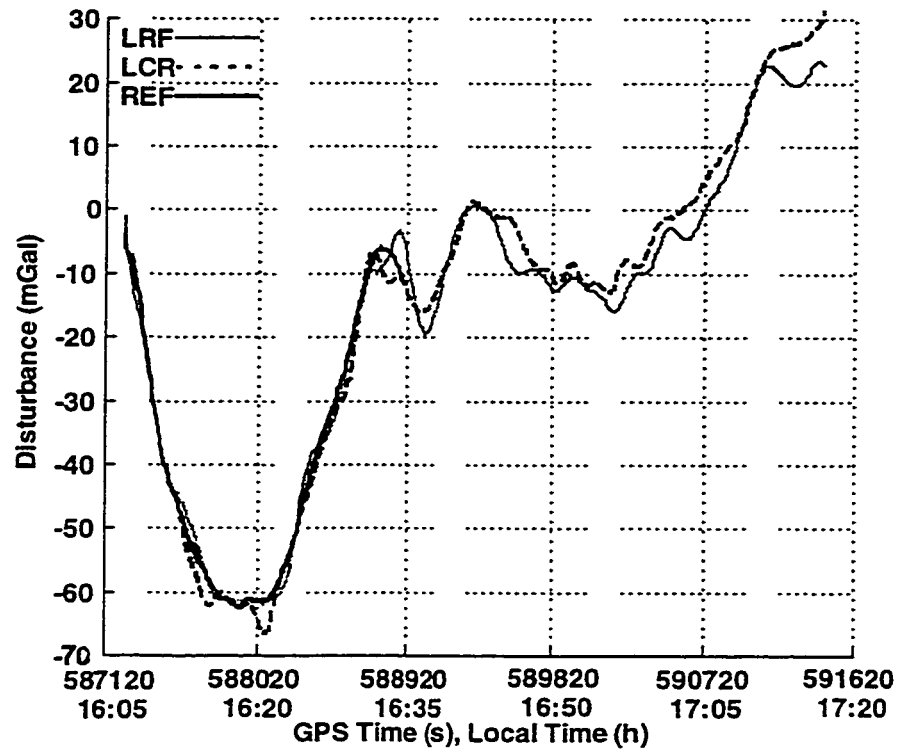


**Figure 5.7:** Reference, LCR and LRF III (SISG) Estimates, Line A, June 6 ($T_c = 200$ sec)
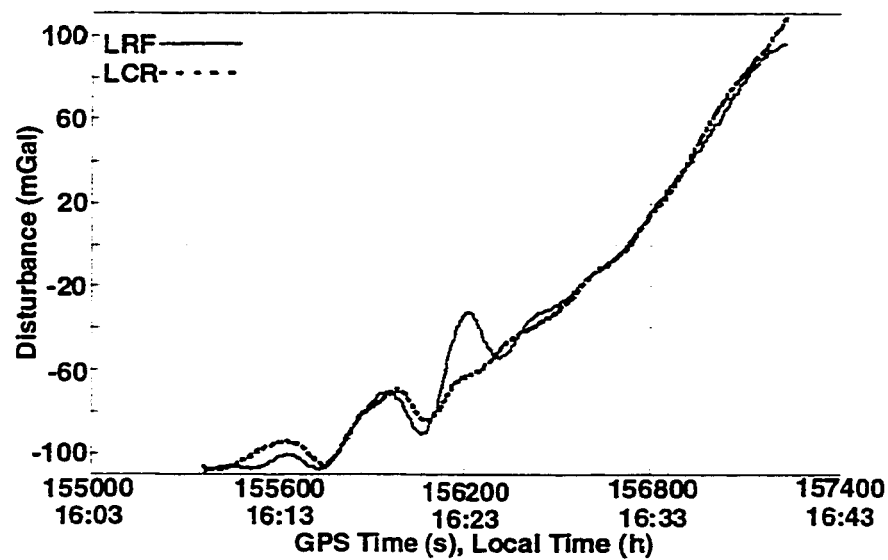


**Figure 5.8:** LCR and LRF III (SISG) System Estimates, Line F, June 8 ($T_c = 200$ sec)
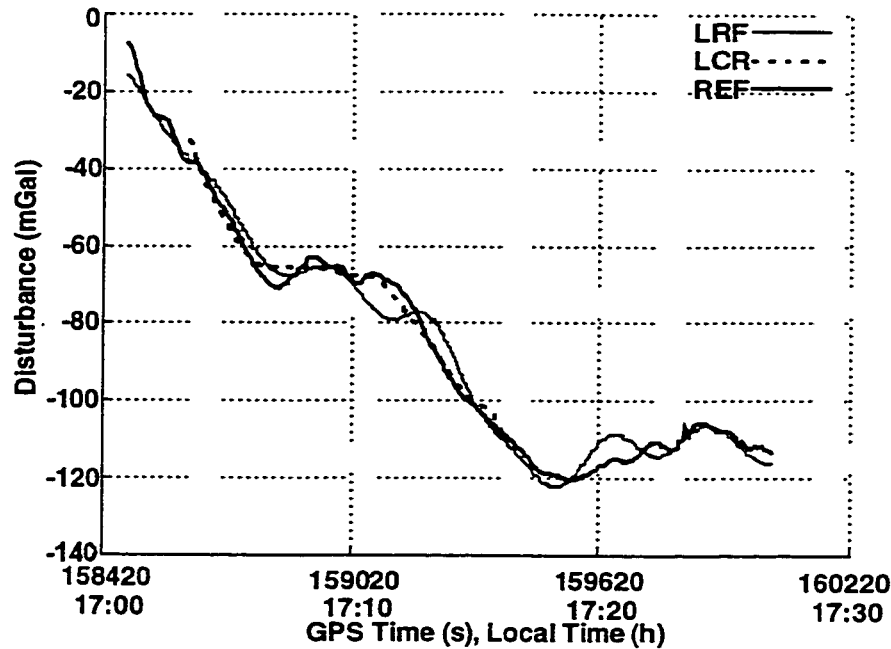
**Figure 5.9:** Reference, LCR and LRF III (SISG) Estimates, Line G1, June 8 ($T_c$=200 sec)

For June 6th (Lines A, B, C) the agreement between the LRF III and LCR estimates is quite good, with an average RMS difference of 2.3 mGal for the SISG estimates and 2.8 mGal for the RISG estimates. These agreements would appear to be close to the combined expected noise levels of the two measuring systems. Crossover point results for the LCR system from the AGMASCO project yielded RMS differences of 2.3 mGal (Olesen et al., 1997), and the LRF III system showed a noise level of 1.6 mGal for crossover point results (section 5.1.3). The RISG results show slightly poorer agreement, which is consistent with the conclusions of the September 1996 test. In addition, for flight line A, the LCR and LRF III estimates also agree quite well with the ship gravity reference. This excellent agreement is displayed in Figure 5.7. Note that the LCR data is not available for the first five minutes of flight line A. This is due to a problem nulling the LCR gravimeter at the beginning of the flight line.

The agreement between the system estimates for the second day (June 8th, Lines F and G1) are worse than those found for the first day. The difference between the SISG and LCR estimates is fairly large. In addition, the RISG estimates show considerably worse results for this second day. Figure 5.8 displays a graph of the LRF III SISG and LCR gravity disturbance estimates for flight line F. The graph shows that the two

estimates agree quite well, except for a three minute period in the LRF III estimate at approximately 156200 seconds. In fact, if this deviation is removed the RMS agreement between the two estimates is below 3.0 mGal, which is consistent with the June 6th results. The RISG results also show a large jump in their residuals at approximately the same time, which explains their poor performance.

The estimates for flight line G1 are given in Figure 5.9. Note that the LCR estimate is only available for approximately half of the flight line displayed, as some data at both ends had to be discarded due to hardware problems. The agreement between the LCR and the reference is quite good. However, the LRF III SISG estimate shows two small jumps at approximately 159150 and 159650. Again if these small jumps are ignored the LRF III and LCR estimates show the same level of agreement as June 6th. The RISG results show larger jumps at these two time periods, and therefore, the RISG results are considerably worse.

At the current time there is no reasonable explanation for the three jumps experienced in the LRF III estimates on flight lines F and G1. There does not appear to be any significant changes in aircraft dynamics at these time periods. In fact, the aircraft dynamics experienced on June 8th are not significantly different from those on June 6th. It simply appears that there is an unexplained irregularity in the LRF III data. This is confirmed by examining Figure 5.10, which shows the difference between the INS predicted easting and DGPS easting at one second intervals immediately before the INS Kalman filter is updated.
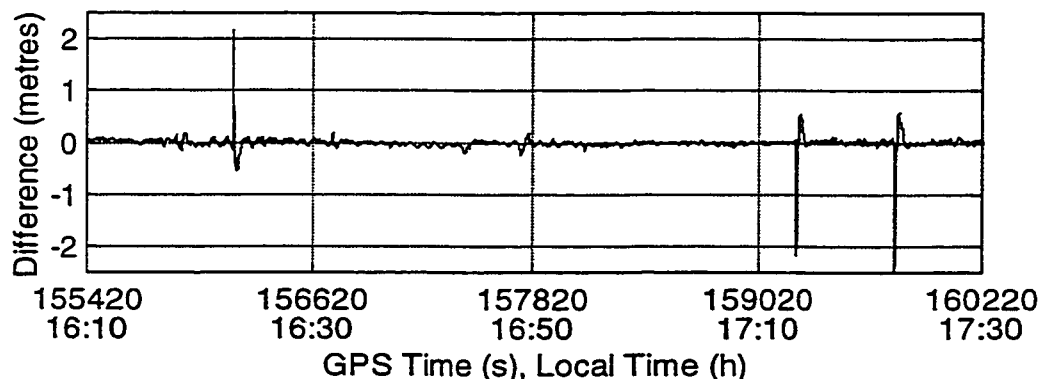


**Figure 5.10:** Difference Between INS Predicted Easting and DGPS Easting Update (One Second Update Interval), June 8th, 1998

Figure 5.10 clearly shows three large discrepancies between the INS and DGPS easting estimates at the exact time periods of the jumps in the LRF III gravity estimates. The periods of large differences between the INS and DGPS positions at each jump lasts approximately 60 seconds. At the present time the cause of these irregularities is unknown. To the author's knowledge this is the first time in which these type of discrepancies have appeared in an airborne data set collected with the LRF III inertial system, and therefore, they should be considered an extremely rare occurrence.

Based on the analysis of profiles A, B, and C it can be concluded that the accuracy of relative gravity determination from the LRF III unit and the LCR gravimeter appear to be at the same level. An RMS agreement of approximately 2 − 3 mGal is obtained for all three lines. The three jumps in the LRF III results on June 8th need further examination. To put them into perspective, they account for a total of about 9 minutes (out of 265 minutes of gravity profiles). A total of 22 minutes of data was discarded for the LCR system due to erroneous results. It can be concluded that the strapdown INS/DGPS approach to airborne gravity gives the same level of gravity field information as the more established LCR gravimeter. Because it is a fully digital system, airborne gravity by strapdown INS/DGPS has better potential for in-flight and post-mission outlier detection and data analysis.

All results for the June 1998 test in Greenland were obtained using a low-pass filter with an averaging time of 200 seconds. This filtering period was used because the LCR data is normally filtered to this level. However, the strapdown INS estimates presented for the September 1996 test showed very good results with 60, 90 and 120 second filter lengths. Initially, these filtering periods were also used for the Greenland strapdown INS data. However, the results were significantly worse than those found in the September 1996 test. A detailed analysis has shown that the GPS data collected in Greenland were of significantly poorer quality than that obtained in September 1996. For example, the typical size of the double difference phase residuals was 5 to 10 times larger and showed significant short and long-term oscillations. The most likely source for this increase in the residual errors is high ionospheric activity during the test. A geomagnetic

observatory located in Greenland reported significant geomagnetic activity during both the $6^{th}$ and $8^{th}$ of June (Kyoto, 1998).

## 5.3 Selection of the Optimal Filtering Period

It has previously been stated that the filtering period used for strapdown airborne gravity cannot be blindly chosen. Several criteria must be weighted before making this choice. Obviously, the most important question to be answered is what type of accuracy and resolution of gravity disturbances is required. Secondly, and closely linked to the first question is the flight speed. The faster the airplane flies the shorter the filtering period required to give the same resolution. Thirdly, the variation in the gravity field under the flight area needs to be considered. For a rough gravity field a shorter filtering time is required in order to extract all of the features. When flying in an area with an unsurveyed gravity field it may be difficult to quantify the gravity field variation. However, some information may be inferred from the topography of the area; in general rough topography will give larger variations of the gravity field. Finally, the expected noise levels of the INS specific force and DGPS acceleration must be considered. The INS specific force noise level is very predictable (except for vibrations) and should not vary from flight to flight; a good indication of the INS noise can be obtained from a static data set. The DGPS acceleration errors are more difficult to quantify because they are not constant and depend on a variety of environmental factors such as: multipath, the troposphere, ionosphere activity, satellite geometry, and baseline length. There does not seem to be any way to reliably predict DGPS acceleration accuracy, and therefore DGPS acceleration accuracy appears to be a critical factor in the final choice of a filtering period. This can be verified by comparing the June 1998 and September 1996 tests. The June test used a filtering period that was twice as long as the September test because the DGPS accelerations were noisy due to increased ionosphere activity. Therefore, although expected values for the filtering period can be inferred prior to flying, it would appear that the most reliable way to choose the final filtering period is through careful post-mission analysis of the data and results by an experienced operator.

# CHAPTER 6
## Multiple Observations of the Gravity Signal

In principle, strapdown inertial systems allow the estimation of the gravity signal in two ways, using the RISG and the SISG approach. The question that arises is do these two approaches exhibit significantly different errors? If they do, then an advantage might be obtained by combining the two solutions. Alternatively, one method could be used as a consistency check for the other. In Chapter 2, the error models of the RISG and SISG approaches were theoretically compared and examined under actual aircraft dynamics. It was found that the errors for the two approaches were similar, and that minimal advantage would likely result from combining the two solutions. To validate the conclusions of the error model analysis, a comparison of RISG and SISG results from a whole day of testing are presented and discussed. Based on this comparison and analysis some possible problems with the RISG approach that were uncovered are also examined. Finally, a discussion of possible accuracy improvements using independent multiple observations of the gravity vector is presented. The test data from September of 1996 is analyzed to determine the improvement in accuracy obtained when multiple measurements of specific force or multiple measurements of kinematic aircraft acceleration are combined.

## 6.1 Comparison of SISG and RISG Results

Section 2.3 demonstrated that the errors for the SISG and RISG approaches should be quite similar. In order to verify the expected small differences between the two approaches a comparison of the RISG and SISG results for one day of testing in September 1996 was undertaken. The SISG and RISG estimates were compared at the four filtering periods (30, 60, 90 and 120 sec.) for all fourteen flight lines of Day 1 of the test. The results of the comparison are given in Table 6.1. An average spectrum of the residuals between the two approaches is also given in Figure 6.1.

| $T_c$ | 30 sec | 60 sec | 90 sec | 120 sec |
|---|---|---|---|---|
| RMS Diff | 3.8 | 2.5 | 2.7 | 2.7 |

**Table 6.1:** Comparison of RISG and SISG Estimates (mGal), Day 1
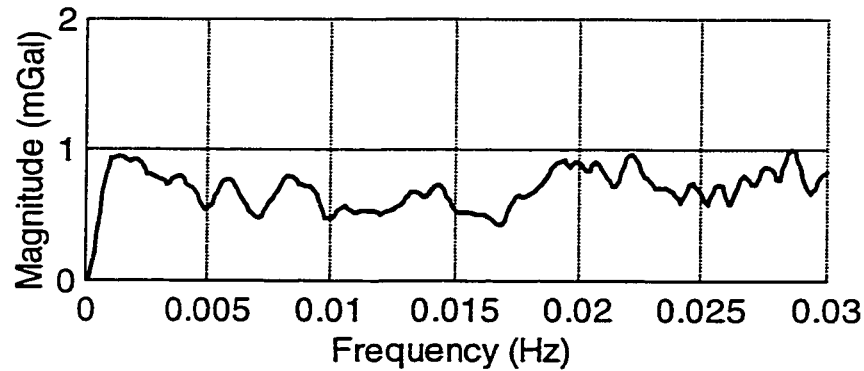


**Figure 6.1:** Average Spectrum of Residuals, RISG v. SISG Estimates, Day 1

The results in Table 6.1 and Figure 6.1 were generated using the same DGPS acceleration estimates. Therefore, the differences presented in the table and figure should be due only to differences in estimation approaches plus possible differences due to the filtering process applied to the data (for a further discussion, see section 6.2). An analysis of Figure 6.1 shows that the average residual spectrum resembles white noise with an amplitude of approximately 1.0 mGal. It is interesting to note that there is no noticeable increase in the residual spectrum in Figure 6.1 at the phugoid oscillation period.

If the residual differences truly have white noise characteristics, then an averaging of the two solutions should give an improvement on the order of the RMS residual differences divided by $\sqrt{2}$. Therefore, the SISG and RISG solutions for Day 1 were averaged, and the resulting average was compared with the upward continued reference. The result of the averaged estimate compared with the reference is given in Table 6.2. The RMS residuals of the original RISG and SISG estimates with respect to the reference presented in Chapter 5 are also repeated here for convenience. The RMS values represent an average of the RMS for all fourteen flight lines on Day 1 of testing.

| Estimate Type | 30 sec | 60 sec | 90 sec | 120 sec |
|---|---|---|---|---|
| SISG | 10.9 | 3.8 | 3.2 | 3.5 |
| RISG | 11.9 | 4.3 | 3.8 | 4.3 |
| SISG/RISG Avg | 11.3 | 4.0 | 3.4 | 3.8 |

**Table 6.2:** Comparison of SISG, RISG and SISG/RISG Average Estimates with Upward Continued Reference (mGal), Day 1

The results in Table 6.2 clearly show that the residuals between the RISG and SISG estimates are not white noise. An averaging of the estimates merely averaged the individual RISG and SISG RMS residuals and did not offer any level of improvement. Based on these results it is reasonable to conclude that an averaging of the RISG and SISG results will not improve the results. Currently, the best results are obtained simply by using a SISG estimate.

## 6.2 Possible Problems with the RISG Approach

In the analysis of the agreement of the RISG estimates with the upward continued reference in Chapter 5 some anomalous flight lines can be found, for example, flight lines 1, 2 and 3 on Day 2, and flight line 1 on Day 3. For these lines the SISG agreement with the reference is quite good, however, the RISG results for these flight lines are poor. This seems to contradict the conclusions of sections 2.3 and 6.1 that the errors for the RISG and SISG approach are similar, and therefore further investigation is warranted. Flight line 2 from Day 2 has been selected for a detailed analysis.

In Chapter 5 the RISG and SISG estimates for line 2 of Day 2 were compared with the upward continued reference. RISG results were available for both INS systems, while SISG results were only available for the LRF III. In addition, the RISG estimates of the two systems were also compared. For convenience, a summary of these comparison results is given in Table 6.3.

| Comparison | 30 sec | 60 sec | 90 sec | 120 sec |
|---|---|---|---|---|
| LRF SISG v. Reference | 9.2 | 2.9 | 2.7 | 3.1 |
| LRF RISG v. Reference | 28.0 | 22.3 | 19.2 | 17.6 |
| LTN RISG v. Reference | 54.6 | 23.9 | 20.5 | 18.9 |
| LRF RISG v. LTN RISG | 55.1 | 8.0 | 4.5 | 3.9 |

**Table 6.3:** Comparison Results, Flight Line 2, Day 2 (mGal)

The LRF III SISG results are quite good, while the RISG results for both systems are poor. However, the two RISG estimates agree quite well with each other (especially for the 60, 90 and 120 second filter periods). A plot of the residuals with respect to the reference for all three estimates is presented in Figure 6.2.
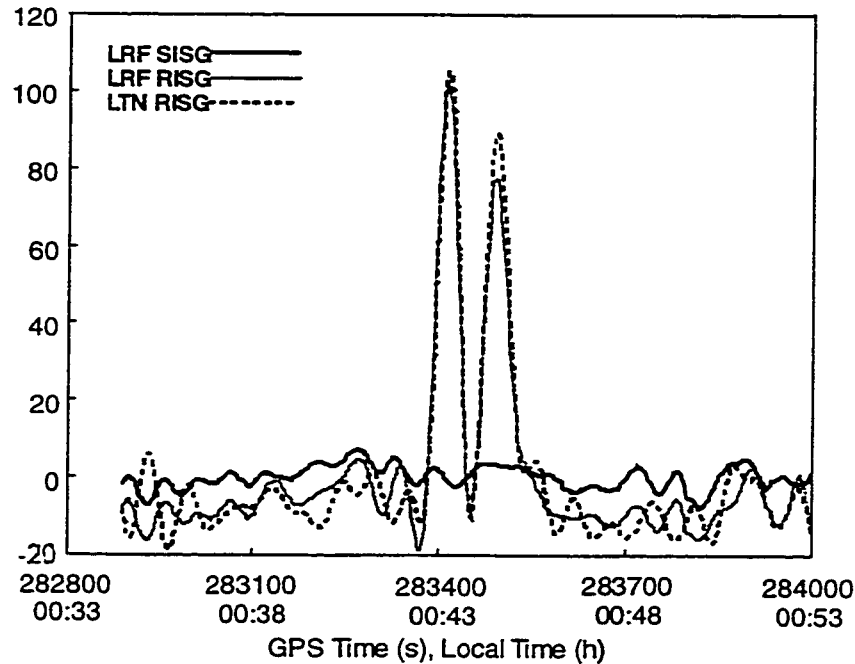


**Figure 6.2:** LRF RISG, SISG and LTN RISG Residuals, Comparison with Upward Continued Reference, Line 2, Day 2 ($T_c$ = 60 sec)

Figure 6.2 shows that in the middle of flight line two there are two large jumps in the RISG residual plots. The SISG results do not show the same jump. Therefore, this rules out possible errors in the vertical component of GPS or INS acceleration. The results for both inertial systems were computed using the same DGPS master-remote combination. This therefore points to a possible error in horizontal DGPS acceleration determination. However, an analysis of all possible combinations of master and remote pairs for this flight line has failed to show any significant differences in acceleration determination between receiver pairs. The average RMS differences for all combinations are near 2.0 mGal ($T_c$ = 60 sec). This cannot be considered significant given the size of the jumps in the RISG results. It is also possible that the results could be poor due to bad

satellite geometry. However, Figure 6.3 displays the PDOP for flight line 2 and clearly shows that this is not the case.
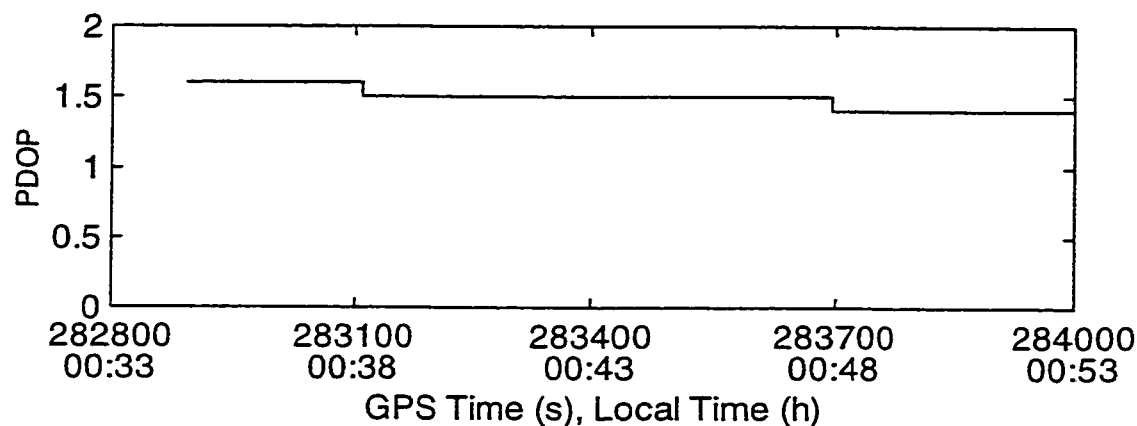


**Figure 6.3:** PDOP, Flight Line 2, Day 2

Seven satellites are tracked for the entire flight line, with no loss of lock or GPS cycle slips. In addition, the double difference phase residuals for the six satellite pairs do not show a significant jump or spike in the area of the large RISG residuals. Therefore, based on this evidence, it seems fairly certain that the error in the RISG results is not being caused by errors in horizontal DGPS acceleration. Other possible sources of this error could be the lever-arm correction, Coriolis correction, or possible INS specific errors. An analysis of the lever-arm correction and Coriolis correction show no significant jumps of the size of the errors in the RISG results, and therefore, errors in these corrections are considered an unlikely source of the problem.

A thorough analysis of the raw data and the data processing methods has not discovered the cause of the jumps in the RISG residuals. However, in the process of examining the data, an interesting correlation with the RISG residuals was observed. To explain the correlation a brief explanation of the INS data format and processing is first required.

The INS specific force data are output from KINGSPAD at the raw INS data collection rate, which is 50 Hz. KINGSPAD outputs six specific force measurements: the x, y and z accelerometer measurements in the b-frame, and the east, north, and up

accelerometer measurements that have been transformed from the b-frame to the l-frame by the gyroscope determined transformation matrix. The x, y and z measurements are used in the RISG approach, while the up measurement is used for the SISG approach. However, since GPS acceleration is only available at 1 Hz the INS data must first be low-pass filtered to 1 Hz. All six specific force measurements are individually low-pass filtered using the same response function. This low-pass filtering occurs in two steps, from 50 Hz to 10 Hz, and from 10 Hz to 1 Hz.

At 50 Hz, the magnitude of the specific force vector in the local level frame ($|f^l|$) is identical to the magnitude of the specific force vector in the body frame ($|f^b|$). However, after low-pass filtering to 10 Hz and 1 Hz, the two magnitudes are no longer identical. Figure 6.4 shows the differences in the specific force vector magnitudes at both 10 Hz and 1 Hz. Note the difference in scale between the top and bottom graphs.
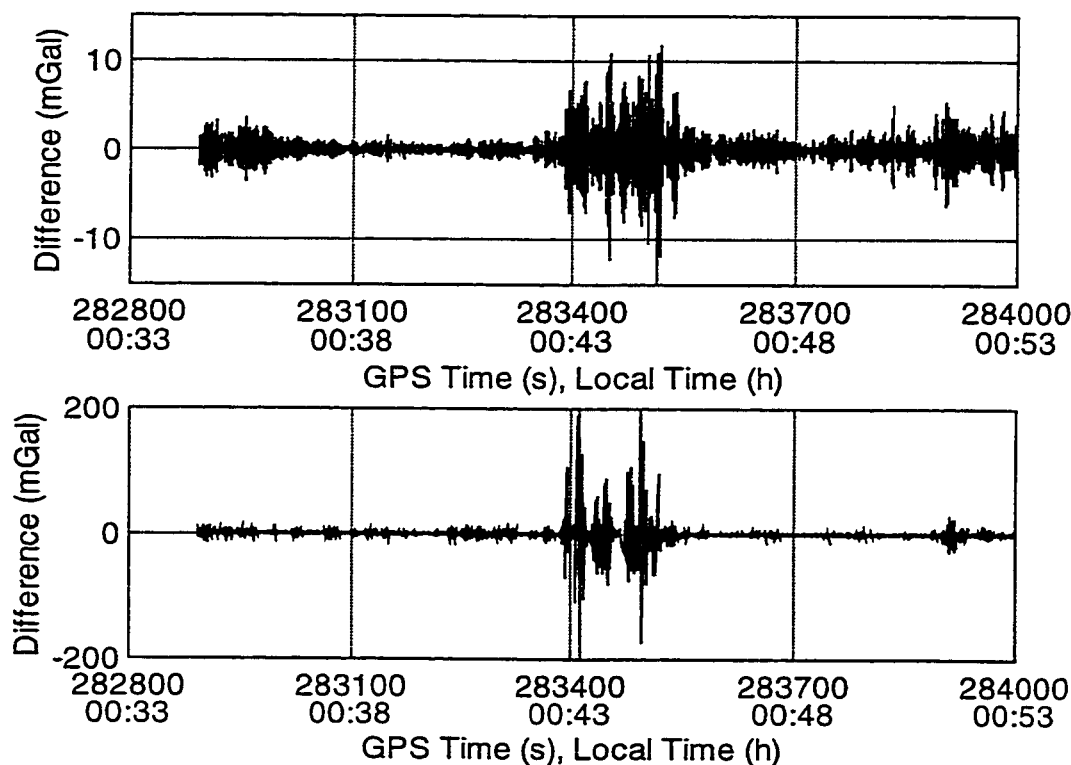


**Figure 6.4:** ($|f^b|$ - $|f^l|$) at 10 Hz (top) and 1 Hz (bottom), Flight Line 2, Day 2

Figure 6.4 clearly shows that the difference in vector length gets worse with more low-pass filtering. At time intervals where the vector lengths show larger discrepancies (eg. from 283400 – 283550) there is no significant change in the aircraft dynamics, i.e. the larger differences do not appear to be caused by, for example, atmospheric turbulence. The differences in the vector lengths are not a problem with the low-pass filter design; the error response of the filter is far too small to cause a significant deviation. The problem arises due to the fact that the six specific force measurements are low-pass filtered separately, and therefore, no property of vector length preservation is built into the filtering process. It was observed that the RISG residuals showed a high correlation with the difference in the specific force vector lengths at 1 Hz. Figure 6.5 shows a plot of the (RISG-SISG) residuals at a 30 second filtering period and the difference ($|f^b| - |f^i|$) at 1 Hz.
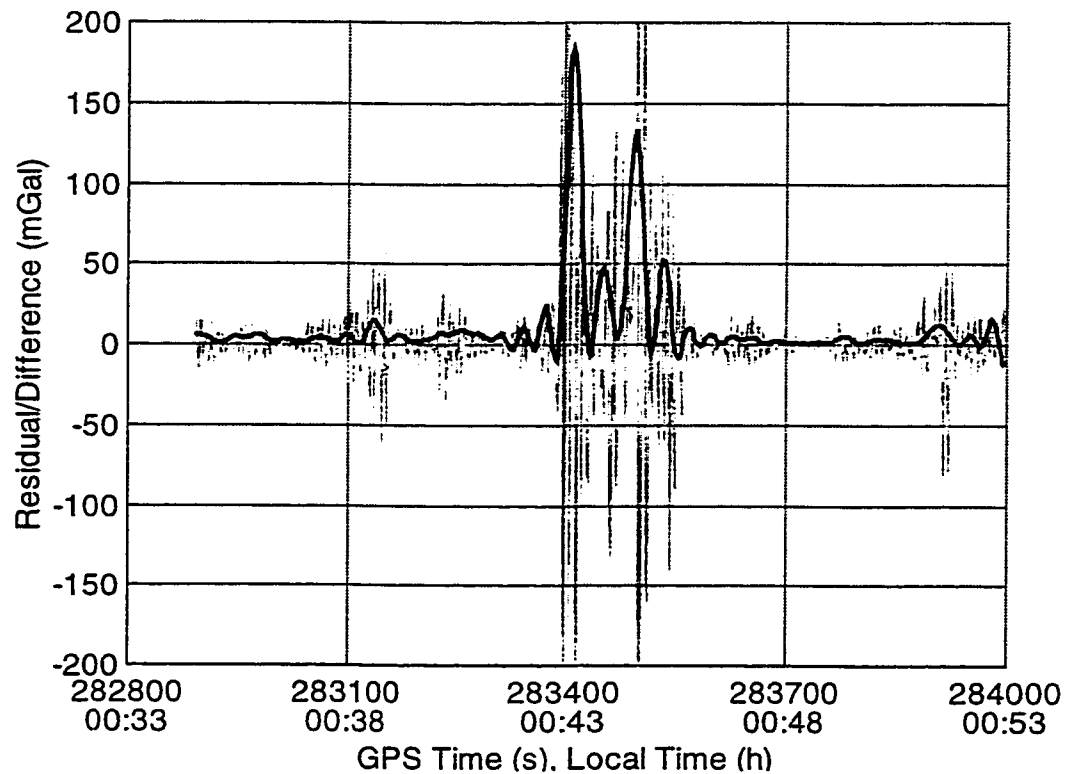


**Figure 6.5:** RISG-SISG at 30 sec. (black), and ($|f^b| - |f^i|$) at 1 Hz (grey), Flight Line 2, Day 2

It should be noted that similar correlation was found for all other flight lines examined. However, this does not mean that the problem is related to the non-preservation of vector length; it just shows a high degree of correlation with it. At the current time there is no reasonable explanation for the erroneous RISG results. Obviously, a resolution of this issue should be accomplished before a full-scale design and purchase of a RISG only configuration is undertaken. However, it should also be noted that of the three days of testing, totalling 42 flight lines and nearly 15 hours of flight time, large erroneous jumps only appeared four or five times and affected only about 10% of the flight lines. In addition, these jumps only caused problems for a portion of each affected flight line, and therefore, only about 1% of the RISG data was erroneous. If this percentage can be considered representative of all situations then this level of discarded data may be considered acceptable.

## 6.3 Improving Accuracy Using a Multi-Sensor Configuration

The analysis contained herein has so far concentrated on utilizing one set of sensors that allow a unique determination of the signal (gravity disturbances) of interest. To date there has been little work presented or published which deals with the possibility of multiple simultaneous observations of the gravity disturbances. Schwarz and Glennie (1998) have presented some preliminary analysis and ideas regarding multi-sensor configurations, and these ideas will be expanded upon here. A multi-sensor approach is an attractive alternative. The noise for two systems will be different, however, the signal will remain the same. Therefore, it is reasonable to suggest that a better separation of signal and noise can be expected. In addition, a multi-sensor approach obviously has a much better reliability than a single sensor system, as the possibility of all sensors failing simultaneously would be considerably lower. If the remaining sensor noise in the gravity disturbance estimates is white, then an improvement of 30% ( $\sqrt{2}$ ) can be expected by averaging the estimates. This would make the additional cost of multiple sensors very attractive, especially coupled with the increased reliability.

The September 1996 test allows a unique opportunity to explore the possibility of using multiple sensor configurations. Two inertial systems were flown in parallel, and there were two GPS receivers on the airplane and four reference GPS receivers on ground stations. Day 1 will be used for the analysis because the results of the two inertial systems are of similar quality for this flight test (see section 5.1.1.1) and there appear to be no flight lines which suffer from significantly degraded RISG results due to the problems discussed in section 6.2.

## 6.3.1 Multiple Specific Force Measurements

To determine the improvement in disturbance estimates using multiple specific force sensors the RISG and SISG estimates of the LTN 101 and LRF III were averaged. The averaged estimate was then compared with the upward continued reference. Table 6.4 lists the results of this comparison. The RMS values are averages for all fourteen flight lines. The comparison of the individual system estimates with the reference is also listed in Table 6.4.

| Estimate | SISG | | | | RISG | | | |
|----------|--------|--------|--------|---------|--------|--------|--------|---------|
| Type | 30 sec | 60 sec | 90 sec | 120 sec | 30 sec | 60 sec | 90 sec | 120 sec |
| LRF III | 10.9 | 3.8 | 3.2 | 3.5 | 11.9 | 4.6 | 4.1 | 4.6 |
| LTN 101 | 21.7 | 5.1 | 3.4 | 3.6 | 20.9 | 5.2 | 3.7 | 3.8 |
| Average | 11.9 | 3.9 | 3.1 | 3.4 | 11.7 | 4.4 | 3.7 | 4.1 |

**Table 6.4:** LRF, LTN, and LRF-LTN Average, RMS of Residuals with Reference (mGal), Day 1

Table 6.4 shows that the improvement in the gravity estimate is nowhere near the 30% improvement that would be expected if the remaining system errors were white noise. The improvements at the 90 and 120 second filtering periods are quite small, and considering the accuracy of the reference, may be considered negligible. The improvement at the 30 and 60 second filtering times is somewhat better, especially considering the fact that the LTN 101 estimates at these periods are considerably worse than the LRF III estimates. This would suggest that the higher frequency errors of the

INS systems are more like white noise. However, a flight test of two identical systems, or two systems of comparable accuracy across the spectrum, is needed to verify this.

The fact that the low frequency errors do not appear to be white noise makes the idea of multiple specific force measurements a little less attractive. It means that simple multi-sensor approaches such as mounting parallel vertical accelerometers on the same platform will not significantly improve the results. A more complex design of the system that takes into account the effect of aircraft dynamics on specific force estimation is most likely required. Obviously, a detailed analysis of accelerometer response under varying dynamics and configurations is required before a design could be selected which would significantly improve the accuracy of a multiple specific force measurement system.

## 6.3.2 Multiple Measurements of Kinematic Acceleration

Multiple observations of DGPS kinematic acceleration can also be utilized in an airborne gravity system. This is an attractive approach, as multiple ground stations can normally be set up quite quickly and easily. In addition, GPS receivers are considerably cheaper than an additional IMU for specific force estimation. To determine the improvement in gravity disturbance estimation, measurements using the LRF III with two different master-remote DGPS receiver pairs were averaged. The resulting estimate was then compared with the upward continued reference. Table 6.5 presents the results of this comparison. The RMS values given are an average of all fourteen flight lines. For comparison, the agreement of the individual estimates for the DGPS pairs with the reference are also given.

| DGPS | SISG | | | | RISG | | | |
|------|------|------|------|--------|------|------|------|---------|
| Estimate | 30 sec | 60 sec | 90 sec | 120 sec | 30 sec | 60 sec | 90 sec | 120 sec |
| Pair 1 | 10.9 | 3.8 | 3.2 | 3.5 | 11.9 | 4.6 | 4.1 | 4.6 |
| Pair 2 | 11.2 | 3.7 | 3.2 | 3.5 | 12.2 | 4.5 | 4.1 | 4.5 |
| Average | 10.5 | 3.5 | 3.1 | 3.5 | 11.5 | 4.4 | 4.1 | 4.5 |

**Table 6.5:** Individual and Averaged DGPS Acceleration Estimates, RMS of Residuals with Reference (mGal), Day 1

Table 6.5 shows that the improvement in accuracy for the averaged DGPS accelerations is negligible for the 90 and 120 second filtering periods. For the 30 and 60 second periods there is a small amount of improvement.

The DGPS acceleration average used to compute the results in Table 6.5 was simply that, an average of the two estimates. However, it is well known that DGPS errors have a time and spatial correlation. For discussions of these error sources the interested reader is referred to Tiberius (1998) or Raquet (1998). The spatial correlation therefore leads to the possibility of using more sophisticated techniques to try and estimate kinematic aircraft acceleration using multiple GPS reference and remote receivers. Additional methods of data combination were therefore tested. In the first method attempted, the simple averaging of the estimates was replaced by a weighted average. The acceleration estimates were weighted based on the distance between the master and remote receiver. The shorter the baseline distance, the higher the weight for that acceleration estimate. This weighting procedure did not produce results significantly different from the simple averaging of the accelerations.

Secondly, a more sophisticated method of combining multiple reference receivers, called NetAdjust, was tested. NetAdjust is a method based upon an optimal linear minimum variance estimator that uses multiple reference receivers to reduce differential GPS measurement errors. A detailed description of the NetAdjust algorithm is given in Raquet (1998). The NetAdjust method requires that the carrier phase ambiguities between reference receivers be fixed. Unfortunately, for the September 1996 test, the reference receiver at the Calgary airport was impossible to use in the NetAdjust method. This was because it was an L1 only receiver, and therefore, the ambiguities between it and the other reference receivers could not be fixed due to the long baseline lengths. As a result only the Banff and Invermere reference stations were used to calculate a NetAdjust DPGS acceleration for the aircraft. The results using the NetAdjust acceleration were nearly identical to the simple averaging of the independent receiver pair estimates. This result is most likely due to the fact that only two reference receivers were used. It is likely that using more than two reference receivers in the NetAdjust method would offer improvement over simple averaging. However, it is impossible to quantify the

improvement, and unfortunately a data set was not available to test the method with more than two reference receivers. In addition, the covariance function used in the NetAdjust method has been developed based on ground remote receiver positioning. It is likely that the form of the covariance function used would have to be modified in order to optimize the NetAdjust method for acceleration determination for airborne gravity.

In the course of examining the DGPS accelerations from the September 1996 and June 1998 tests, it was observed that the quality of the DGPS accelerations had a strong correlation with the double difference phase residuals of the DGPS position solution. In fact, the DGPS acceleration results were considerably improved by a method which monitored the phase residuals of individuals satellites and removed them from the solution for times when they showed significant deviation from expected levels. Based on these promising results it is proposed that a weighting scheme using the size of the phase residuals for different receiver pairs might provide better results than simple averaging. This is an attractive alternative to the NetAdjust approach due to its significantly reduced complexity.

# CHAPTER 7
## Conclusions and Recommendations

## 7.1 Conclusions

A detailed analysis of airborne scalar gravity by strapdown INS/DGPS using both the SISG and RISG approach was presented. The analysis encompassed both theoretical aspects and a numerical study using real data from two flight tests.

The first flight test in September 1996 allowed a detailed study of the accuracy and repeatability of airborne gravity by strapdown INS/DGPS. Two strapdown inertial systems were flown side-by-side over an area with dense ground gravity coverage. Therefore, the results could be compared in three ways: an inter-comparison of system estimates, a comparison with an upward continued reference, and a comparison of crossover point residuals. Based on this test, the following conclusions on system accuracy and repeatability were drawn:

- The prototype LRF III system showed a best agreement of 2.8 mGal with an upward continued reference when using the SISG method with a 90 second filtering time at a flight height of 4300 metres. This level of accuracy was obtained for both the north-south and east-west flight directions, and therefore the results showed no direction dependancy.

- At a flight height of 7300 metres the prototype system had an agreement with the reference of 1.1 mGal using the SISG approach. For the higher flight height a 120 second filter showed the best agreement. This shows that the filtering period must be chosen based on factors such as flight height, gravity field variation, and the accuracy of the sub-systems (INS and DGPS) used. The optimal period is therefore a trade-off between removal of measurement noise and over-smoothing of results.

- The RISG results for the LRF III were in general significantly worse than the SISG results, by as much as 30-40% over the three days of testing.

- Crossover point differences for the LRF III showed that the long-term accuracy of the SISG estimates was approximately 1.6 mGal. This accuracy is close to the combined expected noise level of the INS accelerometers and DGPS accelerations. Thus, it can be concluded that the resolution of the current prototype system has been reached. The RISG comparison at crossover points was approximately 30% worse than the SISG results.

- The LTN 101 inertial system that was also flown in the September 1996 test showed results which were less accurate than the LRF III. This was to be expected based on the higher noise level of the LTN accelerometers. The LTN-101 agreements with the reference were 3.4 and 2.1 mGal for the lower and higher flight heights, respectively.

- The accuracy of the gravity estimation results degrades significantly at the phugoid motion frequency for the airplane. The effect of phugoid motion appears to be inertial system dependent.

The September 1996 test flights are each nearly six hours in duration, and an accurate reference field is available for the entire flight. This allowed an analysis of the long-term drift of the prototype strapdown system's gravity disturbance estimates. The long-term drift showed a $3^{rd}$ order polynomial behaviour. It is felt that this effect is most likely due to a temperature dependency of the accelerometers. To analyze the short-term drift of the estimates a $3^{rd}$ order polynomial was removed from the raw accelerometer measurements. An attempt was then made to model the residual errors with both a Gauss-Markov and random walk process. However, the INS Kalman filter was unable to estimate the residual biases to the level of accuracy required. Adding the actual gravity disturbances to the normal graviy model in the mechanization did not significantly affect the long or short-term accelerometer bias estimation. It was concluded that the filtering scheme applied has reached its resolution in terms of accelerometer bias estimation. Therefore, accelerometers with better bias stability, or a method of correcting for the non-linear drift, possibly using other sources of gravity information in the flight area, is required to refer the relative airborne measurements to the absolute gravity field.

A theoretical analysis of the SISG and RISG approaches to airborne gravity showed that these two methods would show similar error characteristics if the b-frame was aligned with the l-frame, and if a constant height and velocity flight was undertaken. In order to verify this theoretical analysis a comparison of the error models for the two approaches was undertaken using actual aircraft dynamics for two flight lines. In addition, the RISG and SISG results for an entire day of the September 1996 test were compared. Based on the above investigation the following conclusions can be drawn.

- The RISG and SISG error models show similar characteristics. The RISG results are slightly worse due to an omission of the deflections of the vertical in the RISG formulation and erroneous results for approximately 1% of the RISG data.

- An averaging of the RISG and SISG results did not improve the gravity estimation results. The best results are obtained simply by using the SISG estimate. This shows that the residual errors for both approaches do not have white noise characteristics.

- The time synchronization accuracy required for airborne gravity by both the SISG and RISG approach is very stringent. It appears that the accuracy of time synchronization should be at the millisecond level for a filtering period of 30 seconds.

- There are some problems associated with the RISG approach on certain flight lines. Large erroneous results were observed with RISG on approximately 10% of the flight lines. At the current time the cause of this problem is unknown, however, it shows a high correlation with the non-preservation of vector length during the low-pass filtering of the INS specific force measurements. Although 10% of the flight lines were affected, only about 1% of the RISG data produced erroneous results.

An investigation of possible accuracy improvements using multiple observations of the gravity signal and kinematic aircraft acceleration was also undertaken. Again, the data from the September 1996 test was used. The two inertial systems flown in this test allowed the investigation of multiple specific force measurements. In addition, the multiple GPS receivers deployed during the test allowed several independent determinations of kinematic aircraft acceleration. Based on this investigation the following discoveries were made.

- An averaging of the specific force measurements from the two inertial systems did not significantly improve the accuracy of estimation at 90 and 120 seconds. There appeared to be a slight improvement for the 30 and 60 second averaging times.

- The small accuracy improvement obtained by simply averaging the specific force measurements shows that more complex multiple sensor configurations which take into account aircraft dynamics may be required. It is unlikely that the results will be improved by simple designs, for example, mounting several vertical accelerometers.

- A simple averaging, and a weighted average based on baseline distance, for two DGPS solutions did not provide a significant improvement in gravity estimation accuracy for 90 and 120 second filtering times. A slight improvement was observed at the 30 and 60 second filtering times however.

- A more sophisticated method of utilizing multiple GPS reference receivers, the NetAdjust method, showed the same results as averaging of the two independent acceleration estimates of the DGPS pairs. However, it is felt that this approach may show improvements with more than two reference receivers, and with a covariance function which has been modified for airborne acceleration determination.

Finally, the June 1998 test allowed the comparison of strapdown airborne gravity with the more established airborne gravity system using a modified LaCoste and Romberg air/sea gravimeter. The agreement between the two systems was at the 2-3 mGal level for a 200 second averaging time. This agreement appears to be at the expected level of the combined noise of the two systems. It shows that strapdown airborne gravity is a promising method, especially considering the fact that the averaging times required for the strapdown system appear to be significantly less than those required for the LCR gravimeter. In addition, the strapdown system allows more possibility for post-mission data analysis and error detection.

## 7.2 Recommendations

This detailed analysis has answered a number of questions regarding the accuracy and promise of strapdown airborne gravity. However, there are a number of areas in which significant further work is required. The following list attempts to state the areas where future effort should be concentrated.

- All of the comparisons undertaken in this thesis have been done at flight level. However, for the solution of the geodetic boundary value problems the gravity disturbances are needed at the boundary surface, i.e. the surface of the earth (Molodensky's problem) or on the geoid (classical boundary value problems). Therefore, a detailed analysis of the downward continuation of actual strapdown airborne gravity data is required.

- Strapdown airborne gravity shows high accuracy for relative gravity field determination. However, methods must be developed to refer these relative measurements to the absolute gravity field. These methods should focus on optimal merging of all data available in a flight area to provide the best estimates of gravity.

- Alternative methods of accelerometer bias estimation must be developed in order to compensate for the non-linear drift of the gravity disturbance estimates. Conversely, a system of accelerometers having a more stable bias could also be realized.

- An investigation into the differing response of INS systems to phugoid motion is needed, with the objective of estimating this effect rather than removing it by low-pass filtering. This would considerably increase the resolution of the system.

- Analysis of the response of the specific force estimates to aircraft dynamics to facilitate the intelligent formulation of a multiple sensor system is needed.

- The possible low frequency errors in the upward continued reference that were observed should be evaluated to determine their cause.

- Investigation into using the NetAdjust Method with more than two reference receivers and with a covariance model optimized for airborne acceleration determination should be undertaken. Additionally, an acceleration weighting scheme based on the double difference phase residuals should also be attempted.

- The problems encountered in the RISG approach should be examined to determine the cause of the poor results obtained for approximately 1% of the RISG data.

In the past four years strapdown airborne gravity has quickly reached a significant level of maturity. However, as can be gauged by the large number of recommendations given, considerable research needs to be done to further improve the system and processing methods. It is hoped that efforts in the near future will bring about the resolution of many of these remaining questions.

# REFERENCES

Argeseanu, V. (1995). Upward Continuation of Surface Gravity Anomaly Data. In: *Proc. of Airborne Gravity*, IAG Symposium G4, Boulder, Colorado, July 2-14, pp. 95-102.

Babister, A.W. (1980). *Aircraft Dynamic Stability and Response*. Permagon Press, Toronto.

Bastos, L., S. Cunha, R. Forsberg, A. Olesen, A. Gidskehaug, U. Meyer, T. Boebel, L. Timmen, G. Xu, M. Nesemann, K. Hehl (1998) An Airborne Geoid Mapping System for Regional Sea-Surface Topography: Application to the Skagerrak and Azores Areas. In: *Proc of International Association of Geodesy Symposia 'Geodesy on the Move'*. Forsberg R Feissel M Dietrich R (eds) Vol. 119, Springer Berlin Heidelberg NewYork, pp 30-36.

Boedecker, G., and H. Neumayer (1995). An Efficient Way to Airborne Gravimetry: Integrationof Strapdown Accelerometer and GPS. In: *Proc. of Airborne Gravity*, IAG Symposium G4, Boulder, Colorado, July 2-14, pp. 23-28.

Britting, K. (1971). *Inertial Navigation System Analysis*. Wiley-Interscience, Toronto.

Brown, R.G., and P.Y.C. Hwang (1992). *Introduction to Random Signals and Applied Kalman Filtering*, 2$^{nd}$ Ed. John Wiley & Sons Inc., Toronto.

Brozena, J.M., M.F. Peters and V.A. Childers (1997). The NRL Airborne Gravity Program. In: *Proc. of International Symposium on Kinematic Systems in Geodesy, Geomatics and Navigation (KIS97)*, Banff, Canada, June 3-6, pp. 553-556.

Brozena, J.M., and M.F. Peters (1994). Airborne Gravity Measurement at NRL. In: *Proc. of International Symposium on Kinematic Systems in Geodesy, Geomatics and Navigation (KIS94)*, Banff, Canada, August 30- September 2, pp. 495-506.

Brozena, J.M. (1992). The Greenland Aerogeophysics Project: Airborne Gravity, Topographic and Magnetic Mapping of an Entire Continent. In: *Proc. Of IAG Symposium G3: Determination of the Gravity Field by Space and Airborne Methods*, Springer Verlag, pp. 203-214.

Brozena, J.M., G.L. Mader, and M.F. Peters (1989). Interferometric Global Positioning System: Three-Dimensional Positioning Source for Airborne Gravimetry. *Journal of Geophysical Research*, 94, pp. 12153-12162.

Bruton, A.M., C. Glennie, and K.P. Schwarz (1999). Differentiation for High Precision GPS Velocity and Acceleration Determination. *GPS Solutions*, Vol. 2, No. 4.

Bryson, A.E. (1994). *Control of Spacecraft and Aircraft*. Princeton University Press, Princeton, New Jersey.

Childers, V.A., M.F. Peters and J.M. Brozena (1997). Error Analysis of the NRL Airborne Gravity System. In: *Proc. of International Symposium on Kinematic Systems in Geodesy, Geomatics and Navigation (KIS97)*, Banff, Canada, June 3-6, pp. 625-632.

Czompo, J. (1994). Airborne Scalar Gravimetry System Errors in the Spectral Domain. Ph.D. Thesis, *UCGE Report #20067*, Dept. of Geomatics Engineering, The University of Calgary.

Foote, S.A., and D.B. Grindeland (1992). Model QA-3000 Q-Flex Accelerometer: High Performance Test Results. In: *Proc. Of IEEE PLANS 92*, IEEE, Piscataway, NJ, pp. 534-543.

Forsberg, R., and S. Kenyon (1994). Evaluation and Downward Continuation of Airborne Gravity Data – The Greenland Example. In: *Proc. of International Symposium on Kinematic Systems in Geodesy, Geomatics and Navigation (KIS94)*, Banff, Canada, August 30- September 2, pp. 531-538.

Gelb, A., Editor. (1974). *Applied Optimal Estimation*. The M.I.T. Press, Cambridge, Massachusetts.

Glennie, C., and K.P. Schwarz (1999). A Comparison and Analysis of Airborne Gravimetry Results from Two Strapdown Inertial/DGPS Systems. Accepted by: *Journal of Geodesy*.

Glennie, C., and K.P. Schwarz (1997). Airborne Gravity by Strapdown INS/DGPS in a 100 km by 100 km Area of the Rocky Mountains. In: *Proc. of International Symposium on Kinematic Systems in Geodesy, Geomatics and Navigation (KIS97)*, Banff, Canada, June 3-6, pp. 619-624.

Hehl, K., L. Bastos, S. Cunha, R. Forsberg, A.V. Olesen, A. Gidskehaug, U. Meyer, T. Boebel, L. Timmen, G. Xu and M. Nesemann (1997). Concepts and First Results of the AGMASCO Project. In: *Proc. of International Symposium on Kinematic Systems in Geodesy, Geomatics and Navigation (KIS97)*, Banff, Canada, June 3-6, pp. 557-563.

Jekeli, C., and R. Garcia (1997). GPS Phase Accelerations for Moving Base Vector Gravimetry. *Journal of Geodesy*, 71, 10, pp. 630-639.

Klingele, E.E., M. Cocard, M. Halliday, H.G. Kahle (1996). The Airborne Gravimetric Survey of Switzerland. *Report Number 31, Contribution to the Geology of Switzerland – Geophysical Series*, Swiss Geophysical Commission.

Klingele, E.E., M.E. Halliday, M. Cocard and H.G. Kahle (1995). Airborne Gravimetric Survey of Switzerland. *Vermessung, Photogrammetrie, Kulturtechnik*, No. 4, pp. 248-253.

Klingele E.E., and M.E. Halliday (1995). Airborne Gravity Survey of Switzerland. In: *Proc. of Airborne Gravity*, IAG Symposium G4, Boulder, Colorado, July 2-14, pp. 109-115.

Knickmeyer, E. (1990). Vector Gravimetry by a Combination of Inertial and GPS Satellite Measurements. Ph.D. Thesis, *UCGE Report #20035*, Dept. of Geomatics Engineering, The University of Calgary.

Kyoto University (1998). *Provisional Geomagnetic Data Plots No. 17 – (January – June, 1998)*. Data Analysis Center for Geomagnetism and Space Magnetism, Graduate School of Science, Kyoto, Japan.

LaCoste, L.J.B. (1988). The Zero-Length Spring Gravity Meter. *Geophysics*, 7, pp. 20-21.

LaCoste, L.J.B. (1983) LaCoste and Romberg Straight Line Gravity Meter. *Geophysics*, 48, 5, pp. 606-610.

LaCoste and Romberg Model 'S' Air-Sea Dynamic Gravity Meter with 'Airsea 3.0' Digital Control System – Instruction Manual (1998). LaCoste and Romberg LLC, Austin, Texas.

Leick A. (1995). *GPS Satellite Surveying*, 2nd Ed. John Wiley & Sons Inc, Toronto.

Li, Z., and K.P. Schwarz (1994). Chaotic Behaviour in Geodetic Sensors and Fractal Characteristics of Sensor Noise. *Geodetic Theory Today, Third Hotine-Marussi Symposium on Mathematical Geodesy, IAG Symposium Series No. 114*, Springer-Verlag, pp. 246-258.

Maybeck, P.S. (1994). *Stochastic Models, Estimation, and Control, Volume I*. Navtech Book & Software Store, Arlington, Virginia.

Nettleton, L.L., L.J.B. LaCoste, and J.C. Harrison (1960). Tests of an Airborne Gravity Meter. *Geophysics*, 25, 1, pp. 181-202.

Olesen, A.V., R. Forsberg and A Gidskehaug (1997). Airborne Gravimetry Using the LaCoste and Romberg Gravimeter - An Error Analysis. In: *Proc. of International*

*Symposium on Kinematic Systems in Geodesy, Geomatics and Navigation (KIS97)*, Banff, Canada, June 3-6, pp. 613-618.

Raquet J.F. (1998). Development of a Method for Kinematic Carrier-Phase Ambiguity Resolution Using Multiple Reference Receivers. Ph. D. Thesis, *UCGE Report #20116*, Department of Geomatics Engineering, The University of Calgary.

Salychev, O.S. (1998). *Inertial Systems in Navigation and Geophysics*. Bauman MSTU Press, Moscow.

Salychev, O.S. (1995). *Inertial Surveying: ITC Ltd. Experience*. Bauman MSTU Press, Moscow.

Salychev, O.S., and K.P. Schwarz (1995). Airborne Gravimetric Results from the ITC-2 Inertial Platform System. In: *Proc. of Airborne Gravity*, IAG Symposium G4, Boulder, Colorado, July 2-14, pp. 125-141.

Savage, P. (1978). Strapdown Sensors. *AGARD Lecture Series No. 95, Strapdown Inertial Systems*.

Schwarz, K.P., and C. Glennie (1998). Improving Accuracy and Reliability of Airborne Gravimetry by Multiple Sensor Configurations. In: *Proc of International Association of Geodesy Symposia 'Geodesy on the Move'*. Forsberg R Feissel M Dietrich R (eds) Vol. 119, Springer Berlin Heidelberg NewYork, pp 11-17.

Schwarz, K.P., and M. Wei (1997). Inertial Surveying and INS/GPS Integration. *ENGO 623 Lecture Notes*, Department of Geomatics Engineering, The University of Calgary.

Schwarz, K.P., and Z. Li (1996). An Introduction to Airborne Gravimetry and its Boundary Value Problems. *Lecture Notes, IAG International Summer School*, Como, Italy, May 26 - June 7.

Schwarz, K.P., and M. Wei (1994). Some Unsolved Problems in Airborne Gravimetry. *IAG Symposium 'Gravity and Geoid'*, Graz, Austria, September 11-17, pp. 131-150.

Schwarz, K.P., O. Colombo, G. Hein, and E.T. Knickmeyer (1991). Requirements for Airborne Vector Gravimetry. In: *Proc. Of IAG Symposium No. 110, From Mars to Greenland: Charting Gravity with Space and Airborne Instruments*, Springer Verlag, New York, pp. 273-283.

Schwarz, K.P., and M. Wei (1990). A Framework for Modelling Kinematic Measurements in Gravity Field Applications. *Bulletin Géodésique*, 64, pp. 331-346.

Siouris, G.M. (1993). *Aerospace Avionics Systems – A Modern Synthesis*. Academic Press Inc., Toronto.

Škaloud, J. (1999). Optimizing Georeferencing by INS/GPS for Airborne Survey Systems. Ph. D. Thesis, Department of Geomatics Engineering, The University of Calgary (in preparation).

Škaloud, J. (1995). Strapdown INS Orientation Accuracy with GPS Aiding. M. Sc. Thesis, *UCGE Report #20079*, Dept. of Geomatics Engineering, The University of Calgary.

Thompson, L.G.D. (1959). Airborne Gravity Meter Test. *Journal of Geophysical Research*, 64, 488.

Thompson, L.G.D., and L.J.B. LaCoste (1960). Aerial Gravity Measurements. *Journal of Geophysical Research*, 65, 1, pp. 305-322.

Tiberius, C.C.J.M. (1998). Recursive Data Processing for Kinematic GPS Surveying. *NCG Netherlands Geodetic Commission*, Delft, The Netherlands.

Valliant, H.D. (1992). The LaCoste and Romberg Air/Sea Gravity Meter: An Overview. *CRC Handbook of Geophysical Exploration at Sea*, 2nd Ed. Hydrocarbons, CRC Press Inc, pp. 141-176.

Van Dierendonck, K.J., M.E. Cannon, M. Wei, and K.P. Schwarz (1994). Error Sources in GPS-Determined Acceleration for Airborne Gravimetry. In: *Proc. Of ION National Technical Conference*, San Diego, California, pp. 811-820.

Wei, M., and K.P. Schwarz (1998). Flight Test Results from a Strapdown Airborne Gravity System. *Journal of Geodesy*, 72, pp. 323-332.

Wei, M., and K.P. Schwarz (1996). Comparison of Different Approaches to Airborne Gravimetry by INS/DGPS. In: *Proc. of the Int. Symposium Gravity, Geoid and Marine Geodesy (GraGeoMar96)*, Tokyo, September 30 - October 5, pp. 155-162.

Wei, M., and K.P. Schwarz (1995). Analysis of GPS-Derived Acceleration From Airborne Tests. In: *Proc. of Airborne Gravity*, IAG Symposium G4, Boulder, Colorado, July 2-14, pp. 175-188.

Wei, M., and K.P. Schwarz (1994). An Error Analysis of Airborne Vector Gravimetry. In: *Proc. of International Symposium on Kinematic Systems in Geodesy, Geomatics and Navigation (KIS97)*, Banff, Canada, August 30 - September 2, pp. 509-520.

Wei, M., and K.P. Schwarz (1990). A Strapdown Inertial Algorithm Using an Earth-Fixed Cartesian Frame. *Navigation: Journal of the Institute of Navigation*, 37, 2, pp. 153-167.

Zhang Q.J., and K.P. Schwarz (1996). A Testing of Double Difference GPS Multipath Errors Under Kinematic Conditions. In: *Proc. of IEEE PLANS Symposium*. IEEE, New York, pp. 285-291.

# APPENDIX

## Mechanization and Error Model for Strapdown INS

The output of a strapdown inertial system includes the orthogonal triad of three accelerometers specific force estimates, and the assembly of gyroscopes measurements of angular velocity with respect to an inertial frame of reference. The motion of the vehicle is a dynamic process (i.e. changing with time). Typically, a set of differential equations can be formulated to describe a dynamic process. However, for use with standard estimation schemes such as Kalman filtering the arbitrary system of differential equations is transformed into a system of first-order differential equations (or state equations). The variables of such a system are called state variables and are generally composed of the quantities that are of interest, for example, the position, velocity and attitude of a vehicle. Using the set of first-order equations, the kinematic measurements from the accelerometers and gyroscopes can be used to determine the state variables. In KINGSPAD, the INS measurements are mechanized (i.e. processed) in the e-frame. The state equations for vehicle motion in the e-frame are given in Wei and Schwarz (1990) as:

$$\dot{x}^e = \begin{bmatrix} \dot{r}^e \\ \dot{v}^e \\ \dot{R}_b^e \end{bmatrix} = \begin{bmatrix} v^e \\ R_b^e f^b - 2\Omega_{ie}^e v^e + g^e \\ R_b^e \left( \Omega_{ib}^b - \Omega_{ie}^b \right) \end{bmatrix} \tag{A.1}$$

where,

$r^e, v^e$      are the position and velocity vector respectively in the e-frame,

$R_b^e$      is the transformation matrix from the b-frame to the e-frame,

$g^e$      is normal gravity in the e-frame,

$\Omega_{ie}^b$      is a skew-symmetric matrix of earth rotation, $\omega_{ie}$,

$f^b$      is specific force (measured by the accelerometers) and,

$\Omega_{ib}^{b}$ is a skew-symmetric matrix of angular velocities, $\omega_{ib}^{b}$, of the b-frame with respect to the i-frame (measured by the gyroscopes).

The dot above a quantity denotes time differentiation.

Using the above mechanization equations the measurements from the strapdown INS can be related to the variables of interest (position, velocity and attitude). However, the measurements obtained from the INS contain errors that can have deterministic and stochastic components. Therefore, an error model of the mechanization is required for error analysis and estimation. To facilitate the use of Kalman filtering for estimation of errors a set of state equations for the error model is derived. The general model of the state equations used in Kalman filtering is:

$$\dot{x} = Fx + Gw \qquad (A.2)$$

where,

x      denotes the error states,

F      is the dynamics matrix,

w      is the random forcing functions (considered as Gaussian white noise), and

G      is the shaping matrix.

An error model of this form can be obtained by linearizing equation (A.1), details of the linearization can be found in Schwarz and Wei (1990). In addition to the error state variables for position, velocity and attitude, additional variables are normally added to describe gyro drift errors (d) and residual accelerometer bias errors (b). Generally, these terms represent errors correlated in time and are modeled as either random walk or first-order Gauss-Markov processes. When modeled as first-order Gauss-Markov processes the state equations are of the form:

$$\dot{d} = -\kappa d + w_{d} \qquad (A.3)$$

and

$$\dot{b} = -\beta b + w_{b} \qquad (A.4)$$

where $\kappa$ and $\beta$ are diagonal matrices containing the inverse of the time correlation for the processes, and $w_d$ and $w_b$ are vectors of white noise. The general form for the error states in the e-frame is then given by (Schwarz and Wei (1997)):

$$\dot{x}^e = \begin{bmatrix} \delta \dot{r}^e \\ \delta \dot{v}^e \\ \dot{\varepsilon}^e \\ \dot{d} \\ \dot{b} \end{bmatrix} = \begin{bmatrix} \delta v^e \\ -F^e \varepsilon^e + N^e \delta r^e - 2\Omega^e_{ie} \delta v^e + R^e_b b \\ -\Omega^e_{ie} \varepsilon^e + R^e_b d \\ -\kappa d + w_d \\ -\beta b + w_b \end{bmatrix} \tag{A.5}$$

where,

$\delta r^e, \delta v^e$      are errors in position and velocity, respectively and,

$N^e$      is a coefficient matrix relating normal gravity errors to position errors.

All other quantities have been previously defined. The above error equations can then be used via Kalman filtering for INS error prediction and estimation using GPS position and velocity updates. The Kalman filtering procedures will not be discussed here but can be found in numerous references, for example, Gelb (1974), Brown and Hwang (1992), and Maybeck (1994). It should be noted that the state vector in equation (A.5) contains navigation errors as well as correlated sensor noise terms. Other effects such as non-orthogonality of the sensor triad and sensor scale factors are normally calibrated beforehand in laboratory testing and are therefore not modeled. A discussion of calibration procedures for inertial systems can be found in Salychev (1998).